

The Plausibility of Iron-Sulfur Peptides on the Early Earth

by

Yin Juan Hu

A thesis submitted in partial fulfillment of the requirements for the degree of

Master of Science

Department of Chemistry  
University of Alberta

© Yin Juan Hu, 2022

## **Abstract**

Iron-sulfur clusters are recognized widely as ancient cofactors that are proposed to have impacted the prebiotic chemistry that led to life. Previous work done by our lab has shown that iron-sulfur clusters could be synthesized prebiotically on cysteine containing tripeptides, but it remains unclear if such complexes could survive under the environmental conditions of the early Earth.

In this thesis, I investigated the stability of iron-sulfur peptides under prebiotically plausible environments. Seven different peptides with various sequences and lengths were used to synthesize iron-sulfur clusters, and these iron-sulfur peptides were tested under different chemical conditions. The results suggested that the types of iron-sulfur clusters formed are dependent on environmental conditions and the peptidyl ligands. Glutathione coordinated iron-sulfur clusters were the most stable among all conditions. The duplication of the tripeptide, i.e., a hexapeptide, would make the corresponding iron-sulfur clusters more stable. This demonstrated the possibility that modern iron-sulfur proteins could have emerged from short peptides that coordinated iron-sulfur clusters from the beginning, and thereby facilitated the emergence of primordial metabolic pathways that then give rise to the life.

# Acknowledgement

I would like to acknowledge all those who in one way or another assisted me throughout my undergraduate and graduate studies here at the University of Alberta. I want to say thank you all for being here.

I would first want to thank my supervisor, Dr. Sheref S. Mansy, who allowed me to enter this new field of the research on the origin of life. I also am very grateful for his constant encouragement and support during the research. In addition, I want to thank the other members of my supervisory committee, Dr. Julianne M. Gibbs and Dr. Gabriel Hanna, for their time, comments, and suggestions on my project.

Many thanks to Craig Walton from the University of Cambridge for his collaboration on this project and the many constructive suggestions he provided from a geochemistry perspective.

I also want to thank Mark Miskolzie for his patient help with paramagnetic  $^1\text{H}$  NMR and all of staff at the Chemistry Department for their continuous support during my studies at the University of Alberta.

Another thanks to all the past and present members of the Mansy group, most especially Daniele Rossetto, Luca Valer, Dr. Shibaji Basak, and Dr. Serge Nader for their help and advice during my research. They also provided me with a friendly and joyful working environment.

A very special thanks to my family and friends for their endless love and encouragement; without them, I am not sure if I would ever been able to finish this endeavor.

Lastly, I would like to thank Dr. Anna D. Jordan for her precious advice on my thesis writing.

# Table of Contents

CHAPTER 1 .....	1
Introduction.....	1
1.1 The Origins of Life .....	1
1.2 The Prebiotic Earth .....	2
1.3 The Importance of Metals.....	3
1.4 Iron-Sulfur Clusters .....	5
CHAPTER 2 .....	10
Results and Discussion .....	10
2.1 Research Aims and Strategy .....	10
2.2 The Stability Test of Iron-Sulfur Peptides under Individual Chemical Condition .....	12
2.2.1 Experimental Design.....	12
2.2.2 Method to Analyze UV-vis Spectral Data .....	17
2.2.3 Assessment of Glutathione Stabilized [2Fe-2S] <sup>2+</sup> Clusters .....	19
2.2.4 Assessment of N-acetyl-L-Cysteine Methyl Ester Stabilized [4Fe-4S] <sup>2+</sup> Cluster .....	24
2.3 The Stability Test of Iron-Sulfur Peptides Under Mimicked Prebiotic Environments .....	27
2.3.1 Experimental Design.....	27
2.3.2 Assessment of Iron-Sulfur Peptides under Mimicked Prebiotic Environment.....	29
CHAPTER 3 .....	38
Conclusion and Future Work .....	38
CHAPTER 4 .....	40
Experimental .....	40
4.1 Materials .....	40
4.2 Solid Phase Peptide Synthesis .....	40
4.3 [2Fe-2S] <sup>2+</sup> Cluster Synthesis.....	41
4.4 [4Fe-4S] <sup>2+</sup> Cluster Synthesis.....	41
4.5 UV-Visible Absorption Spectroscopy .....	41
4.6 Fit-FeS .....	42
4.7 Paramagnetic <sup>1</sup> H NMR .....	42
4.8 Statistics and Reproducibility .....	42

References.....	43
Appendix.....	46

## List of Tables

2.1. List of Ubiquitous Species .....	11
2.2. List of Phosphorus Species .....	12
2.3. Four Prebiotic Plausible Environmental Conditions.....	12
2.4. The Changes of pH after Adding Different Additives.....	17
2.5. List of Ligands Tested under Prebiotic Plausible Environmental Conditions.....	29
A.1. Chemical Structures of Tested Peptide Sequences .....	46
A.2. Standard Errors of Mean for Figure 2.4.....	47
A.3. Standard Errors of Mean for Figure 2.9 .....	49
A.4. Standard Errors of Mean for Figure 2.15.....	51

# List of Figures

1.1. A timeline of the elemental composition of the Earth. ....	3
1.2. The functions of iron-sulfur clusters.....	6
1.3. The structures of different types of clusters.....	7
1.4. UV-vis absorption spectra of iron-sulfur clusters.....	8
2.1. The stability of a glutathione coordinated $[2\text{Fe-2S}]^{2+}$ cluster under different temperatures.....	15
2.2. The stability of iron-sulfur clusters coordinated by different ligands.....	16
2.3. Formation of glutathione coordinated iron-sulfur clusters .....	19
2.4. Cluster composition of glutathione coordinated iron-sulfur clusters after 110 min .....	21
2.5. A two-dimensional representation of a glutathione coordinated $[2\text{Fe-2S}]^{2+}$ cluster .....	23
2.6. A proposed $[2\text{Fe-2S}]^{2+}$ glutathione hydrolysis mechanism via counterion mediated pathway .....	23
2.7. Cluster composition of glutathione coordinated iron-sulfur clusters under different additive concentrations.....	24
2.8. Hofmeister series .....	25
2.9. Cluster composition of N-acetyl-L-cysteine methyl ester coordinated iron-sulfur clusters after 7 h.....	27
2.10. Cluster composition at pH 5–10 .....	29
2.11. Paramagnetic $^1\text{H}$ NMR spectra of glutathione stabilized iron-sulfur clusters ...	31
2.12. Cluster composition of peptide GCGGCG coordinated iron-sulfur clusters under lost city condition over time .....	32
2.13. Cluster composition of glutathione coordinated iron-sulfur clusters under seawater condition over time .....	33
2.14. Cluster composition of peptide GCG coordinated iron-sulfur clusters under glacial brine condition over time .....	35
2.15. Cluster composition of iron-sulfur peptides after 20 h .....	37

A.1. Individual absorption spectra for iron-sulfur glutathione under 100 $\mu$ M additive conditions.....	52
A.2. Individual absorption spectra for iron-sulfur glutathione under 100 mM additive conditions.....	56
A.3. Individual absorption spectra for iron-sulfur glutathione under 0.5 M additive conditions.....	59
A.4. Individual absorption spectra for iron-sulfur N-acetyl-L-cysteine methyl ester under 100 $\mu$ M additive conditions.....	62
A.5. Individual absorption spectra for iron-sulfur N-acetyl-L-cysteine methyl ester under 100 mM additive conditions.....	65
A.6. Individual absorption spectra for iron-sulfur N-acetyl-L-cysteine methyl ester under 0.5 M additive conditions.....	68
A.7. Individual absorption spectra for iron-sulfur peptides under alkaline lake conditions.....	71
A.8. Individual absorption spectra for iron-sulfur peptides under lost city conditions.....	73
A.9. Individual absorption spectra for iron-sulfur peptides under seawater conditions.....	75
A.10. Individual absorption spectra for iron-sulfur peptides under glacial brine conditions.....	77
A.11. Paramagnetic $^1\text{H}$ NMR spectra of iron-sulfur peptides under alkaline lake conditions.....	79
A.12. Paramagnetic $^1\text{H}$ NMR spectra of iron-sulfur peptides under lost city conditions.....	83
A.13. Paramagnetic $^1\text{H}$ NMR spectra of iron-sulfur peptides under seawater conditions.....	87
A.14. Paramagnetic $^1\text{H}$ NMR spectra of iron-sulfur peptides under glacial brine conditions.....	91



## List of Abbreviations

A	Alanine
AA	Amino acid
Ac-Cys-OMe	<i>N</i> -acetyl-l-cysteine methyl ester
C	Cysteine
ca.	Circa
cm	Centimeter
Cys	Cysteine
D	Aspartic acid
ddr	Direct digital receiver
DNA	Deoxyribonucleic acid
E	Glutamic acid
Fmoc	Fluorenylmethoxycarbonyl protecting group
G	Glycine
h	Hour
Hz	Hertz
H <sub>α</sub>	Alpha proton
H <sub>β</sub>	Beta proton
I	Isoleucine
K	Lysine
L	Leucine
min	Minute
mM	Milli-molar
M	Molar
nm	Nanometer
NMR	Nuclear magnetic resonance
P	Proline
ppm	Parts per million
RNA	Ribonucleic Acid
s	Second

S	Serine
SPPS	Solid phase peptide synthesis
T	Threonine
UV-vis	Ultra-violet visible
W	Tryptophan
$\alpha$	Alpha
$\beta$	Beta
$\gamma$	Gamma
$\mu\text{M}$	Micro-molar
$\mu\text{s}$	Micro-second
$\rho$	Rho
$^{\circ}\text{C}$	Degree Celsius

# CHAPTER 1

## Introduction

### 1.1 The Origins of Life

What is life and how did it emerge? This question has puzzled scientists for many years.<sup>1</sup> The history of research on the origins of life goes back to the early 19<sup>th</sup> century where the concept of spontaneous generation was explored. It was believed that “life was inherent to matter; it was eternal and appeared spontaneously whenever the conditions were favorable.”<sup>2</sup> However, by the middle of the 19<sup>th</sup> century, this idea was rejected after the invention of the microscope and the technique of sterilization,<sup>3</sup> which showed that life comes from life.

Around the same time, Charles Darwin published *The Origins of Species*. Although in the book he avoided to discuss the origins of life, he did mention in a letter to Joseph D. Hooker that a warm little pond with a mixture of inorganic salts and simple organic molecules could have provided an optimal environment for life to originate through natural processes.<sup>4</sup> Alexander Oparin was inspired by this idea and proposed that life may have formed in a hot primordial soup of simple chemicals that combined together to form modern macromolecules.<sup>5</sup> Later on, Stanley Miller tested whether the building blocks of life could be built through prebiotically plausible mechanisms in the laboratory. He exposed a mixture of methane (CH<sub>4</sub>), ammonia (NH<sub>3</sub>), hydrogen (H<sub>2</sub>), and water (H<sub>2</sub>O) to an electric discharge, and a number of amino acids were formed.<sup>6</sup> For many, this experiment represents the beginning of the modern era of research on the origins of life.

Since the discovery of the central dogma of molecular biology, efforts have focused on the role of nucleic acids on the origins of life. Models such as the RNA world,<sup>7</sup> metabolism-first world,<sup>8</sup> and lipid world came out,<sup>9</sup> and each has its own strengths. The ability of RNA to perform jobs of DNA and protein-like enzymes supports the RNA world hypothesis,<sup>7</sup> but it does not explain life’s other essential feature, such as metabolism. This raises the concept of “metabolism first”.<sup>8</sup> An early form of metabolism could have led to the synthesis of the building blocks of life.

Generally, it also is accepted that lipid vesicles aided the emergence of Darwinian evolution and metabolism.<sup>9</sup>

Obviously, one model cannot explain the origins of life as a whole, but the combination of these models can give us some insights. Although we have a long way to go to obtain a comprehensive picture about how life emerged, we can begin to take small steps. For example, prebiotic chemistry was constrained by the environmental conditions of our young planet. Therefore, by simply subjecting what are thought to be prebiotically plausible reactions deciphered in the laboratory to more plausible early Earth conditions, we can begin to constrain chemical space towards more plausible scenarios.

## **1.2 The Prebiotic Earth**

The Earth was formed ca. 4.6 billion years ago by accretion from the solar nebula.<sup>10</sup> At this stage, the core of Earth consisted of metallic Fe, Ni, and a mantle of silicate.<sup>11</sup> 100 million years later, the young Earth shaped into a partially solid surface as temperature decreased gradually. This young planet was unstable due to its heavy weight, and thus underwent melting and solidification processes, resulting in the formation of the crust and finally the continents.<sup>11</sup>

Meanwhile, the primary atmosphere of the Earth was formed by the degassing of the mantle,<sup>11</sup> which consisted of carbon dioxide (CO<sub>2</sub>), water vapour (H<sub>2</sub>O), and nitrogen (N<sub>2</sub>) as major components, in addition to lesser amounts of methane (CH<sub>4</sub>), molecular hydrogen (H<sub>2</sub>), ammonia (NH<sub>3</sub>), hydrogen sulfide (H<sub>2</sub>S), and other components.<sup>10</sup> Free oxygen likely did not exist at this point. Once the Earth's atmosphere was cooled enough to below the condensation point, water vapour condensed and started to fall as rain, forming oceans and other bodies of water on the surface of the earth. The ultraviolet and infrared radiation, together with CO<sub>2</sub> and other greenhouse gases, provided enough energy to maintain a temperature range compatible with the presence of liquid water.<sup>11</sup>

In general, both the physical and chemical conditions of the early Earth's atmosphere and ocean fulfilled the requirements necessary for the formation of complex chemical compounds, as suggested by the Miller–Urey experiment.<sup>4</sup>

Specifically, the formation of a water layer introduced bio-essential elements, such as iron and sulfur, to the ocean. Most of the iron was in the form of dissolved  $\text{Fe}^{2+}$  complexes, while sulfur was in the form of insoluble sulfide minerals.<sup>12</sup> Besides these two, the ocean also contained an abundance of transition metals, such as manganese, cobalt, nickel, copper, zinc, and molybdenum (Figure 1.1). These metals were proposed to participate in the construction of biological macromolecules.<sup>13-14</sup>

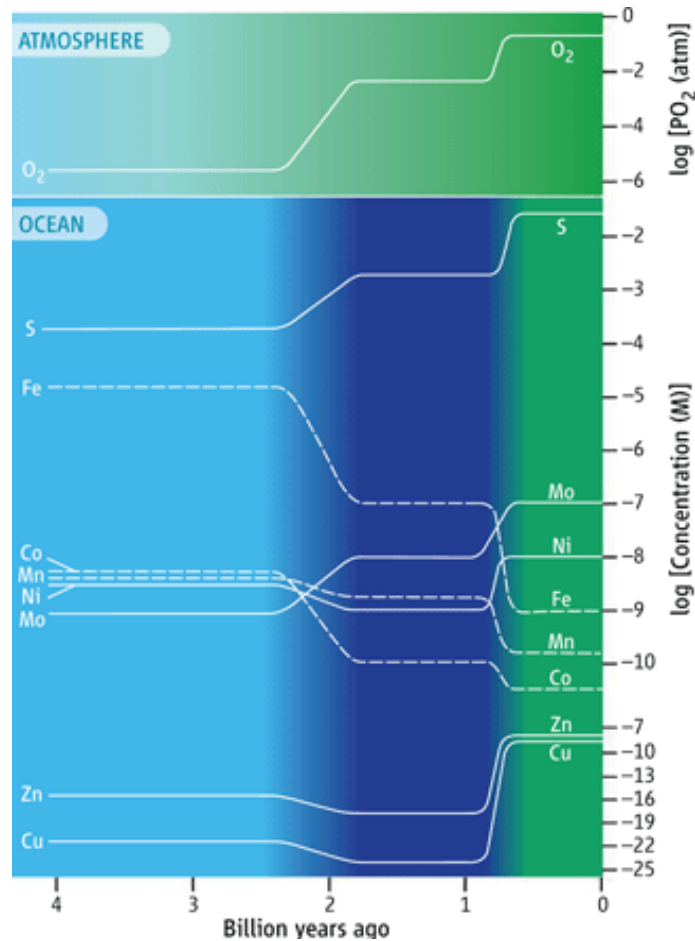


**Figure 1.1.** A timeline of the elemental composition of the Earth. Colour gradients indicate a transition from anoxic, S poor oceans (light blue), to  $\text{H}_2\text{S}$ -rich oceans (dark blue), finally to complete oxygenation of ocean (green). Dashed lines represent decreasing concentrations. (Adapted from Anber, A. D.)<sup>12</sup>

### 1.3 The Importance of Metals

Certainly, metals are essential for contemporary life. Informatics studies suggest that more than 30% of all proteins in cells require one or more metals to perform their

specific functions,<sup>13</sup> and over 40% of all enzymes contain metals.<sup>14</sup> These metalloproteins and metalloenzymes can be found in every living organism, and metals, in particular, play crucial roles in life's three fundamental subsystems: information molecules, compartmentalization, and metabolism.

Among all metals,  $\text{Na}^+$ ,  $\text{K}^+$ ,  $\text{Mg}^{2+}$ , and  $\text{Ca}^{2+}$  are bulk metals, as they form 1–2% of the human body weight<sup>15</sup> and are responsible for transmitting nerve impulses and muscle contraction through transmembrane concentration gradients. Iron and copper often participate in electron transfer due to their redox nature.<sup>16</sup> In respiration and photosynthesis, small redox-active metalloproteins facilitate electron transfer reactions by alternately binding to specific integral membrane proteins that often contain several metal sites. Additionally, iron and copper are involved in dioxygen ( $\text{O}_2$ ) storage and transportation via metalloproteins such as hemoglobin, myoglobin, and hemocyanin.<sup>17</sup> In contrast, zinc helps to stabilize the folding of proteins and enzymes as well as DNA and ribozymes.<sup>18</sup> Most of the other trace metals have been identified as parts of metalloenzymes.<sup>14</sup> For instance, cobalt can be found in  $\text{B}_{12}$  cofactors, which act in humans as a cofactor for methylmalonyl-coenzyme A mutase and methionine synthase,<sup>17</sup> and these two enzymes are important for health. Furthermore, nickel functions in several hydrogenases to mediate the reversible oxidation of  $\text{H}_2$ , and both molybdenum and vanadium can be found in nitrogenase, assisting the fixation of  $\text{N}_2$ .<sup>17</sup> Noticeably, these are just a few examples of how metal ions perform in biological systems; numerous unmentioned metals also play important roles in living organisms.

Since metals participate in so many biological activities and were abundant in the prebiotic Earth, it also is reasonable to consider metals as the possible progenitors of contemporary metalloproteins. For example, iron ions catalyze the decomposition of hydrogen peroxide ( $\text{H}_2\text{O}_2$ ), and divalent cations (i.e.,  $\text{Mn}^{2+}$ ,  $\text{Mg}^{2+}$ ,  $\text{Zn}^{2+}$ ,  $\text{Co}^{2+}$ ,  $\text{Ni}^{2+}$ , etc.) can catalyze transphosphorylation independently.<sup>19</sup> Within a solution of iron ions, inorganic sulfide, and thiolate ligands, catalytically active iron-sulfur clusters can be formed easily.<sup>20</sup> Both cases suggest the ability of metal ions to act as catalysts without coordination to proteins that were not found on the prebiotic Earth. Furthermore, Markus Ralser and co-workers demonstrated that  $\text{Fe}^{2+}$  could catalyze most of the

glycolysis and the pentose phosphate pathways.<sup>21</sup> Additionally,  $\text{Fe}^{2+}$  functionally replaces  $\text{Mg}^{2+}$  in the  $\text{Mg}^{2+}$  dependent catalytic site of *Tetrahymena thermophila* Group I intron P4-P6 domain.<sup>22</sup> Combined with the high concentration of dissolved iron in the ancient ocean,<sup>12</sup>  $\text{Fe}^{2+}$  displayed a higher possibility to be used as a catalyst on the prebiotic Earth when compared to other metal ions.

However, the pathway from free metal ions to modern metalloproteins remains unclear. Researchers proposed a pathway via metallopeptide intermediates, which formed by free metal ions and prebiotically plausible peptides.<sup>23</sup> Insights into the sequences of these prebiotic peptides may be determined by bioinformatics analysis of modern-day proteins. Besides sequence analysis alone, it is also worth synthesizing and testing metal coordinating peptides to understand better the likelihood of these metallopeptides existing prebiotically. Thus, these experiments help to reveal the potential role of metallopeptides in facilitating the emergence of a primordial metabolic-like pathways.

## **1.4 Iron-Sulfur Clusters**

Iron-sulfur clusters could be one of the valuable metallopeptides to investigate deeply since these clusters have been recognized widely as among the first catalysts that appeared on Earth. This may be due to the high concentration of iron and sulfur on the early Earth and their ability to form spontaneously.<sup>20</sup> Iron-sulfur clusters often act as versatile prosthetic groups that enable their associated proteins to perform numerous functions, ranging from electron transport to substrate ligation, structural support, and DNA repair (Figure 1.2).<sup>24</sup>

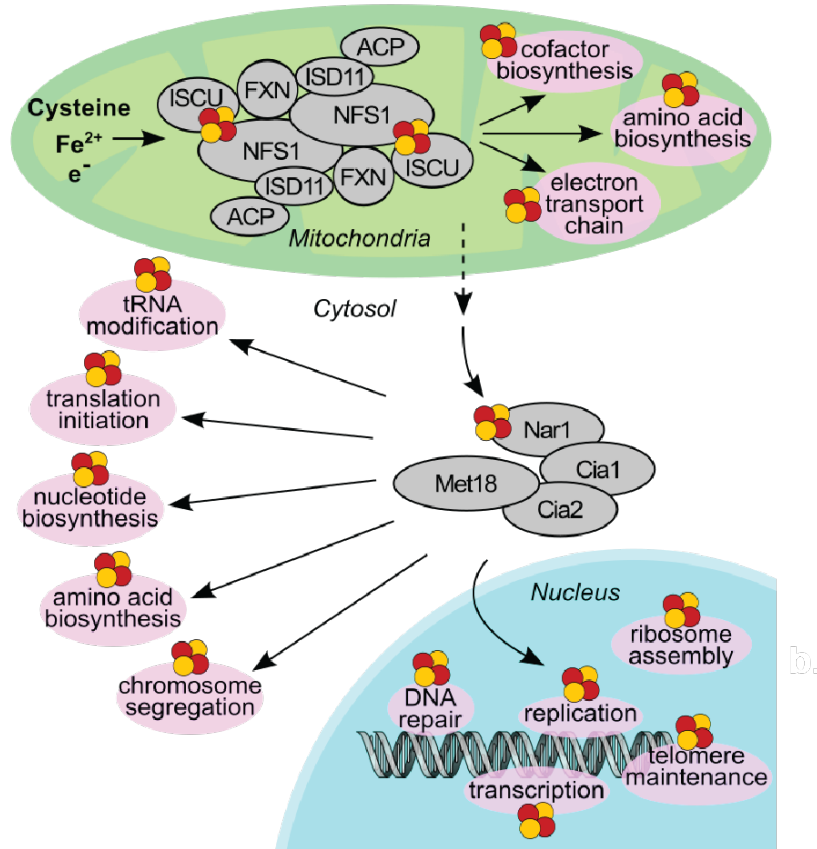


**Figure 1.2.** The functions of iron-sulfur clusters (red/yellow). These can be assembled by mitochondrial protein complexes. The cytosolic complexes then deliver iron-sulfur clusters to proteins that function in a wide range of processes. (Adapted from Drennan research and education laboratory).<sup>25</sup>

The most common iron-sulfur clusters found in biology are [1Fe-0S], [2Fe-2S], and [4Fe-4S] clusters with different charges since both iron and sulfur exist in more than one oxidation state. In all these clusters, iron ions typically are tetrahedrally coordinated by the thiolate sidechains of cysteines (Figure 1.3). Often, polynuclear iron-sulfur clusters are coordinated by additional inorganic sulfide. Conversely, iron atoms in proteins such as Rieske and mitoNEET are coordinated by histidine, whereas Biotin synthetase exploits an arginine ligand.



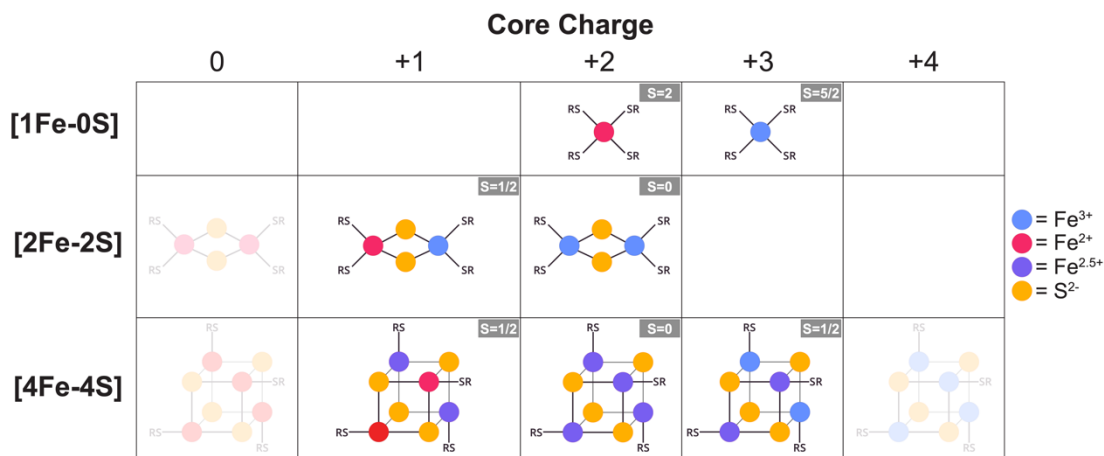


**Figure 1.3.** The structures of different types of clusters. [2Fe-2S]<sup>0</sup>, [4Fe-4S]<sup>0</sup>, and [4Fe-4S]<sup>+4</sup> clusters do not typically form. (Adapted from Valer, L. et al.)<sup>26</sup>

Due to a large variety of iron-sulfur clusters, it is necessary to have proper tools to characterize these clusters in a precise and efficient way. In fact, the earliest discovery of iron-sulfur clusters in proteins was by spectroscopic studies.<sup>27</sup> Till now, more than a dozen of different spectroscopic techniques have been developed and used to identify and characterize iron-sulfur proteins.<sup>24</sup> These techniques can be classified into three main categories: optical, magnetic, and X-ray techniques. In particular, optical techniques include electron absorption (ultraviolet-visible region), circular dichroism (CD), infrared (IR), and Raman spectroscopies. Magnetic techniques include electron paramagnetic resonance (EPR), Mössbauer, magnetic CD (MCD), and nuclear magnetic resonance (NMR) spectroscopies. X-ray techniques include X-ray absorption, X-ray emission, and nuclear resonance vibrational spectroscopies. These techniques explore almost the entire electromagnetic spectrum from microwave frequency (MW) to X-ray frequency.<sup>24</sup> Among all, UV-visible absorption spectroscopy would be used most commonly, as it is inexpensive, efficient, and readily available. In the UV-vis region, the broad absorption features result from S to Fe charge transfer. The spectral peaks are varied in different types of clusters.<sup>28</sup> [1Fe-0S]<sup>2+</sup> clusters often display a peak around 310 nm and another one at 350 nm (Figure 1.4). In addition, [2Fe-2S]<sup>2+</sup> clusters give peaks at 420 nm and 450 nm, and [4Fe-4S]<sup>2+</sup> clusters often show a broad peak around the 400–420 nm region.

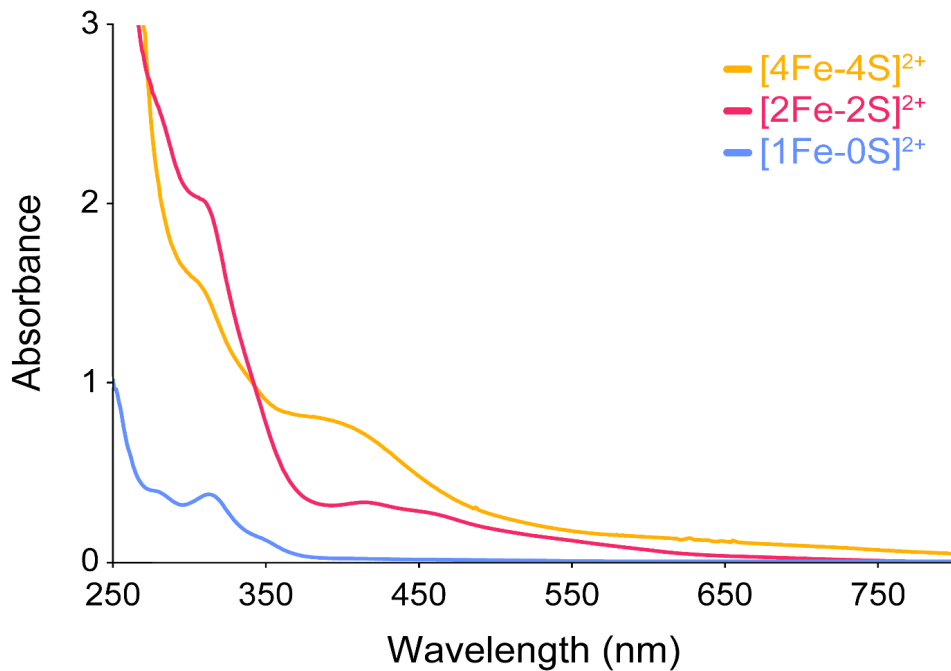


**Figure 1.4.** UV-vis absorption spectra of iron-sulfur clusters. Spectra are of peptide GCPLCG coordinated [1Fe-0S]<sup>2+</sup> cluster (blue line), peptide PESCKAGACSTCAGPDLTCT coordinated [2Fe-2S]<sup>2+</sup> cluster (red line), and peptide KLCEGGCIACGACGGW coordinated [4Fe-4S]<sup>2+</sup> cluster (yellow line). (Adapted from Valer, L. et al.)<sup>26</sup>

After the first successful synthesis of iron-sulfur clusters *in vitro* by Holm and colleagues in the 1970s,<sup>29</sup> people started to realize that iron-sulfur clusters could interconvert and assemble independently of a protein scaffold. Originally, these reactions happened in nonaqueous conditions. Later on, researchers demonstrated the possibility to synthesize clusters in aqueous buffer,<sup>30</sup> then recently, even just in water.<sup>31</sup> Indeed, our lab also made big efforts in investigating iron-sulfur cluster synthesis. We showed that iron-sulfur clusters can be synthesized with simple, prebiotically plausible ligands (cysteine-containing tripeptides) under UV light.<sup>32</sup> In this case, the UV light was responsible for the generation of sulfide ions from thiol containing ligands as well as ferric ions through photooxidation of ferrous ions. Notably, this pathway was similar to the modern biosynthetic pathway in terms of donation of sulfide ions during the synthesis of iron-sulfur clusters. We also demonstrated that the duplication of an iron-sulfur tripeptide (glutathione) sequence to longer peptides increased the cluster's stability;<sup>33</sup> this suggested that the formation of protoferredoxin may emerge from simple and small peptides. These experimental observations reveal that simple iron-

sulfur peptides could form under prebiotically plausible conditions. However, these early studies did not investigate the impact of environmental conditions thoroughly.

# CHAPTER 2

## Results and Discussion

### 2.1 Research Aims and Strategy

Iron-sulfur clusters are recognized widely as ancient cofactors, which are proposed to have participated in the prebiotic chemical reactions that led to the Earth's first cells.<sup>34</sup> Previous work done by our lab has shown that iron-sulfur clusters could be synthesized prebiotically on cysteinyl peptides,<sup>32</sup> but it remains unclear if such complexes would survive the environmental conditions of the early Earth.

As a first attempt to address this question, we decided to test the impact of different chemical conditions on iron-sulfur peptides, in particular,  $[2\text{Fe-2S}]^{2+}$  and  $[4\text{Fe-4S}]^{2+}$  peptides. Two main categories were focused on: one set was a geologically ubiquitous species that any particular prebiotic reaction scheme would need to survive (Table 2.1), and another set was on key biologic element P species with their various forms<sup>35</sup> (Table 2.2). In addition, different concentrations (100  $\mu\text{M}$ , 100 mM, and 0.5 M) were used for each additive to see if certain concentrations are lethal or not to the formation of iron-sulfur clusters. Indeed, we also mimicked four prebiotically plausible environmental conditions<sup>36-41</sup> (Table 2.3) and then determined their effects on different iron-sulfur peptides. The overall data will help to reveal the plausibility of iron-sulfur peptides on the early Earth.

**Table 2.1.** List of Ubiquitous Species

<b>Ubiquitous species</b>	$\text{Ca}^{2+}$	$\text{Fe}^{2+}$	$\text{Mg}^{2+}$	$\text{K}^{+}$	$\text{Na}^{+}$	$\text{SiO}_3^{2-}$	$\text{Cl}^{-}$	$\text{F}^{-}$	$\text{Br}^{-}$
<b>Added as...</b>	$\text{CaCO}_3$	$\text{Fe(II)CO}_3$	$\text{MgCl}_2$	$\text{K}_2\text{CO}_3$	$\text{Na}_2\text{CO}_3$	$\text{Na}_2\text{SiO}_3$	$\text{NaCl}$	$\text{NaF}$	$\text{KBr}$

<b>Ubiquitous species</b>	$\text{SO}_4^{2-}$	$\text{SO}_3^{2-}$	$\text{BO}_3^{3-}$
<b>Added as...</b>	$\text{Na}_2\text{SO}_4$	$\text{Na}_2\text{SO}_3$	$\text{H}_3\text{BO}_3$

**Table 2.2.** List of Phosphorous Species

<b>P species</b>	Phosphate	Phosphite	Pyrophosphate	Cyclo-trimeta-phosphate	Diphosphate pentoxide	Amido phosphate
<b>Added as...</b>	NaH <sub>2</sub> PO <sub>4</sub> 2H <sub>2</sub> O	Na <sub>2</sub> HPO <sub>3</sub> 5H <sub>2</sub> O	Na <sub>2</sub> H <sub>2</sub> P <sub>2</sub> O <sub>7</sub>	Na <sub>3</sub> P <sub>3</sub> O <sub>9</sub>	P <sub>2</sub> O <sub>5</sub>	(C <sub>2</sub> H <sub>5</sub> O) <sub>2</sub> PONH <sub>2</sub>

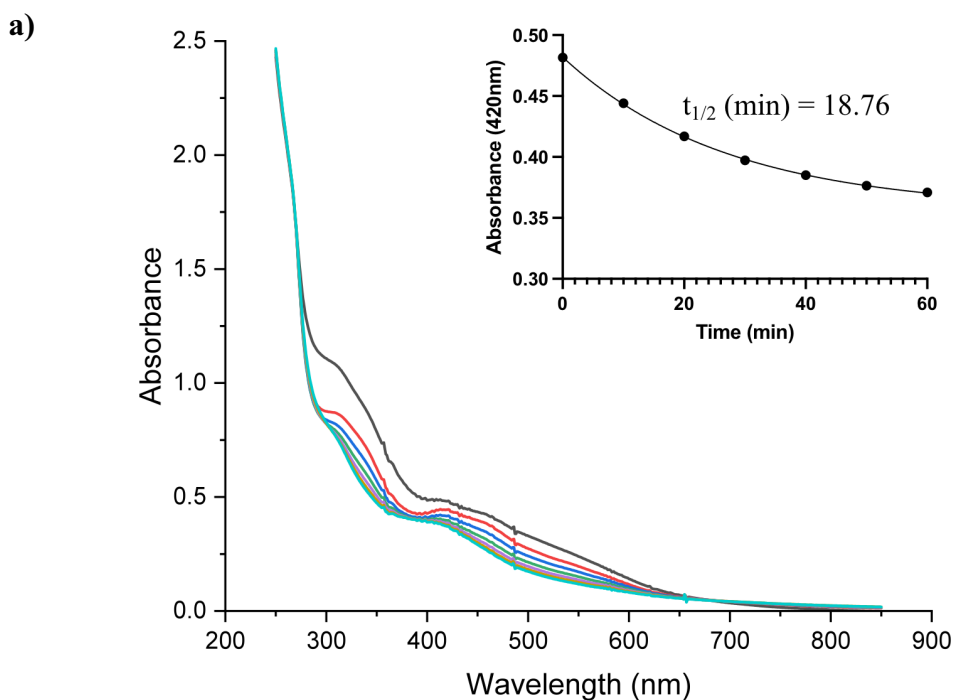
**Table 2.3.** Four Prebiotic Plausible Environmental Conditions

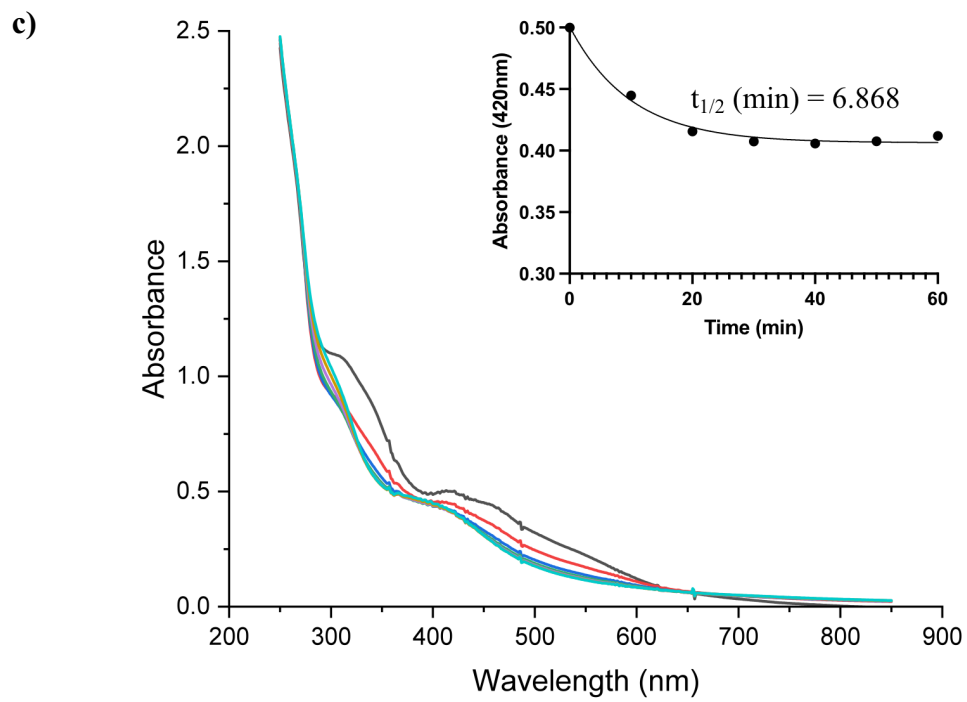
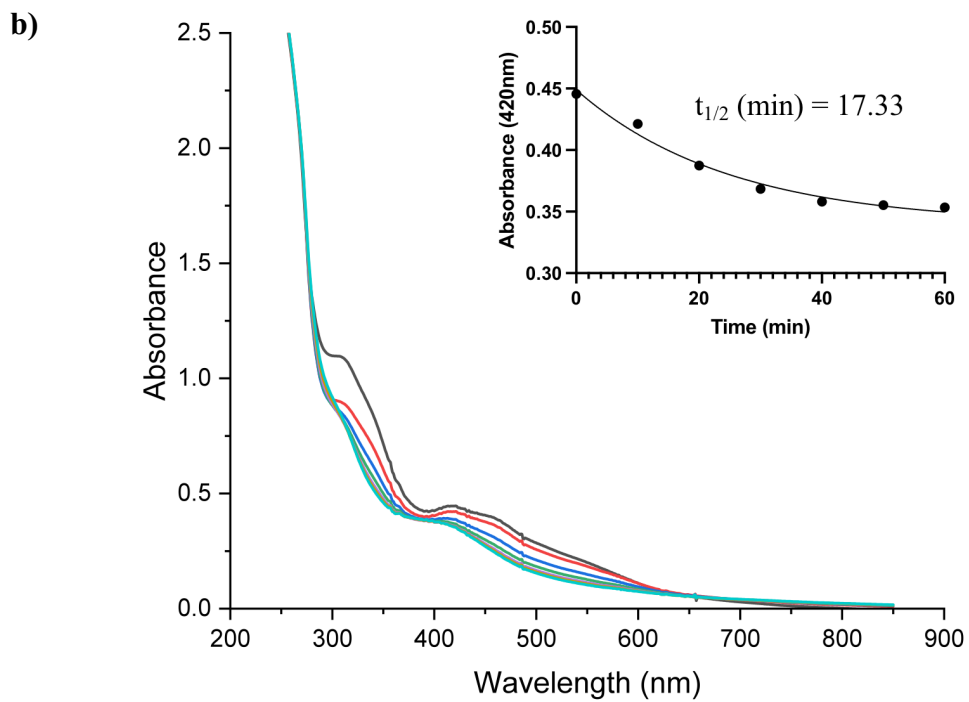
<b>Interference Species</b> (mM)	<b>Alkaline lake</b> <sup>37</sup> (pH = 10)	<b>Alkaline (Lost city)</b> <sup>38,39</sup> (pH = 9)	<b>Seawater</b> <sup>40</sup> (pH =6.5)	<b>Glacial brine</b> <sup>41</sup> (pH = 5)
PO <sub>4</sub> <sup>3-</sup>	1E+3	< 1E-3	< 1E-3-0.1	< 1E-3-0.1
Br-	100	0.1	1	2
SO <sub>4</sub> <sup>2-</sup>	1E+3	0	1E-3	60
Na <sub>2</sub> SO <sub>3</sub> – follow Rimmer et al 2018 SA (0.1 mmol) <sup>36</sup>	0.24	0.24	0.24	0.24
Li <sup>+</sup>	10	50	0.015	0.7
BO <sub>3</sub> <sup>3-</sup>	1E+3	0.03	0.5	2
Cl <sup>-</sup>	2E+3	600	500	2E+3
Ca <sup>2+</sup>	10	40	50	80
Mg <sup>2+</sup>	10	1	10	200
K <sup>+</sup>	1E+3	10	10	30
Na <sup>+</sup>	1E+4	50	500	2E+3
SiO <sub>3</sub> <sup>2-</sup>	2.2	1	2.2	0.5

## 2.2 The Stability Test of Iron-Sulfur Peptides under Individual Chemical Condition

### 2.2.1 Experimental Design

The prebiotic chemical synthesis of iron-sulfur clusters in aqueous solution typically is accomplished by mixing  $\text{Fe}^{3+}$ ,  $\text{HS}^-$ , and suitable thiolate ligands under anaerobic conditions.<sup>31-33</sup> We began by using glutathione ( $\gamma\text{ECG}$ ) as the thiolate ligand because this tripeptide has been shown previously to coordinate an iron-sulfur cluster<sup>31-33</sup> and because glutathione is readily available. We ran a series of kinetic tests to determine a convenient temperature to assess the survival of the coordinated iron-sulfur cluster (Figure 2.1). An experimental temperature of 35 °C was chosen, as this temperature was demonstrated to stabilize the glutathione coordinated  $[\text{2Fe-2S}]^{2+}$  clusters the most when compared with the other three temperatures tested (40 °C, 45 °C, and 50 °C). Furthermore, a slight pH change was detected as different species were added to the solution (Table 2.4). In order to keep the consistency of the experiment, we adjusted the pH to 8.7 after mixing.





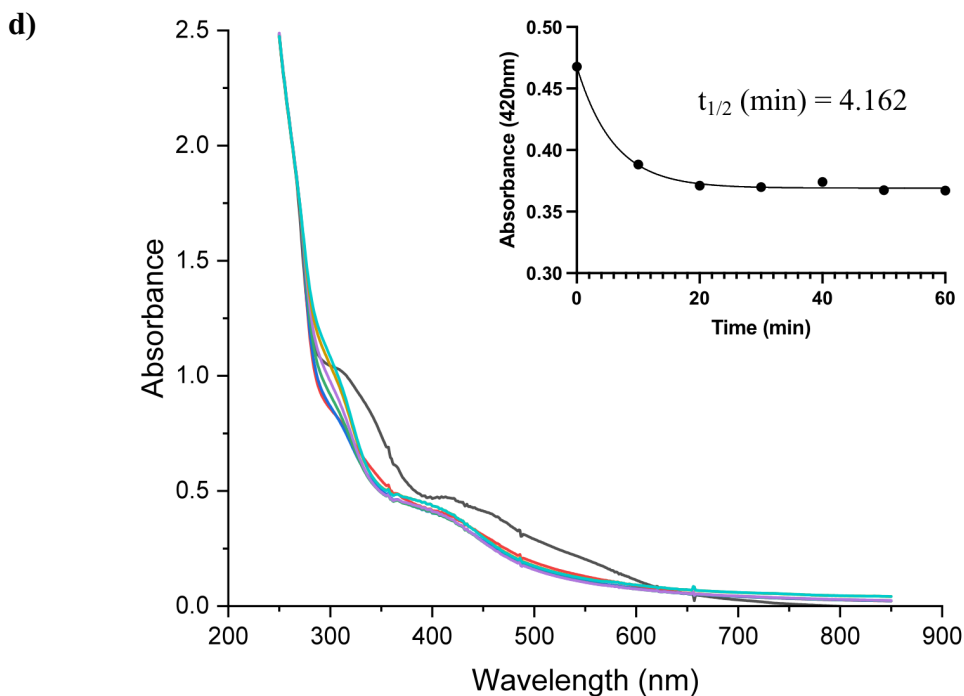


**Figure 2.1.** The stability of a glutathione coordinated  $[2\text{Fe-2S}]^{2+}$  clusters under different temperatures. The solution consisted of 0.185 mM  $\text{Na}_2\text{S}$ , 0.5 mM  $\text{FeCl}_3$ , and 40 mM glutathione, pH 8.7, and was monitored by UV-vis absorption for 1 h at a) 35 °C, b) 40 °C, c) 45 °C, and d) 50 °C.

To explore the impact of the ligand, we also tested the stability of iron-sulfur clusters coordinated by Ac-Cys-OMe (N-acetyl-L-cysteine methyl ester) instead of glutathione. The experiment showed that in a solution of 0.8 mM  $\text{HS}^-$  and 0.4 mM  $\text{Fe}^{3+}$ , Ac-Cys-OMe coordinated  $[4\text{Fe-4S}]^{2+}$  clusters were more stable than glutathione coordinated  $[4\text{Fe-4S}]^{2+}$  clusters over time (Figure 2.2). Ac-Cys-OMe appears to have a preference for  $[4\text{Fe-4S}]^{2+}$  clusters, whereas glutathione favors the formation of a  $[2\text{Fe-2S}]^{2+}$  cluster.

Once the experimental conditions were defined precisely, we started testing the stability of iron-sulfur glutathione to 100  $\mu\text{M}$  additive, followed by 100 mM and 0.5 M. Iron-sulfur N-acetyl-L-cysteine methyl ester also was tested. Iron-sulfur peptides were synthesized in water at pH 8.7 anaerobically, then different species were added to the solution. All reactions were monitored at 35 °C over time and the UV-vis spectra were collected.



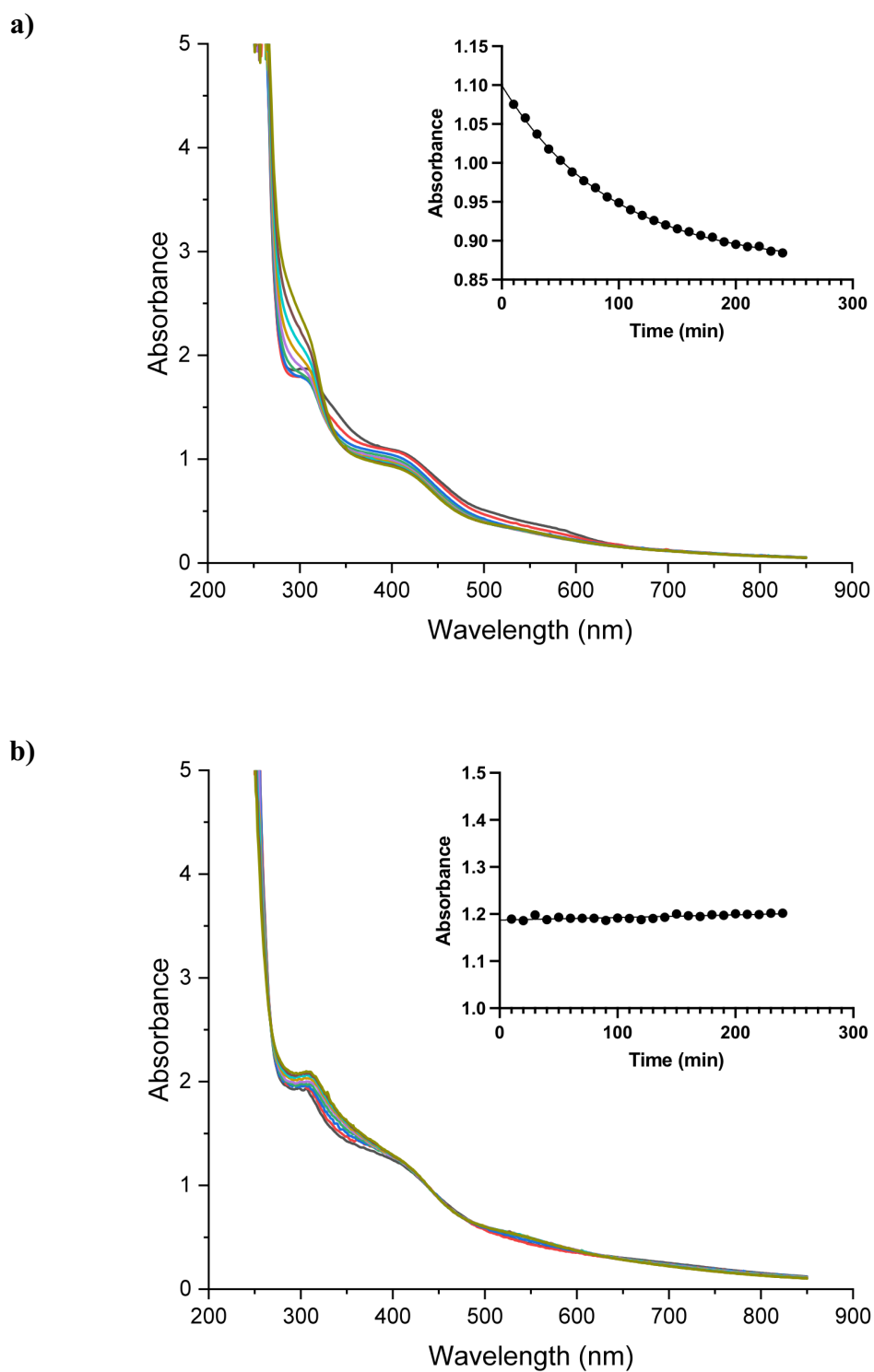


**Figure 2.2.** The stability of iron-sulfur clusters coordinated by different ligands. A solution of a) 40 mM glutathione or b) 5 mM N-acetyl-L-cysteine methyl ester, 0.8 mM Na<sub>2</sub>S, and 0.4 mM FeCl<sub>3</sub>, pH 8.7, and was monitored for 4 h, at 35 °C.

**Table 2.4.** The Changes of pH After Adding Different Additives

<b>Additives</b>	<b>Step 1:</b> H <sub>2</sub> O + Glutathione (40 mM)	<b>Step 2:</b> Na <sub>2</sub> S (0.185 mM) + FeCl <sub>3</sub> (0.5 mM)	<b>Step 3:</b> Additives (100 μM)	<b>ΔpH</b>
CaCO <sub>3</sub>	8.70	8.69	8.66	-0.01
Fe (II) CO <sub>3</sub>	8.70	8.68	8.65	-0.05
MgCl <sub>2</sub>	8.70	8.68	8.64	-0.06
K <sub>2</sub> CO <sub>3</sub>	8.70	8.69	8.69	-0.01
Na <sub>2</sub> CO <sub>3</sub>	8.70	8.69	8.63	-0.07
Na <sub>2</sub> SiO <sub>3</sub>	8.70	8.67	8.66	-0.04
NaCl	8.70	8.69	8.63	-0.06
NaF	8.70	8.68	8.65	-0.05
H <sub>3</sub> BO <sub>3</sub>	8.70	8.69	8.64	-0.06
NaH <sub>2</sub> PO <sub>4</sub> 2H <sub>2</sub> O	8.70	8.69	8.69	-0.01
Na <sub>2</sub> HPO <sub>3</sub> 5H <sub>2</sub> O	8.70	8.67	8.69	-0.01
Na <sub>2</sub> H <sub>2</sub> P <sub>2</sub> O <sub>7</sub>	8.70	8.69	8.67	-0.03
Na <sub>3</sub> P <sub>3</sub> O <sub>9</sub>	8.70	8.69	8.66	-0.04
P <sub>2</sub> O <sub>5</sub>	8.70	8.68	8.64	-0.06
(C <sub>2</sub> H <sub>5</sub> O) <sub>2</sub> PONH <sub>2</sub>	8.70	8.68	8.70	0

### 2.2.2 Method to Analyze UV-vis Spectral Data

The original UV-vis spectral data was analyzed in order to determine the impact of different additives on peptide stabilized iron-sulfur clusters. Normally,  $[2\text{Fe-2S}]^{2+}$  clusters give the most distinctive UV-vis spectra among other common types of iron-sulfur clusters.<sup>42</sup> The spectra showed two diagnostic peaks at 420 nm and 450 nm. Therefore, the formation of  $[2\text{Fe-2S}]^{2+}$  clusters under each condition can be determined easily by plotting the absorbance versus time at 420 nm or 450 nm. The same technique also was applied to  $[1\text{Fe-0S}]^{2+}$  and  $[4\text{Fe-4S}]^{2+}$  clusters (Figure 2.3). However, this measurement was not able to detect multiple clusters in solution as is often the case for peptide stabilized clusters.<sup>32</sup> As a result, the graph of absorbance versus time would misrepresent the true cluster compositions in solution, thereby leading to the calculation of the wrong half-life of the iron-sulfur clusters.

To solve this problem, our group developed an easy-to-use spectral decomposition tool called Fit-FeS.<sup>28</sup> This tool allows quick recognition of individual cluster concentrations in solution at every given point (Figure 2.3). In this case, the spectral fitted graph displayed the immediate formation of a  $[2\text{Fe-2S}]^{2+}$  clusters after the addition of 0.185 mM  $\text{HS}^-$  and 0.5 mM  $\text{Fe}^{3+}$  to 40 mM glutathione, in addition to trace amounts of  $[1\text{Fe-0S}]^{2+}$  and  $[4\text{Fe-4S}]^{2+}$  clusters. This contribution is reasonable since the  $[2\text{Fe-2S}]^{2+}$  cluster should be dominant in glutathione stabilized clusters initially.<sup>31-33</sup> In contrast, monitoring the absorbance at a single wavelength showed mainly formation of the  $[1\text{Fe-0S}]^{2+}$  cluster, which cannot represent the true cluster composition in solution. Therefore, Fit-FeS would be a more proper tool to use in our quantitative analysis of iron-sulfur clusters under various conditions.

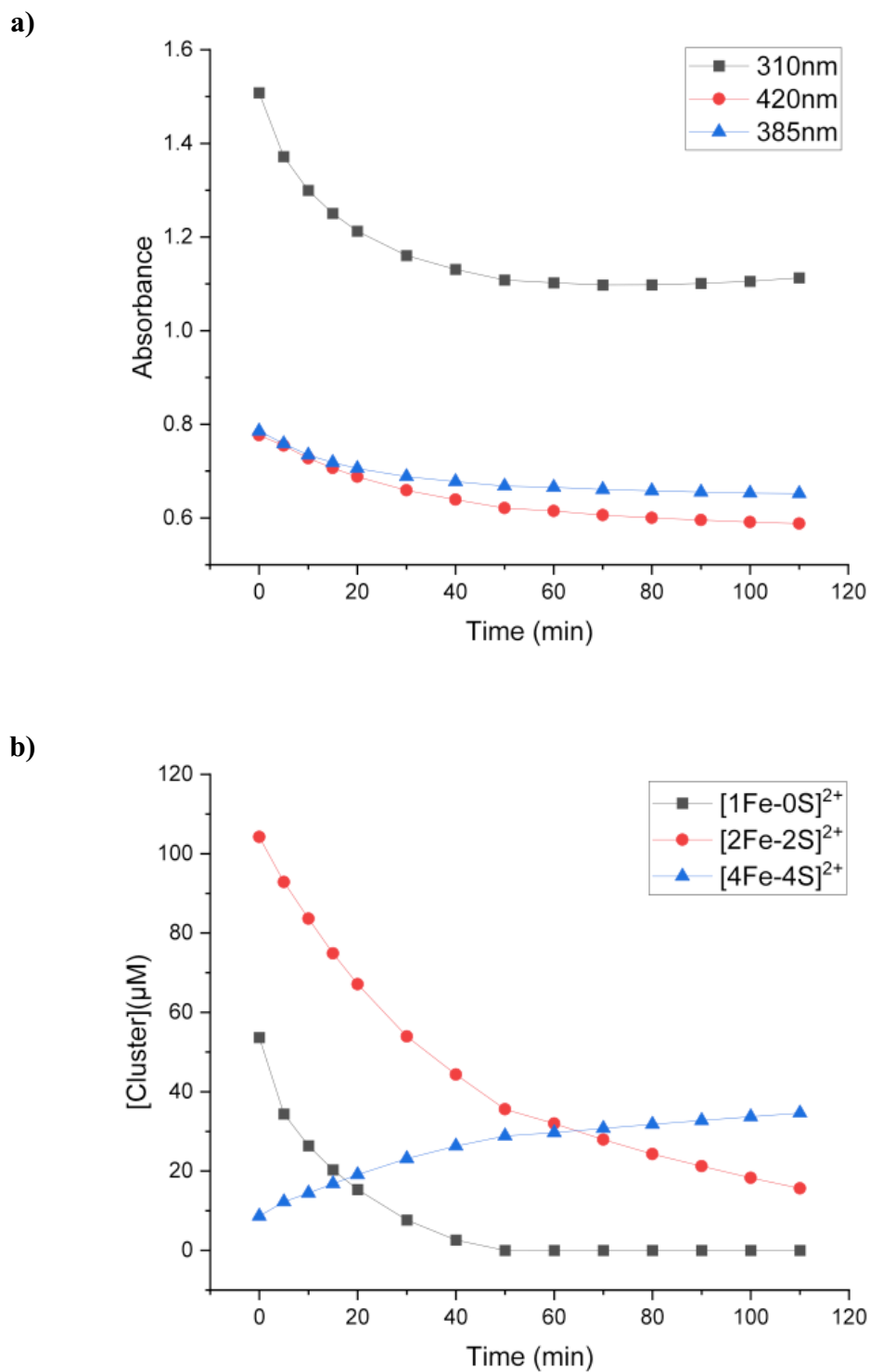


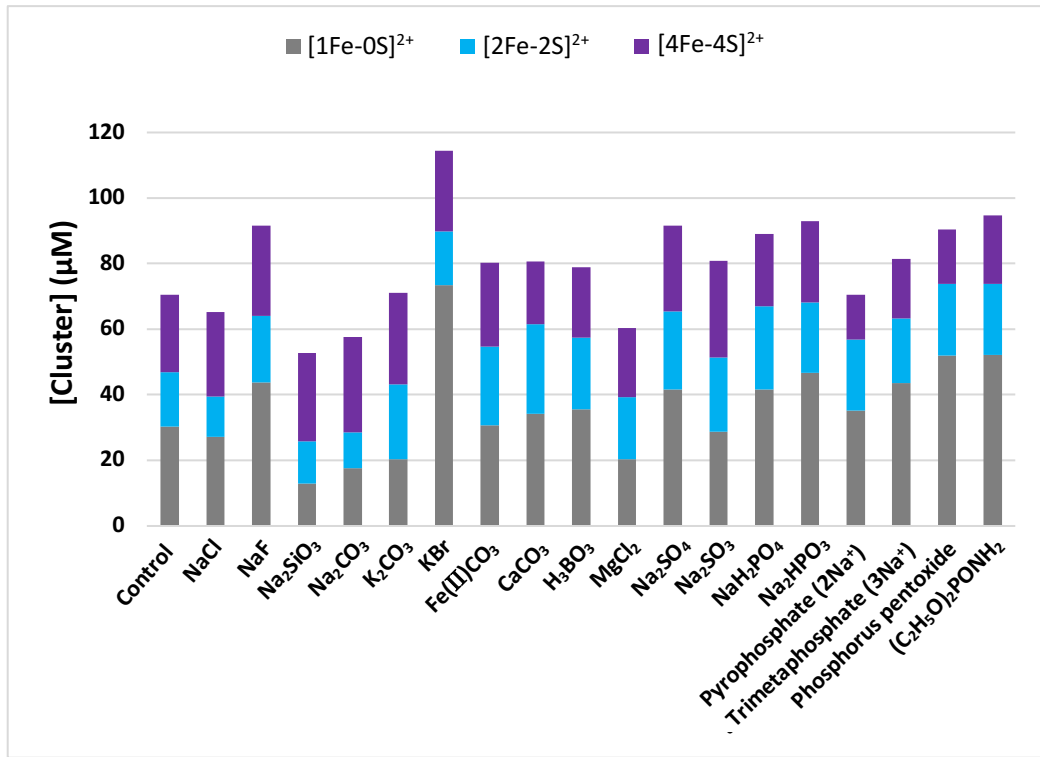
**Figure 2.3.** Formation of glutathione coordinated iron-sulfur clusters. The solution consisted of 0.185 mM Na<sub>2</sub>S, 0.5 mM FeCl<sub>3</sub>, and 40 mM glutathione. a) Monitored cluster formation by measuring absorbance at 310 nm for [1Fe-0S]<sup>2+</sup> cluster, 420 nm for [2Fe-2S]<sup>2+</sup> cluster, and 385 nm for [4Fe-4S]<sup>2+</sup> cluster. b) Monitored cluster formation with Fit-FeS.

### 2.2.3 Assessment of Glutathione Stabilized [2Fe-2S]<sup>2+</sup> Clusters

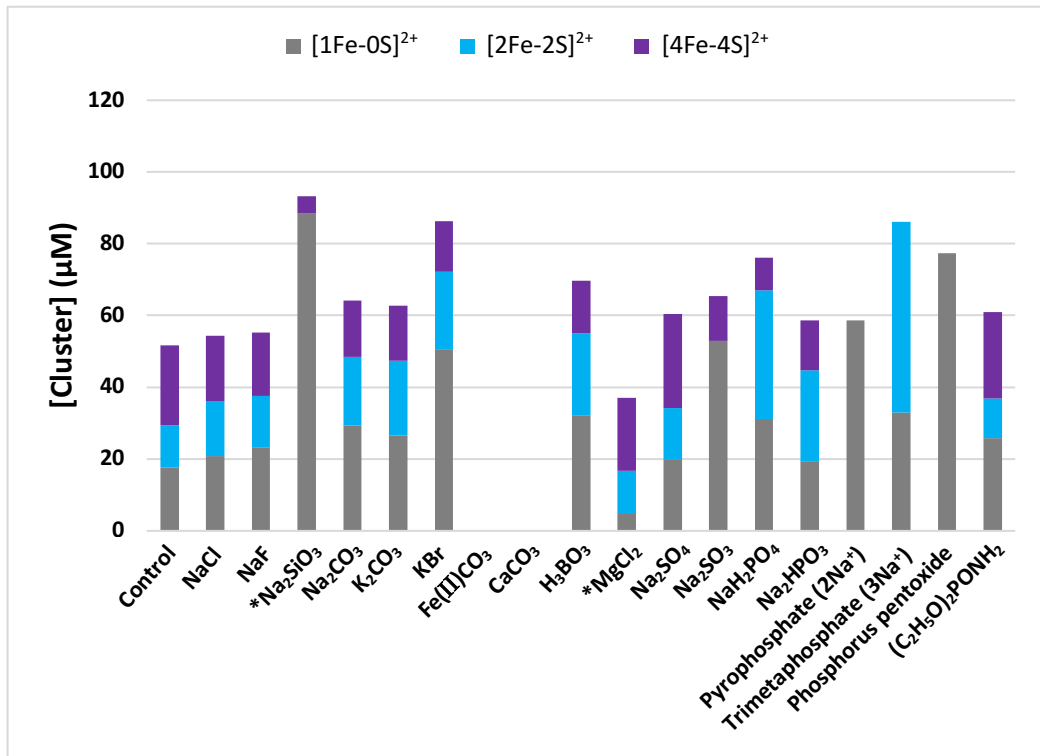
The formation of [2Fe-2S]<sup>2+</sup> clusters was evident from the characteristic dark red-brown colour change and the UV-vis spectra which displayed two prominent peaks at 420 nm and 450 nm. Fit-FeS was used to calculate final cluster concentrations under each chemical condition, and then these results were compared with control samples (same solution without any additives). This way, any chemical condition with a similar or higher [2Fe-2S]<sup>2+</sup> cluster concentration in the final solution may indicate its role in stabilizing or even contributing to the formation of [2Fe-2S]<sup>2+</sup> glutathione.

In general, the impact on the iron-sulfur clusters was more significant as the concentration of additives increased (Figure 2.4). For example, 100 μM additive generally had a very mild influence on the stability of glutathione coordinated [2Fe-2S]<sup>2+</sup> cluster, whereas addition of 100 mM and 0.5 M significantly weakened the formation of clusters in most of the cases.

a)



b)



c)

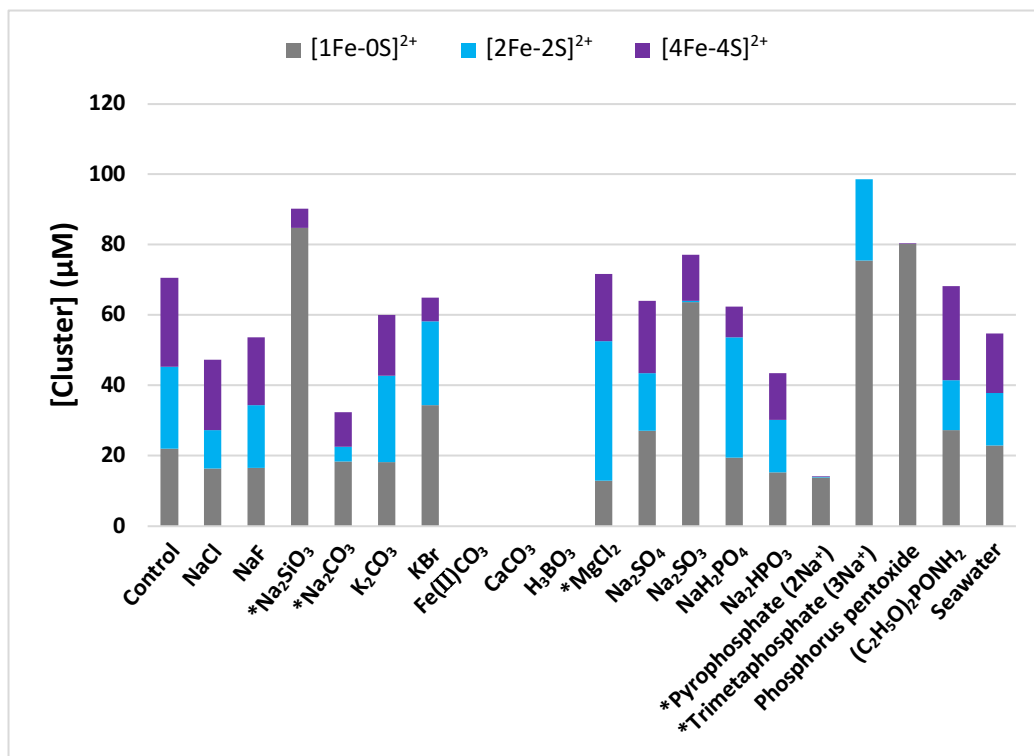


**Figure 2.4.** Cluster composition of glutathione coordinated iron-sulfur clusters after 110 min. The solution consisted of 0.185 mM Na<sub>2</sub>S, 0.5 mM FeCl<sub>3</sub>, and 40 mM glutathione, pH 8.7. All UV-vis spectra were monitored at 35 °C and fit with Fit-FeS. The final concentration of each cluster under a) 100 μM additive condition, b) 100 mM additive condition, and c) 0.5 M additive condition is shown. \*No pH adjustment due to precipitation.

According to previous work done by Cowan's group, they demonstrated that the formation of [2Fe-2S]<sup>2+</sup> glutathione may be facilitated by the tetrameric macrocyclic glutathione through a salt bridge interaction that serves as a pre-assembled iron-sulfur cluster chelate (Figure 2.5).<sup>42</sup> This intramolecular salt bridge was not only important for the formation of [2Fe-2S]<sup>2+</sup> clusters but also responsible for the stabilization of the clusters.<sup>44</sup> Combined with Debye-Hückel theory, the overall poor performance of high level additive conditions would be explained. The high ionic strength salt ions led to an increase in the activity coefficient,<sup>44</sup> and these ions were more likely to disrupt the salt bridge by counterion association,<sup>43</sup> thereby weakening macrocyclic stabilization and exposing the clusters more efficiently to the solvent water (Figure 2.6).

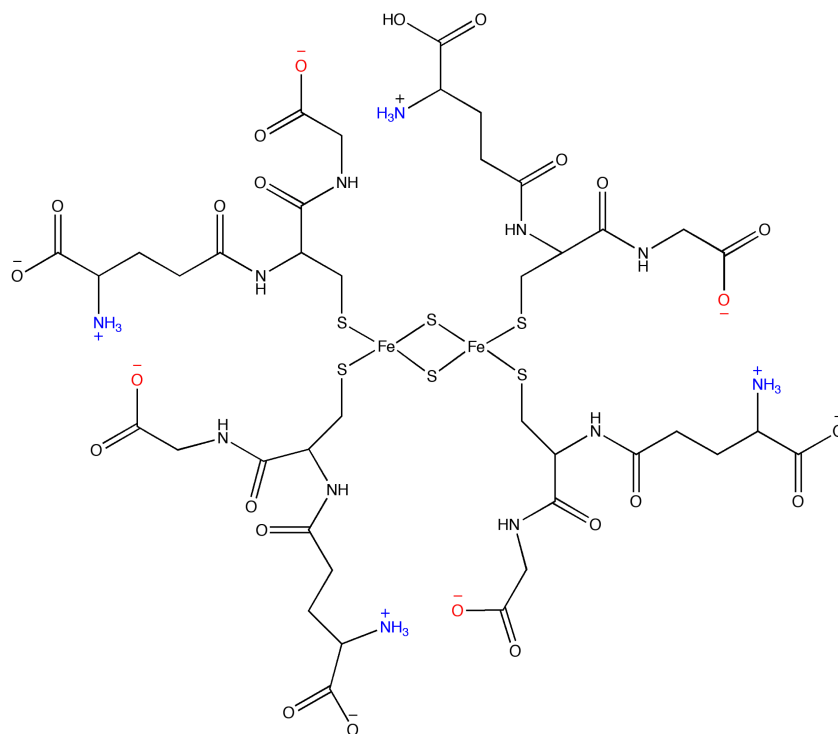


**Figure 2.5.** A two-dimensional representation of a glutathione coordinated  $[2\text{Fe}-2\text{S}]^{2+}$  cluster. (Adapted from Qi, W. et al.)<sup>42</sup>



**Figure 2.6.** A proposed  $[2\text{Fe}-2\text{S}]^{2+}$  glutathione hydrolysis mechanism via counterion mediated pathway. (Adapted from Li, J. et al.)<sup>43</sup>

However, there were a few observations that could not be explained by this theory. Increased concentrations of KBr and phosphate helped stabilize more  $[2\text{Fe}-2\text{S}]^{2+}$  clusters (Figure 2.7). One hypothesis invokes the Hofmeister effect.<sup>46</sup> High ionic strength salt ions would interact with water molecules, which decreased the chance that iron-sulfur clusters form hydrogen bonds with the surrounding water, thereby leading to more glutathione coordinated iron-sulfur clusters salting out of the solution. Since  $\text{H}_2\text{PO}_4^-$  ranked earlier than  $\text{Br}^-$  in the Hofmeister series (Figure 2.8),<sup>46</sup> glutathione was expected to form more  $[2\text{Fe}-2\text{S}]^{2+}$  clusters under phosphate conditions when compared to the same concentration of KBr. This trend was consistent with our findings. The better performance of  $[2\text{Fe}-2\text{S}]^{2+}$  clusters in the presence of high levels



of phosphate also links the idea of 0.1 M phosphate being thought to be present on the early Earth, as concentrated phosphate is required in prebiotic syntheses to overcome the low reactivity of phosphate with organics in water.<sup>37</sup> Furthermore, NaF and NaCl stabilized similar amounts of clusters since they were at a close position in the Hofmeister series.

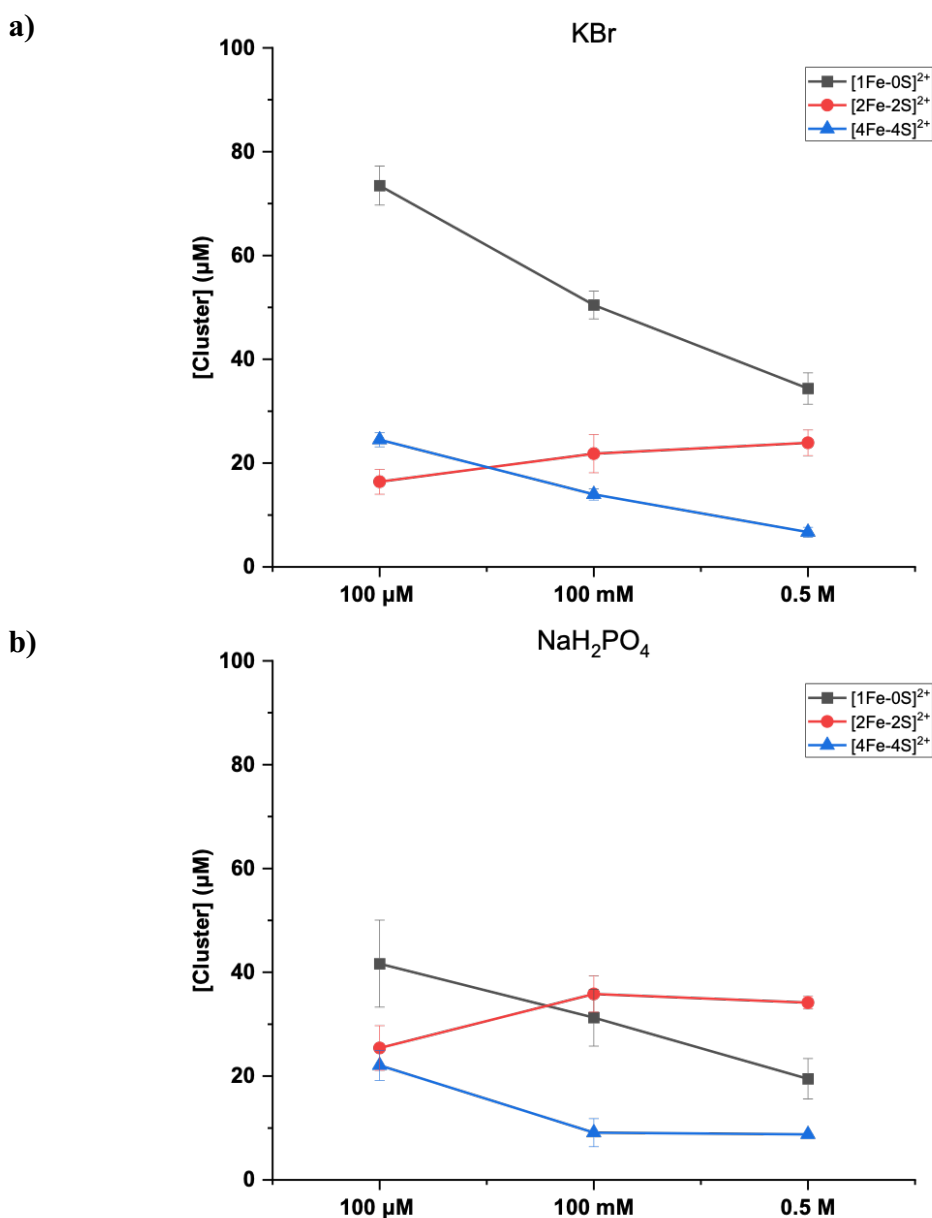


**Figure 2.7.** Cluster composition of glutathione coordinated iron-sulfur clusters under different additive concentrations. The solution consisted of 0.185 mM Na<sub>2</sub>S, 0.5 mM FeCl<sub>3</sub>, 40 mM glutathione, a) KBr and b) NaH<sub>2</sub>PO<sub>4</sub>, pH 8.7. All UV-vis spectra were monitored at 35 °C and fit with Fit-FeS.

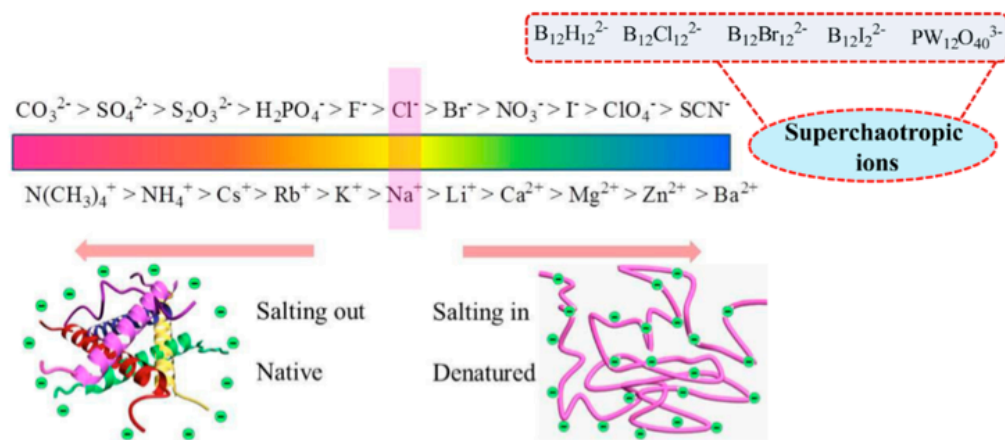


**Figure 2.8.** Hofmeister series. Members have better ability to stabilize proteins (left) or to denature proteins (right). (Adapted from Kang, B. et al.)<sup>46</sup>

Notably, pyrophosphate and phosphorous pentoxide were lethal to  $[2\text{Fe-2S}]^{2+}$  clusters at 100 mM and 0.5 M. These two species may act as better chelating ligands to bind with iron and thus destroy the structure of the iron-sulfur cluster. Conversely, trimetaphosphate with more bulk structure was hard to participate into clusters. The amine group from diethyl phosphoramidate could form hydrogen bonds with thiolate ligand or sulfide, which might weaken the Fe-S bond, but the overall cluster structure would not be affected much. Under modern seawater condition, the  $[2\text{Fe-2S}]^{2+}$  cluster had very minor impact. This is reasonable, as modern seawater consisted mainly millimolar levels of  $\text{Mg}^{2+}$  and  $\text{SO}_4^{2-}$  and molar levels of  $\text{Cl}^-$ , which all helped to stabilize  $[2\text{Fe-2S}]^{2+}$  clusters in individual chemical conditions.

#### 2.2.4 Assessment of N-acetyl-L-Cysteine Methyl Ester Stabilized $[4\text{Fe-4S}]^{2+}$ Cluster

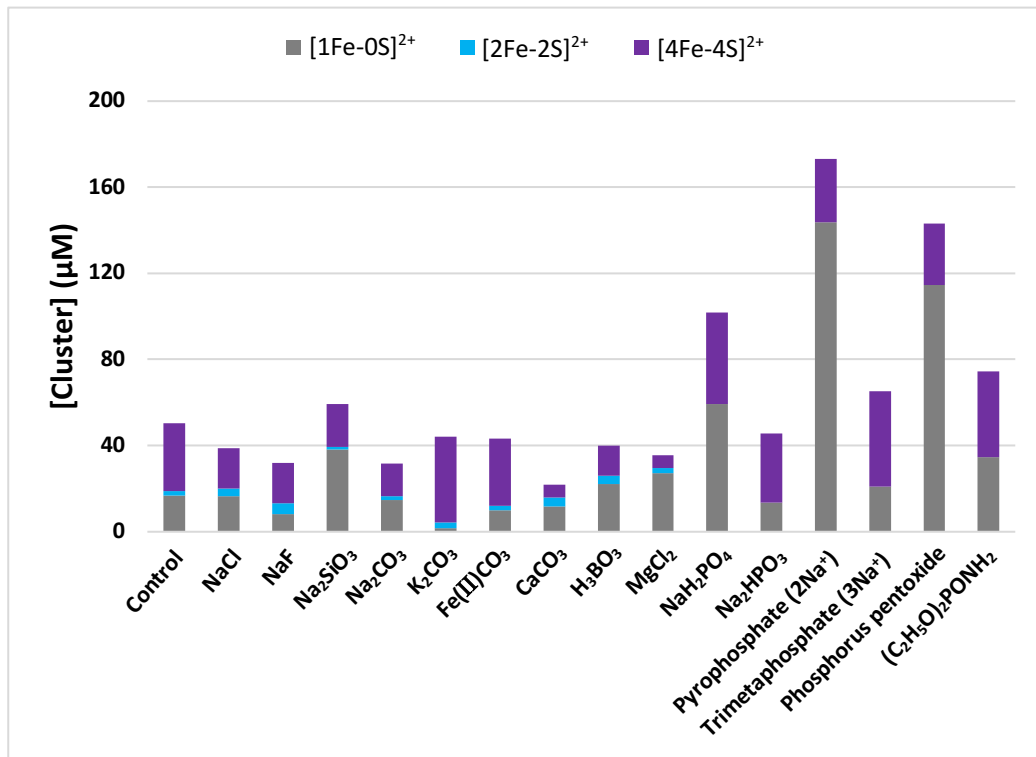
A brown colour change was observed in the formation of Ac-Cys-OME coordinated  $[4\text{Fe-4S}]^{2+}$  clusters, and a broad peak around 400–420 nm was shown by UV-vis spectroscopy. The method to assess the stability of  $[4\text{Fe-4S}]^{2+}$  Ac-Cys-OME was the same as for  $[2\text{Fe-2S}]^{2+}$  glutathione.

Notably, Ac-Cys-OME coordinated  $[2\text{Fe-2S}]^{2+}$  clusters were unstable, regardless of surrounding environments (Figure 2.9). Different from glutathione, Ac-Cys-OME has both carboxyl ester and amine acetylation modifications (Table A.1). We suggested that Ac-Cys-OME was less likely to pre-form a stable binding pocket for a

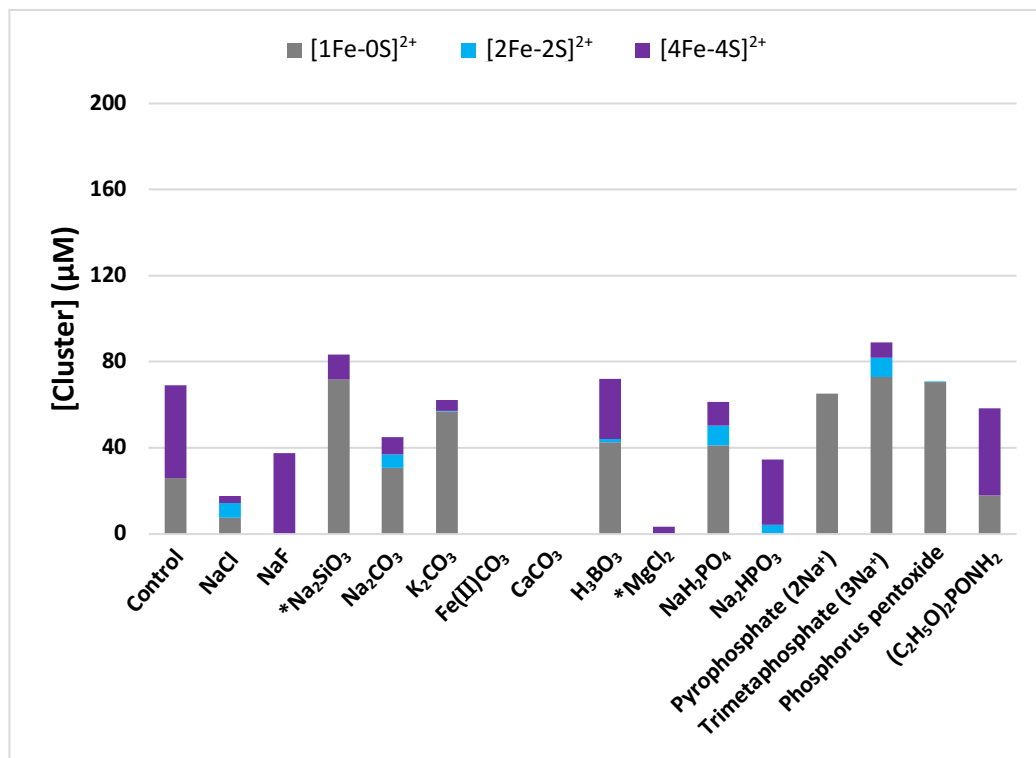
$[2\text{Fe-2S}]^{2+}$  cluster core via salt bridge interaction, thereby, it increased the difficulty to form  $[2\text{Fe-2S}]^{2+}$  clusters and maintain these clusters in a stable structure in water. Water molecules could interact easily with  $[2\text{Fe-2S}]^{2+}$  Ac-Cys-OMe and then enhance the cluster degradation.

Ac-Cys-OMe stabilized  $[4\text{Fe-4S}]^{2+}$  clusters were more sensitive to the surrounding environment as compared to glutathione stabilized clusters. Under 100  $\mu\text{M}$  additive conditions, only P species can stabilize  $[4\text{Fe-4S}]^{2+}$  clusters, with the exception of  $\text{K}_2\text{CO}_3$  and  $\text{Fe(II)CO}_3$  (Figure 2.9). As the earliest member in the Hofmeister series,  $\text{CO}_3^{2-}$  was expected to stabilize iron-sulfur clusters. In contrast, the fact that  $\text{Ca}^{2+}$  and  $\text{Mg}^{2+}$  destabilized  $[4\text{Fe-4S}]^{2+}$  clusters the most also could be explained by the Hofmeister effect due to their very backward location in the series. The increase in additive concentration made  $[4\text{Fe-4S}]^{2+}$  clusters unstable and, in many cases, even destroyed these clusters. Furthermore, modern seawater conditions were not suited for the survival of the  $[4\text{Fe-4S}]^{2+}$  cluster because  $\text{Mg}^{2+}$  and  $\text{Cl}^-$  as main components of modern seawater destabilized  $[4\text{Fe-4S}]^{2+}$  Ac-Cys-OMe under individual additive conditions. The combination of both chemicals would make  $[4\text{Fe-4S}]^{2+}$  clusters even more fragile. Many P species interfered with iron-sulfur cluster structures due to chelate effects, and this effect became stronger as the concentration of P species increased. Diethyl phosphoramidate could form hydrogen bonds with a thiolate group of Ac-Cys-OMe or sulfide, which made the overall structure more rigid.

a)



b)



c)

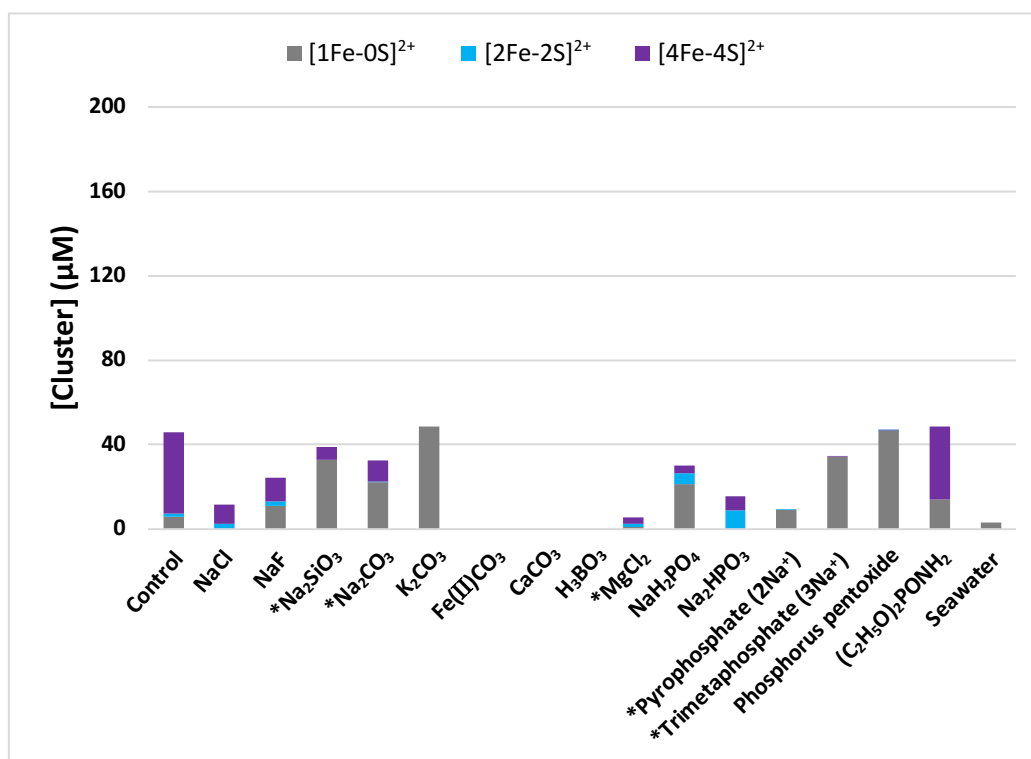


**Figure 2.9.** Cluster composition of N-acetyl-L-cysteine methyl ester coordinated iron-sulfur clusters after 7 h. The solution consisted of 0.8 mM Na<sub>2</sub>S, 0.4 mM FeCl<sub>3</sub>, and 5 mM Ac-Cys-OMe anaerobically, pH 8.7. All UV-vis spectra were monitored at 35°C and fit with Fit-FeS. The final concentration of each cluster under a) 100 μM additive condition, b) 100 mM additive condition, and c) 0.5 M additive condition is shown. \*No pH adjustment due to precipitation.

## 2.3 The Stability Test of Iron-Sulfur Peptides Under Mimicked Prebiotic Environments

### 2.3.1 Experimental Design

The actual environments of the early Earth would not consist of a single element. Indeed, a variety of environments often resulted from a mix of multiple species in different concentrations. Therefore, it is necessary to examine how iron-sulfur clusters behave under such mixed conditions to obtain more convincing results and get a better understanding on the plausibility of iron-sulfur peptides on the early Earth.

The pH stability test of glutathione coordinated iron-sulfur clusters was performed before selecting testable prebiotic plausible environments (Figure 2.10), and it suggested that both polynuclear and mononuclear clusters were more likely to survive at higher pH. Only [1Fe-0S]<sup>2+</sup> clusters existed at pH 5, while [2Fe-2S]<sup>2+</sup> and [4Fe-4S]<sup>2+</sup>

clusters were destroyed at this low pH. In the pH range that a cluster can survive at, four proposed potential environmental settings on the early Earth were selected (Table 2.3): alkaline lake condition at pH 10, lost city condition at pH 9, seawater condition at pH 6.5, and glacial brine condition at pH 5.

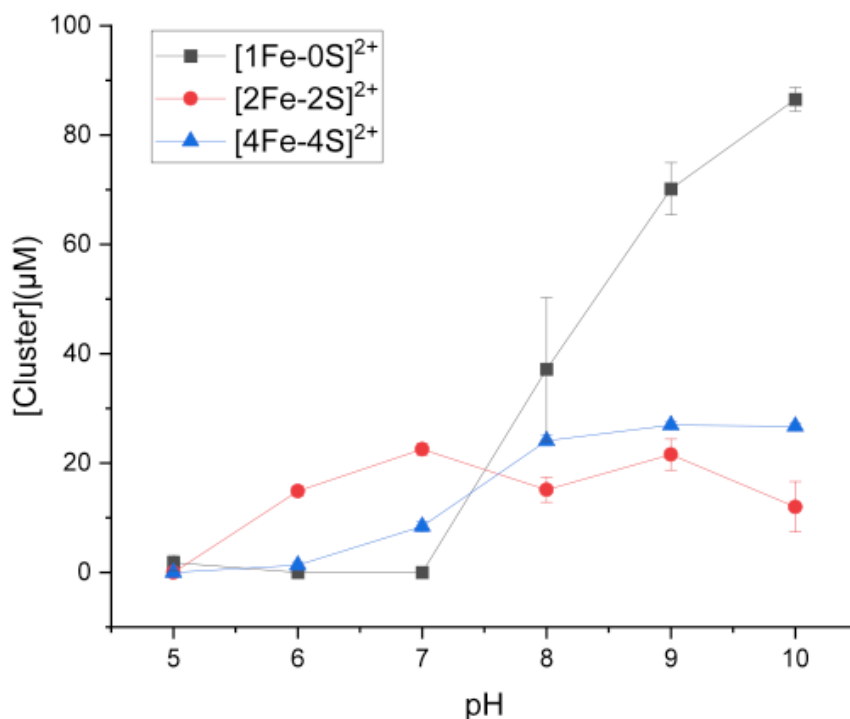


**Figure 2.10.** Cluster composition at pH 5–10. The solution consisted of 0.185 mM Na<sub>2</sub>S, 0.5 mM FeCl<sub>3</sub>, and 40 mM glutathione. The cluster concentrations at each pH were obtained by Fit-FeS after 2 h.

Furthermore, we picked seven peptides to coordinate with iron-sulfur clusters and tested their behaviour under those four given environmental settings (Table 2.5). Besides the five prebiotically plausible peptides,<sup>32</sup> we also chose two long peptides: Peptide PESCKAGACSTCAGPDLTCT derived from *Spirulina platensis* ferredoxin, which is often used as a [2Fe-2S]<sup>2+</sup> peptide model,<sup>47</sup> and peptide KLCEGGCIACGACGGW inspired by the *Peptococcus aerogenes* ferredoxin and often referred to as a [4Fe-4S]<sup>2+</sup> peptide model.<sup>48</sup> This way, different types of peptides would help us determine what are the minimum requirement (i.e., length of peptides or the sequence spacing between cysteines) for the cluster formation on the early Earth.

**Table 2.5.** List of Ligands Tested Under Prebiotic Plausible Environmental Conditions

Peptide sequence	Name
E <sub>γ</sub> CG	Glutathione
N-Acetyl-L-Cysteine Methyl Ester	Ac-Cys-OMe
GCG	-
GCGGCG	-
GCPLCG	-
PESCKAGACSTCAGPDLTCT	<i>Spirulina platensis</i> ferredoxin maquette (Sp FdM)
KLCEGGCIACGACGGW	<i>Peptococcus aerogenes</i> ferredoxin maquette (Pa FdM)

### 2.3.2 Assessment of Iron-Sulfur Peptides under Mimicked Prebiotic Environment

In most cases, a light-yellow colour appeared following the addition of Fe<sup>3+</sup> and HS<sup>-</sup> to the peptide solution at each simulated prebiotic environmental condition. As yellow is not a color typically indicative of either [2Fe-2S]<sup>2+</sup> or [4Fe-4S]<sup>2+</sup> clusters, polynuclear iron-sulfur clusters were not expected at these conditions.

To corroborate the findings from UV-vis spectroscopy, paramagnetic NMR was used. Iron-sulfur peptides frequently display shifted resonances of the protons of ligating cysteines and NH groups, which can be used to identify cluster type.<sup>26</sup> A peak around 100–300 ppm region often indicates the Cys H<sub>β</sub> resonances for [1Fe-0S]<sup>2+</sup> clusters, whereas Cys H<sub>β</sub> resonances are found more upfield in the cases of [2Fe-2S]<sup>2+</sup> and [4Fe-4S]<sup>2+</sup> clusters (Figure 2.11).

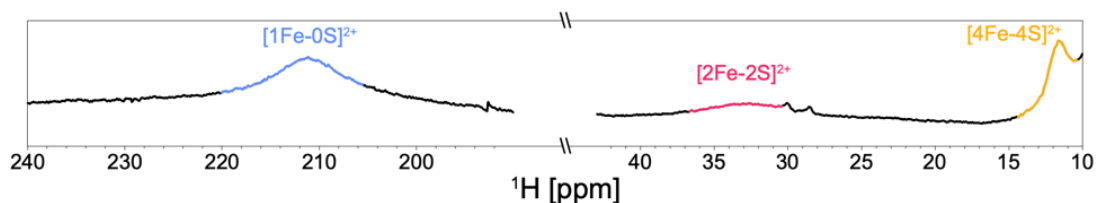
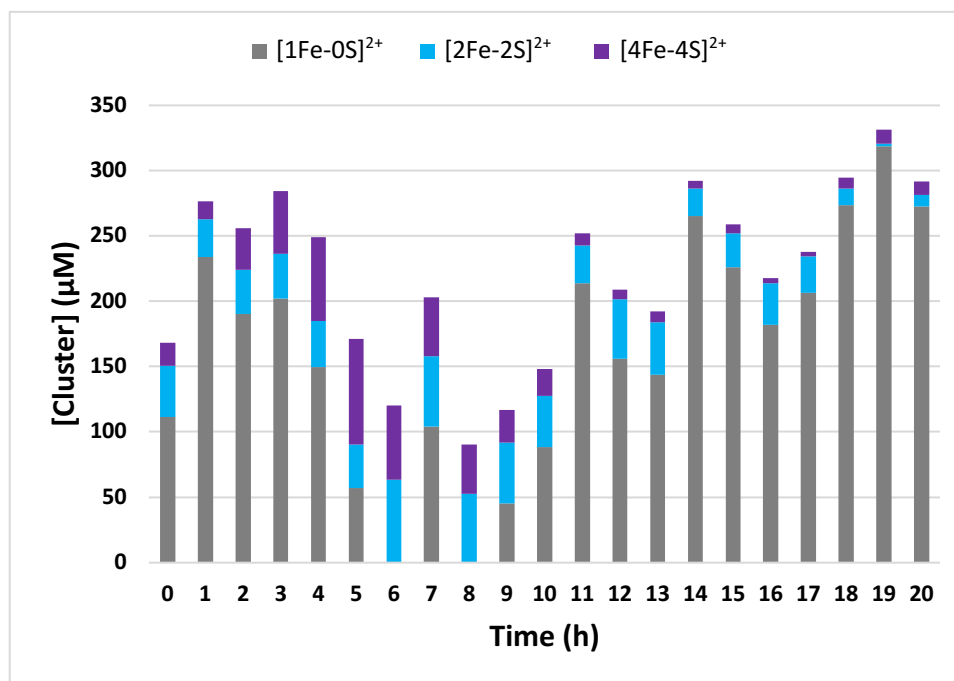


**Figure 2.11.** Paramagnetic  $^1\text{H}$  NMR spectra of glutathione stabilized iron-sulfur clusters. The resonances at 210 ppm (blue), 33 ppm (red), and 11.8 ppm (yellow) are indicative of  $[\text{1Fe-0S}]^{2+}$ ,  $[\text{2Fe-2S}]^{2+}$ ,  $[\text{4Fe-4S}]^{2+}$  clusters, respectively. (Adapted from Valer, L. et al.)<sup>26</sup>

All UV-vis spectra were analyzed by Fit-FeS, and each type of cluster concentration was calculated at every given time point. Then, corresponding paramagnetic NMR spectra under each condition were checked for verification. For example, the peptide GCGGCG under lost city conditions consisted of a high concentration of  $[\text{1Fe-0S}]^{2+}$  clusters with a small amount of  $[\text{2Fe-2S}]^{2+}$  and  $[\text{4Fe-4S}]^{2+}$  clusters at the beginning, and  $[\text{1Fe-0S}]^{2+}$  clusters still remained after 20 h. This finding is consistent with what we observed by paramagnetic NMR (Figure 2.12). The peak near 220 ppm corresponded to Cys  $\text{H}_\beta$  resonances of the  $[\text{1Fe-0S}]^{2+}$  cluster. Since Cys  $\text{H}_\beta$  resonances of both  $[\text{2Fe-2S}]^{2+}$  and  $[\text{4Fe-4S}]^{2+}$  clusters and Cys  $\text{H}_\beta$  resonances of  $[\text{1Fe-0S}]^{2+}$  clusters all appeared around the 10–30 ppm region, the peaks detected around this region were hard to assign. Nevertheless, the presence of  $[\text{1Fe-0S}]^{2+}$  clusters were observed by both UV-vis spectroscopy and paramagnetic NMR since in such slightly alkaline pH, more thiol containing molecules were likely to deprotonate and allowed more easily coordination with  $\text{Fe}^{3+}$  to form  $[\text{1Fe-0S}]^{2+}$  clusters.



a)



b)

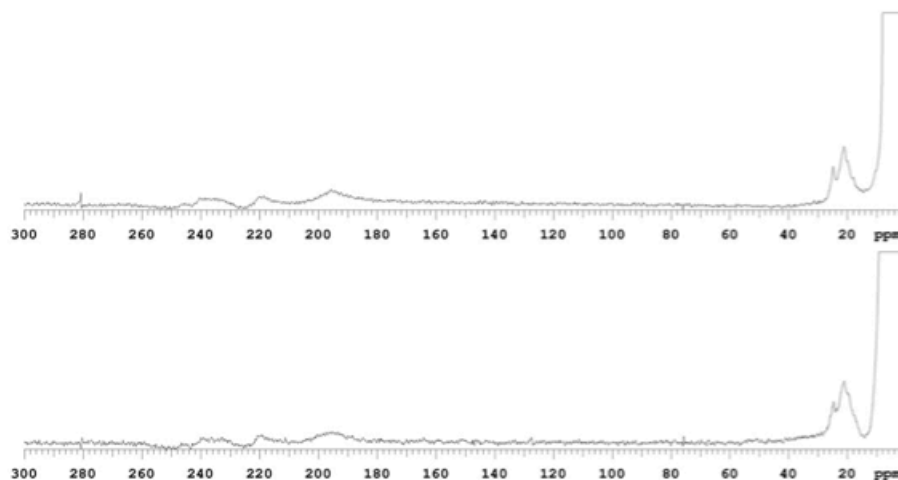
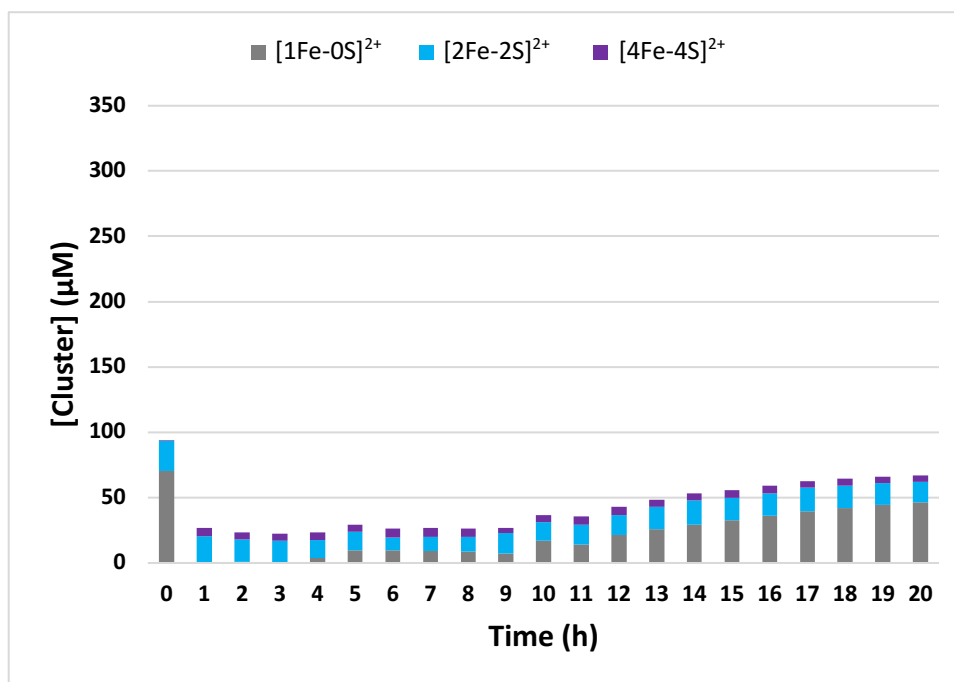


**Figure 2.12.** Composition of peptide GCGGCG coordinated iron-sulfur clusters under lost city condition over time. a) The solution consisted of 0.185 mM Na<sub>2</sub>S, 0.5 mM FeCl<sub>3</sub>, and 10 mM GCGGCG, pH 9. The cluster concentrations at each given time point were obtained by Fit-FeS. b) The solution consisted of 0.75 mM Na<sub>2</sub>S, 1.87 mM FeCl<sub>3</sub>, and 40 mM GCGGCG, pD 9. The clusters were detected by paramagnetic <sup>1</sup>H NMR at 0 h (top) and 20 h (bottom).

In the seawater scenario, glutathione coordinated iron-sulfur clusters showed similar trends as GCGGCG stabilized iron-sulfur clusters under lost city conditions (Figure 2.13). The signal detected by paramagnetic NMR showed a peak at 210 ppm

that indicates the presence of  $[1\text{Fe-0S}]^{2+}$  clusters and a peak at 35 ppm proposed as the Cys  $\text{H}_\beta$  resonances of  $[2\text{Fe-2S}]^{2+}$  clusters. Moreover, the NMR spectra also captured the decrease of  $[2\text{Fe-2S}]^{2+}$  clusters over time, as the signal at 35 ppm was not able to distinguish from noise after 20 h.

a)



b)

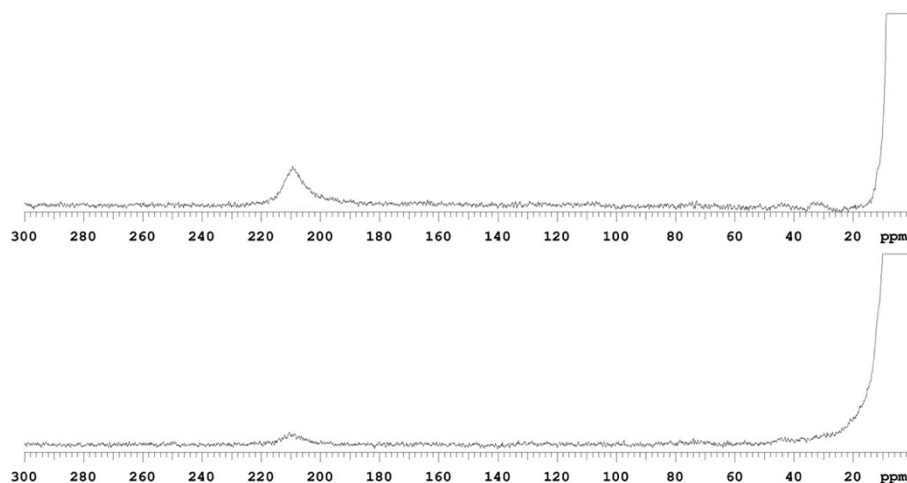
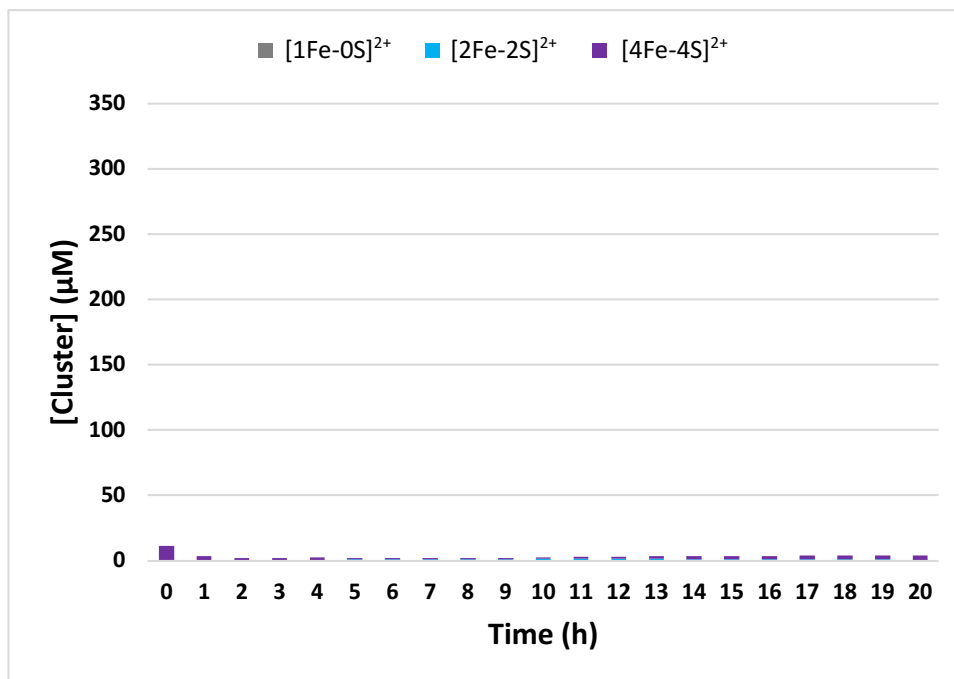


**Figure 2.13.** Composition of glutathione coordinated iron-sulfur clusters under seawater condition over time. a) The solution consisted of 0.185 mM Na<sub>2</sub>S, 0.5 mM FeCl<sub>3</sub>, and 40 mM glutathione, pH 6.5. The cluster concentrations at each given time point were obtained by Fit-FeS. b) The solution consisted of 0.75 mM Na<sub>2</sub>S, 1.87 mM FeCl<sub>3</sub>, and 150 mM glutathione, pD 6.5. The clusters were detected by paramagnetic <sup>1</sup>H NMR at 0 h (top) and 20 h (bottom).

In fact, the deficiency of GCG coordinated clusters detected under glacial brine condition also was suggested by both UV-vis spectroscopy and paramagnetic NMR (Figure 2.14). The cluster composition over time showed zero concentrations of every type of clusters by Fit-FeS. As expected, there were no signals detected in the full spectrum region as well.

a)



b)

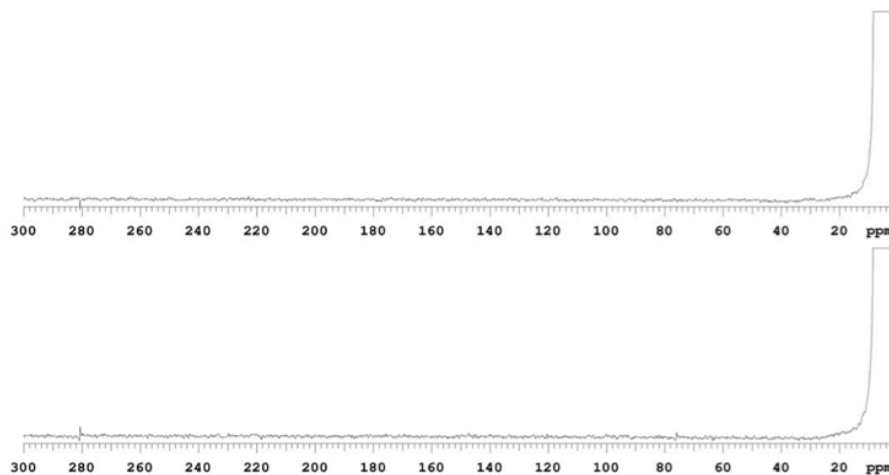


**Figure 2.14.** Composition of peptide GCG coordinated iron-sulfur clusters under glacial brine condition over time. a) The solution consisted of 0.185 mM Na<sub>2</sub>S, 0.5 mM FeCl<sub>3</sub>, and 10 mM GCG, pH 5. The cluster concentrations at each given time point were obtained by Fit-FeS. b) The solution consisted of 0.75 mM Na<sub>2</sub>S, 1.87 mM FeCl<sub>3</sub>, and 150 mM GCG, pD 5. The clusters were detected by paramagnetic <sup>1</sup>H NMR at 0 h (top) and 20 h (bottom).

The final cluster concentrations of each peptide under the same prebiotically plausible conditions are summarized in one graph for analysis purpose (Figure 2.15). In general, all peptides were more stable at conditions with higher pH, except Sp FdM. This long peptide that characterized for  $[2\text{Fe-2S}]^{2+}$  clusters behaved the same under all conditions. Almost no clusters can survive under glacial brine conditions with pH 5, regardless of which kind of peptide is used. Any thiol containing ligands were difficult to deprotonate in order to contribute in the synthesis of iron-sulfur clusters under such low pH. Glutathione coordinated  $[2\text{Fe-2S}]^{2+}$  clusters were more likely to survive under alkaline lake, lost city, and seawater conditions. Interestingly, these  $[2\text{Fe-2S}]^{2+}$  glutathione clusters exhibited a similar stability as GCPLCG coordinated  $[2\text{Fe-2S}]^{2+}$  clusters under alkaline lake and seawater conditions. GCG coordinated  $[2\text{Fe-2S}]^{2+}$  clusters exhibited a similar behaviour with its duplicated form, GCGGCG. They both showed overall poor survivability under four given environmental settings. However,  $[2\text{Fe-2S}]^{2+}$  GCGGCG did a relatively better job when compared with GCG stabilized  $[2\text{Fe-2S}]^{2+}$  clusters. This finding was consistent with our previous studies that duplication of tripeptide increases the overall stability of iron-sulfur clusters.<sup>11</sup> Ac-Cys-OMe was not able to stabilize  $[2\text{Fe-2S}]^{2+}$ , regardless of what environmental condition they were at. Even though the ratio of  $\text{HS}^-$  and  $\text{Fe}^{3+}$  used in this case was responsible for the formation of  $[2\text{Fe-2S}]^{2+}$  clusters, Ac-Cys-OMe still intends to form  $[4\text{Fe-4S}]^{2+}$  clusters. This observation also suggested that Ac-Cys-OMe was more predisposed to the formation of  $[4\text{Fe-4S}]^{2+}$  clusters.

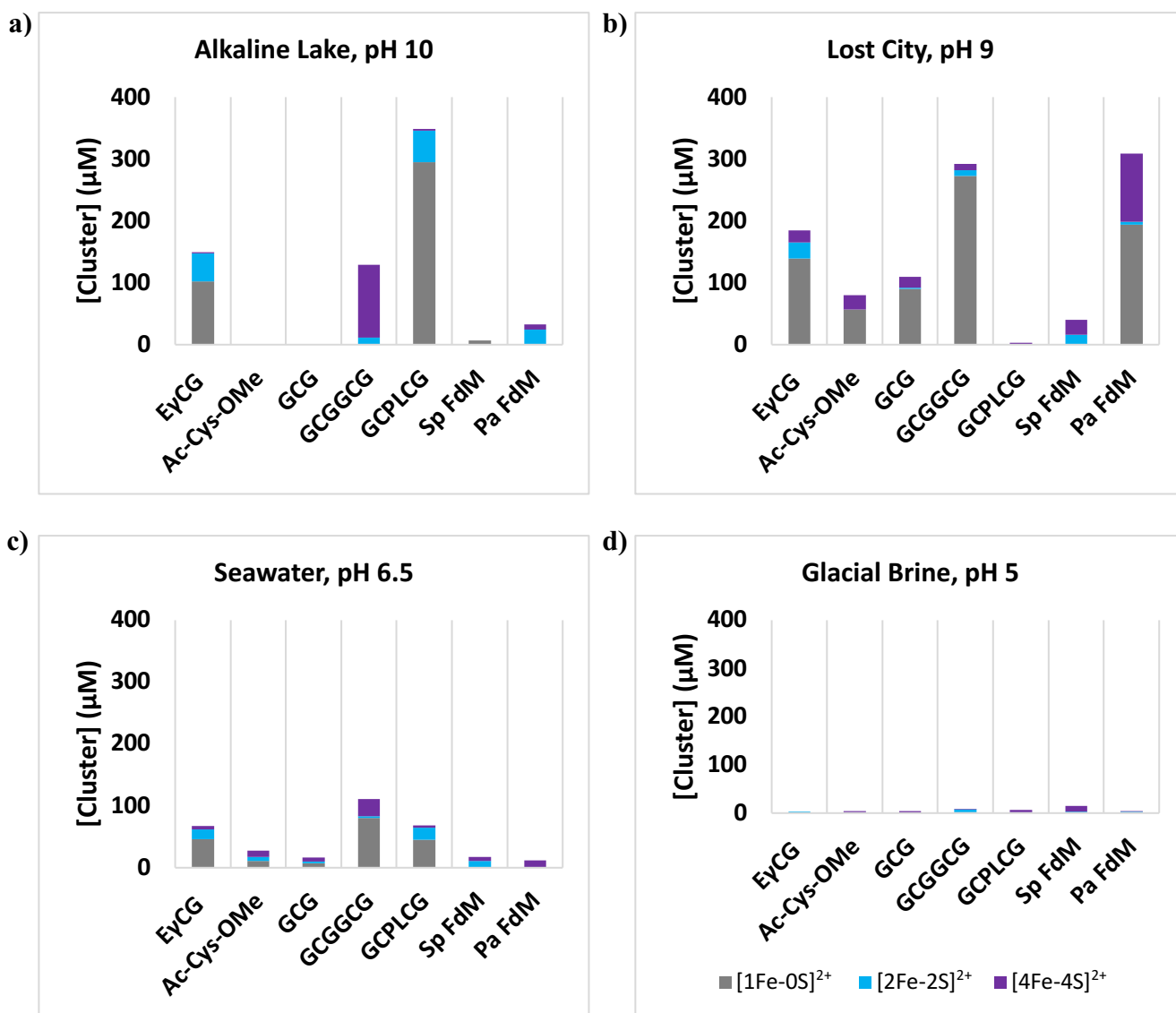


**Figure 2.15.** Cluster composition of iron-sulfur peptides after 20 h. All UV-vis spectra were monitored at 35 °C and fit with Fit-FeS. The final concentration of each cluster under a) alkaline lake condition, b) lost city condition, c) seawater condition, and d) glacial brine is shown. \*No pH adjustment due to precipitation.

While glutathione coordinated [2Fe-2S]<sup>2+</sup> clusters were quite compatible with pH between 10 and 6.5, Pa FdM coordinated [4Fe-4S]<sup>2+</sup> clusters were more sensitive to changes in pH. This [4Fe-4S]<sup>2+</sup> peptide only exhibited better performance under lost city condition at pH 9, which was close to the typical pH required for the synthesis of iron-sulfur clusters. Moreover, all iron-sulfur peptides, especially [1Fe-0S]<sup>2+</sup> peptides, tended to be more stable under this slightly alkaline pH. More free thiolates were deprotonated and ready to react with Fe<sup>3+</sup> to form iron-sulfur clusters.

Besides the influence of pH on the performance of iron-sulfur peptides, the concentrations of different additives also played a crucial role. Molar levels of  $\text{PO}_4^{3-}$ ,  $\text{Cl}^-$ ,  $\text{K}^+$ , and  $\text{Na}^+$  were all responsible for the stabilization of  $[\text{2Fe-2S}]^{2+}$  glutathione under individual additive conditions. The combination of these additives in an alkaline lake scenario stabilized glutathione coordinated  $[\text{2Fe-2S}]^{2+}$  clusters the most. Lost city conditions were expected to have more  $[\text{2Fe-2S}]^{2+}$  glutathione survive than alkaline lake conditions since this condition is closer in pH to the typical conditions used for the synthesis of iron-sulfur clusters. However, glutathione stabilized  $[\text{2Fe-2S}]^{2+}$  clusters did not behave as predicted. This may be explained by the much lower concentrations of  $\text{PO}_4^{3-}$ ,  $\text{Cl}^-$ ,  $\text{K}^+$ , and  $\text{Na}^+$  under lost city condition. These early members of the Hofmeister series with lower ionic strength would be less competitive for the interaction with surrounding water molecules and caused more interactions between the cluster and solvent. Therefore, less  $[\text{2Fe-2S}]^{2+}$  glutathione would be stabilized when compared with alkaline lake condition. As a result, in scenarios of seawater and glacial brine where both pH and Hofmeister effects took place, all iron-sulfur peptides were more difficult to survive.

## CHAPTER 3

### Conclusion and Future Work

In general, glutathione coordinated  $[2\text{Fe-2S}]^{2+}$  clusters could be stabilized by  $\text{K}_2\text{CO}_3$ ,  $\text{KBr}$ ,  $\text{MgCl}_2$ , and  $\text{NaH}_2\text{PO}_4$  with up to 0.5 M concentration. Notably, these additives were the major components of one of the proposed prebiotic conditions, namely the alkaline lake conditions. While iron-sulfur clusters coordinated to the tripeptide glutathione were the most stable, Ac-Cys-OMe stabilized iron-sulfur clusters were more sensitive to the surrounding environments. Only diethyl phosphoramidate from 100  $\mu\text{M}$  to 0.5 M was capable of stabilizing the  $[4\text{Fe-4S}]^{2+}$  coordinated to Ac-Cys-OMe.

Among the seven tested peptides, glutathione stabilized  $[2\text{Fe-2S}]^{2+}$  clusters were more compatible to most of the environmental settings. The  $[2\text{Fe-2S}]^{2+}$  GCPLCG was the second most stable iron-sulfur clusters under these prebiotic plausible environments. Ac-Cys-OMe and GCG coordinated iron-sulfur clusters were only able to survive under lost city conditions. Clearly, environmental conditions were important for both peptides stabilized iron-sulfur clusters. The hexapeptide GCGGCG synthesized  $[2\text{Fe-2S}]^{2+}$  clusters were more favoured at high pH and high salt concentrations. The long peptide PESCKAGACSTCAGPDLTCT, which was used to characterize  $[2\text{Fe-2S}]^{2+}$  clusters were not suitable for all four proposed prebiotic environments. The other long peptide KLCEGGCIACGACGGW acted as  $[4\text{Fe-4S}]^{2+}$  cluster model was incompatible with most of the environmental settings as well.

The overall poor survivability of the two longer peptides suggests that increased stability either requires more complex three-dimensional folds or that the spacing investigated here were far from ideal. Therefore, the transition from short, prebiotically plausible iron-sulfur peptides to longer stable iron-sulfur peptides would have either required unidentified conditions or would have emerged later when machinery was available to give rise to longer peptide scaffolds. Nevertheless, the peptides that would have arisen from a single duplication event of a tripeptide, i.e., a hexapeptide, do coordinate more stable iron-sulfur clusters. This suggests that we simply have not



properly sampled sequence space. If so, then modern iron-sulfur proteins could have emerged from short peptides that coordinated iron-sulfur clusters from the beginning, thereby facilitated the emergence of primordial metabolic pathways that then gave rise to the life.

The future step of this project would be to further expand the peptide library in terms of their sequences and lengths. This way we could give a deeper understanding of the limitations for the formation of iron-sulfur peptides on the early Earth. However, iron-sulfur proteins are known to be fundamental to several physiology processes ranging from photosynthesis, central metabolism, nitrogen fixation to protein and DNA synthesis. Therefore, using the same environmental settings and testing a wide variety of biologically relevant reactions of these iron-sulfur peptides embedded within the protocells could be necessary. Together give a comprehensive picture of what kinds of iron-sulfur peptides are plausible on the prebiotic Earth and play a role in the origin and the evolution of life-like systems.

# CHAPTER 4

## Experimental

### 4.1 Materials

All reagents were from Sigma Aldrich or BOC science and used without any further purification. All peptides were synthesized according to standard solid phase peptide synthesis procedures or purchased from LifeTein LLC. Schlenk lines and Schlenk glassware were used under a controlled nitrogen atmosphere to obtain the procedures for the synthesis. Stock solutions were prepared with deoxygenated water that was made by distilling deionized ultrapure water (Synergy UV Water Purification System) under a nitrogen flow. Stock solutions were stored in anaerobically sealed glass vials with a rubber septum until further use. Hamilton gastight syringes were used to inject reagents or solutions into sealed anaerobic quartz cuvettes for UV-vis detection, and 5 mm NMR tubes were used for paramagnetic  $^1\text{H}$  NMR. Parafilm was wrapped around the caps of the cuvettes or NMR tubes. pH was measured by an Orion Star A211 pH meter and ATC Probes from Thermo Scientific. Adjustment of the pH was done with 5 mM NaOH and 3 mM HCl.

### 4.2 Solid Phase Peptide Synthesis

All peptides were synthesized according standard Fmoc-protected SPPS procedures. N,N-dimethyl formamide (DMF) was used as the solvent and *p*-alkoxybenzyl alcohol resin (Wang resin) was used as the starting polymeric support. Fmoc-protected amino acids were used as building blocks. Normally, the peptide chain was elongated by sequential Fmoc deprotection of the residue anchored to the resin and Fmoc-AA-OH coupling. A 20% (v/v) solution of piperidine in DMF was used to wash the mixture for Fmoc deprotection. Under each coupling, an excess (Fmoc-AA-OH: anchored AA, 3:1) of the Fmoc- $\alpha$ -amino-acid derivatives was added to the resin. Fmoc-Cys(Trt)OH was activated with a N,N'-diisopropylcarbodiimide (DIC)/hydroxyl-benzotriazole (HOBt) mixture, whereas other Fmoc-protected amino acids were activated with a mixture of HOBt, N,N,N',N'-tetramethyl-O-(benzotriazole-1-yl)uranium tetrafluoroborate (TBTU),

and N,N-diisopropylethyl amine (DIPEA). At the end of coupling, the polymers were cleaved from the resin and deprotected by the treatment with a solution of trifluoroacetic acid (TFA), water (H<sub>2</sub>O), triisopropyl silane (TIS), and 1,2-ethanedithiol (EDT) for 2 h. The volume was reduced under a nitrogen atmosphere to avoid cysteinyl thiol oxidation, and the product was precipitated out with a cold solution of diethyl ether/petroleum ether (30:70 (v/v)), followed by centrifugation for 20 min at 8000 x G and -5°C. The wash cycle was repeated four times and finally dried under inert atmosphere.

### **4.3 [2Fe-2S]<sup>2+</sup> Cluster Synthesis**

Peptide solutions were prepared in a glass vial under anaerobic conditions and the pH was adjusted to the desired value. Ferric chloride hexahydrate (FeCl<sub>3</sub>·6H<sub>2</sub>O, final concentration 0.5 mM) and sodium sulfide nonahydrate (Na<sub>2</sub>S·9H<sub>2</sub>O, final concentration 0.185 mM) were added to synthesize the [2Fe-2S]<sup>2+</sup> clusters for UV-vis detection, whereas 0.75 mM Na<sub>2</sub>S·9H<sub>2</sub>O and 1.87 mM FeCl<sub>3</sub>·6H<sub>2</sub>O were used in paramagnetic <sup>1</sup>H NMR measurements.

### **4.4 [4Fe-4S]<sup>2+</sup> Cluster Synthesis**

Peptide solutions were prepared in a glass vial under anaerobic conditions and the pH was adjusted to the desired value. Ferric chloride hexahydrate (FeCl<sub>3</sub>·6H<sub>2</sub>O, final concentration 0.8 mM), sodium sulfide nonahydrate (Na<sub>2</sub>S·9H<sub>2</sub>O, final concentration 0.4 mM), and 2% (v/v) β-mercaptoethanol were added to synthesize the [4Fe-4S]<sup>2+</sup> clusters for both UV-vis and paramagnetic <sup>1</sup>H NMR measurements.

### **4.5 UV-Visible Absorption Spectroscopy**

UV-vis absorption spectra were collected using an Agilent Cary 3500 UV-Vis spectrometer. Parameters were set as follows: integration = 0.02 s, interval = 1 nm. Samples were prepared under anaerobic condition and transferred to sealed quartz cuvettes (path length = 0.5 cm).

## 4.6 Fit-FeS

The spectra library used for all iron-sulfur peptides except glutathione contains [1Fe-0S]<sup>2+</sup> GCPLC, [2Fe-2S]<sup>2+</sup> PESCKAGACSTCAGPDLTCT and [4Fe-4S]<sup>2+</sup> KLCEGGCIACGACGGW. The [2Fe-2S]<sup>2+</sup> peptide reference was replaced by ferredoxin in the case of iron-sulfur glutathione. Additionally, iron-sulfide species were generated by using the same materials required for iron-sulfur cluster synthesis without peptides and were included in the reference spectra as well. Models were generated as a linear combination of the reference spectra. The method of least squares was employed to match the model to a sample spectrum. The concentration of each species after spectra fitting was calculated by the Beer–Lambert law by input of path length and extinction coefficient. By default, the extinction coefficients were 7400 M<sup>-1</sup> cm<sup>-1</sup> at 310 nm for [1Fe-0S]<sup>2+</sup> clusters, 6600 M<sup>-1</sup> cm<sup>-1</sup> at 420 nm for [2Fe-2S]<sup>2+</sup> clusters, and 16100 M<sup>-1</sup> cm<sup>-1</sup> at 385 nm for [4Fe-4S]<sup>2+</sup> clusters.

## 4.7 Paramagnetic <sup>1</sup>H NMR

An Agilent/Varian VNMRS four-channel 600 MHz spectrometer equipped with an autoxid HCN probe was used to acquire NMR spectra at room temperature. All samples contained 100% D<sub>2</sub>O. One dimensional <sup>1</sup>H NMR spectra optimized for paramagnetic samples were acquired with a water presaturation pulse sequence. Acquisition parameters were 1024 scans, 2 μs pulse width, 0.1 s acquisition time, 0.25 s relaxation delay, 36.4 μs ddr time, and 500000 Hz sweep width.

## 4.8 Statistics and Reproducibility

All UV-vis analyses were performed in triplicate, and individual data points in all summary graphs represent the average of three measurements. Standard errors of mean (SEM) were calculated as well.

# References

1. Pross, A. What is Life? How Chemistry Becomes Biology. Oxford University Press: Oxford, 2012.
2. Brack, A. The Molecular Origins of Life: Assembling Pieces of the Puzzle. Cambridge University Press: Cambridge, 1998.
3. Seckbach, J. Origins. Genesis, Evolution and Diversity of Life. Kluwer Academic Publishers: Dordrecht, 2004.
4. Lazcano, A. Historical Development of Origins Research. *Cold Spring Harb Perspect Biol* **2010**, 1-14.
5. Oparin, A. I. The Origins of Life. Dover Publications: New York, 1953.
6. Miller, S. L. A Production of Amino Acid under Possible Primitive Earth Condition. *Science* **1953**, *117*, 528-529.
7. Gilbert, W. Origin of life: The RNA World. *Nature* **1986**, *319*, 618-618.
8. Wächtershäuser, G. Pyrite Formation, the First Energy Source for Life: a hypothesis. *Syst. Appl. Microbiol* **1988**, *10*, 207-210.
9. Sergé, D., Ben-Eli, D., Deamer, D. W. Lancet, D. The Lipid World. *Orig Life Evol Bioph* **2001**, *31*, 119-145.
10. Oschmann, W., Grasshof, M., Gudo, M. The Early Evolution of the Planet Earth and the Origins of Life. *Senckenbergiana lethaea* **2002**, *82*, 284-294.
11. Williams, R. J. P., and Fraústo da Silva, J. J. R. The Chemistry of Evolution: the Development of Our Ecosystem. Elsevier B. V.: Netherland, 2006.
12. Anbar, A. D. Elements and Evolution. *Science* **2008**, *322*, 1481-1483.
13. Gray, H. B. Biological Inorganic Chemistry at the Beginning of 21st Century. *Proc Natl Acad Sci USA* **2003**, *100*, 3563-3568.
14. Bertini, I., Gray, H. B., Lippard, S. J., Valentine, J. S. Bioinorganic Chemistry. University Science Books: USA, 1994.
15. Sigel, A., Sigel, H., Sigel, R. K. O. The Alkali Metal Ions: Their Roles for Life. Springer Publishing: Switzerland, 2016.
16. Fenton, D. E. Biocoordination Chemistry. Oxford University Press: Oxford, 1995.
17. Bhattacharya, P. K., and Samnani, P. B. Metal Ions in Biochemistry. CRC Press: Florida, 2021.
18. Gomes, C. M., and Wittung-Stafshede, P. Protein Folding and Metal Ions: Mechanisms, Biology and Disease. CRC Press: Florida, 2011.
19. Lowenstein, J. M. Transphosphorylations Catalysed by Bivalent Metal Ions. *Biochemical Journal* **1958**, *70*, 222-230.
20. McMillan, R. S., Renaud, J., Reynolds, J. G., Holm, R. H. Biologically Related Iron-Sulfur Clusters as Reaction Centers. Reductions of Acetylene to Ethylene in Systems Based on  $[\text{Fe}_4\text{S}_4(\text{SR})_4]^{3-}$ . *Journal of Inorganic Biochemistry* **1979**, *11*, 213-227.
21. Keller, A. M., Turchyn, A. V., Ralser, M. Non-Enzymatic Glycolysis and Pentose Phosphate Pathway-Like Reactions in a Plausible Archean Ocean. *Molecular Systems Biology* **2014**, *10*.
22. Athavale, S. S., Petrov, A. S., Hsiao, C., Watkins, D., Prickett, C. D., Gossett, J. J., Lie, L., Bowman, J. C., O'Neill, E., Bernier, C. R., Hud, N. V., Wartell, R. M., Harvey, S. C., William, L. D. RNA Folding and Catalysis Mediated by Iron (II). *PLoS One* **2012**, *7*(5).
23. Belmonte, L., and Mansy, S. S. Metal Catalysts and the Origin of Life. *Elements* **2016**, *12*, 413-418.
24. Rouault, T. Iron-Sulfur Cluster in Chemistry and Biology. Walter de Gruyter GmbH: Berlin, 2017.

25. Drennan Research and Education Laboratory. Iron Sulfur Cluster Biogenesis and Delivery. <http://drennan.mit.edu/research/research-interests/iron-sulfur-cluster-biogenesis-and-delivery/> (accessed September 27, 2021).
26. Valer, L., Rossetto, D., Scintilla, S., Hu, Y. J., Anju., Nader, S., Bentinol, I. O., Mansy, S. S. Methods to Identify and Characterize Iron-Sulfur Oligopeptides in water. Submitted.
27. Beinert, H., and Sands, R. H. Studies on Succinic and DPNH Dehydrogenase Preparations by Paramagnetic Resonance (EPR) Spectroscopy. *Biochem Biophys Res Commun* **1960**, 3(1), 41-46.
28. Bentinal, I. O., Nader, S., Mansy, S. S. Spectral Decomposition of Iron-Sulfur Clusters. *Anal. Biochem* **2021**, 629, 114269.
29. Orme-Johnson, W. H., and Holm, R. H. Identification of Iron-Sulfur Clusters in Proteins. *Methods Enzymol* **1978**, 53, 268-274.
30. Rao, P. V., and Holm, R. H. Synthetic Analogues of the Active Sites of Iron-Sulfur Proteins. *Chem Rev* **2004**, 104, 527-559.
31. Qi, W., Li, J., Chain, C. Y., Pasquevich, G. A., Pasquevich A. F., Cowen, J. A. Glutathione Complexed Fe-S Centers. *J. Am. Chem. Soc* **2012**, 134, 10745-10748.
32. Bonfio, C., Valer, L., Scintilla, S., Shah, S., Evans, D. J., Jin, L., Szostak, J. W., Sasselov, D. D., Sutherland, J. D., Mansy, S. S. UV-Light-Driven Prebiotic Synthesis of Iron-Sulfur Clusters. *Nature Chemistry* **2017**, 9, 1229-1234.
33. Scintilla, S., Bonfio, C., Belmonte, L., Forlin, M., Rossetto, D., Li, J., Cowan, J. A., Galliani, A., Arnesano, F., Assfalg, M., Mansy, S. S. Duplications of an Iron-Sulfur Tripeptide Leads to the Formation of a Protoferredoxin. *Chem Commun* **2016**, 52, 13456-13459.
34. Camprubi, E., Jordan, S. F., Vasiliadou, R., Lane, N. Hypothesis: Iron Catalysis at the Origin of Life. *IUBMB Life* **2017**, 69, 373-381.
35. Pasek, M. A. Rethinking Early Earth Phosphorus Geochemistry. *PNAS* **2008**, 105(3), 853-858.
36. Rimmer, P. B., Xu, J., Thompson, S. J., Gillen, E., Sutherland, J. D., Quéloz, D. The Origin of RNA Precursors on Exoplanets. *Science advances* **2018**, 4(8), eaar3302.
37. Toner, J. D., and Catling, D. C. A Carbonate-Rich Lake Solution to the Phosphate Problem of the Origin of Life. *PNAS* **2020**, 117(2), 883-888.
38. Webber, A. P., Roberts, S., Murton, B. J., Hodkinson, M. R. S. Geology, Sulfide Geochemistry and Supercritical Venting at the Beebe Hydrothermal Vent Field, Cayman Trough. *Geophys. Geosyst* **2015**, 16, 2661-2678.
39. Colin-García, M., Heredia, A., Cordero, G., Camprubí, A., Negrón-Mendoza, A., Ortefa-Gutiérrez, F., Beraldi, H., Ramos-Bernal, S. Hydrothermal Vents and Prebiotic Chemistry: a Review. *Bol. Soc. Geol. Mex* **2016**, 68(3), 599-620.
40. Jones, C., Nomosatryo, S., Crowe, S. A., Bjerrum, C. J., Canfield, D. E. Iron Oxides, Divalent Cations, Silica, and the Early Earth Phosphorus Crisis. *Geology* **2015**, 43(2), 135-138.
41. Lyons, W. B., Mikucki, J. A., German, L. A., Welch, K. A., Welch, S. A., Gardner, C. B., Tulaczyk, S. M., Pettit, E. C., Kowalski, J., Dachwald, B. The Geochemistry of Englacial Brine from Taylor Glacier, Antarctica. *Journal of Geophysical Research: Biogeosciences* **2019**, 124, 633-648.
42. Qi, W., Li, J., Chain, C.Y., Pasquevich, G.A., Pasquevich, A. F., Cowan, J. A. Glutathione-Complex Iron-Sulfur Clusters. Reaction Intermediates and Evidence for a Template Effect Promoting Assembly and Stability. *Chem. Commun* **2013**, 49, 6313-6315.
43. Li, J., Pearson, S. A., Fenk, K.D., Cowan, J.A. Glutathione-Coordinated [2Fe-2S] Cluster is Stabilized by Intramolecular Salt Bridge. *J Biol Inorg Chem* **2015**, 20, 1221-1227.
44. Atkins, P., and De Paula, J. *Physical Chemistry for the Life Science*. W. H. Freeman and Company: USA, 2006.

45. Okur, H. I., Hladílková, J., Rembert, K. B., Cho, Y., Heyda, J., Dzubielia, J., Cremer, P. S., Jungwirth, P. Beyond the Hofmeister Series: Ion-Specific Effects on Proteins and Their Biological Functions. *J. Phys. Chem* **2017**, *121*, 1997-2014.
46. Kang, B., Tang, H., Zhao, Z., Song, S. Hofmeister Series: Insights of Ion Specificity from Amphiphilic Assembly and Interface Property. *ACS Omega* **2020**, *5*, 6229-6239.
47. Ueyama, N., Ueno, S., Nakamura, A., Wada, K., Matsubara, H., Kumagai, S., Sakakibara, S., Tsukihara, T. A Synthetic Analogue for the Active Site of the Plant-Type Ferredoxin: Two Different Coordination Isomers by a Four-Cys-Containing [20]-Peptide. *Biopolymers* **1992**, *32*, 1535-1544.
48. Mulholland, S., Gibhey, B. R., Rabanal, F., Dutton, P. I. Characterization of the Fundamental Protein Ligand Requirements of  $[4\text{Fe-4S}]^{2+/+}$  Clusters with Sixteen Amino Acid Maquettes. *J. Am. Chem. Soc* **1998**, *120*, 10296-10302.

# Appendix

Table A.1. Chemical Structures of Tested Peptide Sequences

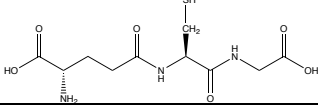
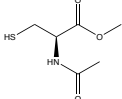
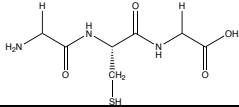
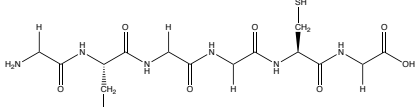
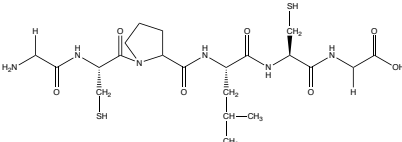
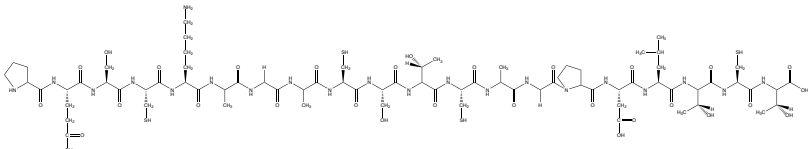
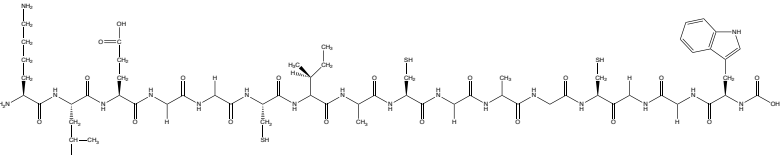
Peptide sequence	Peptide structure
E <sub>γ</sub> CG (Glutathione)	
N-Acetyl-L-Cysteine Methyl Ester	
GCG	
GCGGCG	
GCPLCG	
PESCKAGACSTCAGPDLTCT	
KLCEGGCIACGACGGW	



Table A. 2. Standard Errors of Mean for Figure 2.4

<b>100 <math>\mu\text{M}</math> additive</b>	<b>[1Fe-0S]<sup>2+</sup> SEM (<math>\mu\text{M}</math>)</b>	<b>[2Fe-2S]<sup>2+</sup> SEM (<math>\mu\text{M}</math>)</b>	<b>[4Fe-4S]<sup>2+</sup> SEM (<math>\mu\text{M}</math>)</b>
Control	15.86	6.15	6.13
NaCl	4.96	4.16	3.39
NaF	8.44	7.21	3.14
Na <sub>2</sub> SiO <sub>3</sub>	13.02	6.73	3.42
Na <sub>2</sub> CO <sub>3</sub>	16.66	7.26	3.26
K <sub>2</sub> CO <sub>3</sub>	14.87	9.52	4.16
KBr	3.76	2.39	1.35
Fe(II)CO <sub>3</sub>	15.79	9.56	3.75
CaCO <sub>3</sub>	9.60	1.74	4.76
H <sub>3</sub> BO <sub>3</sub>	6.16	5.95	0.81
MgCl <sub>2</sub>	7.78	3.94	1.53
Na <sub>2</sub> SO <sub>4</sub>	2.61	3.47	2.69
Na <sub>2</sub> SO <sub>3</sub>	4.68	2.96	2.15
NaH <sub>2</sub> PO <sub>4</sub>	8.39	4.30	2.87
Na <sub>2</sub> HPO <sub>3</sub>	8.64	0.36	1.89
Na <sub>2</sub> H <sub>2</sub> P <sub>2</sub> O <sub>7</sub>	3.99	2.40	4.27
Na <sub>3</sub> P <sub>3</sub> O <sub>9</sub>	8.81	2.57	2.27
P <sub>2</sub> O <sub>5</sub>	1.08	3.74	0.58
(C <sub>2</sub> H <sub>5</sub> O) <sub>2</sub> PONH <sub>2</sub>	2.49	4.97	2.47

<b>100 mM additive</b>	<b>[1Fe-0S]<sup>2+</sup> SEM (<math>\mu\text{M}</math>)</b>	<b>[2Fe-2S]<sup>2+</sup> SEM (<math>\mu\text{M}</math>)</b>	<b>[4Fe-4S]<sup>2+</sup> SEM (<math>\mu\text{M}</math>)</b>
Control	2.96	2.94	2.06
NaCl	2.44	3.30	1.86
NaF	3.27	1.56	1.27
Na <sub>2</sub> SiO <sub>3</sub>	12.48	0	0.99
Na <sub>2</sub> CO <sub>3</sub>	1.99	4.07	1.72
K <sub>2</sub> CO <sub>3</sub>	9.67	7.94	4.80
KBr	2.68	3.67	1.11
Fe(II)CO <sub>3</sub>	-	-	-
CaCO <sub>3</sub>	-	-	-
H <sub>3</sub> BO <sub>3</sub>	4.97	6.27	0.30
MgCl <sub>2</sub>	3.57	2.91	1.88
Na <sub>2</sub> SO <sub>4</sub>	2.94	3.20	3.34
Na <sub>2</sub> SO <sub>3</sub>	3.81	0	1.14
NaH <sub>2</sub> PO <sub>4</sub>	5.46	3.49	2.70
Na <sub>2</sub> HPO <sub>3</sub>	8.48	7.11	3.22
Na <sub>2</sub> H <sub>2</sub> P <sub>2</sub> O <sub>7</sub>	16.68	0	0
Na <sub>3</sub> P <sub>3</sub> O <sub>9</sub>	1.07	2.86	0
P <sub>2</sub> O <sub>5</sub>	8.73	0	0
(C <sub>2</sub> H <sub>5</sub> O) <sub>2</sub> PONH <sub>2</sub>	6.57	0.31	2.41

<b>0.5 M additive</b>	<b>[1Fe-0S]<sup>2+</sup> SEM (<math>\mu</math>M)</b>	<b>[2Fe-2S]<sup>2+</sup> SEM (<math>\mu</math>M)</b>	<b>[4Fe-4S]<sup>2+</sup> SEM (<math>\mu</math>M)</b>
Control	1.23	5.55	1.93
NaCl	4.65	3.15	0.96
NaF	5.36	3.39	1.31
Na <sub>2</sub> SiO <sub>3</sub>	8.18	0	1.23
Na <sub>2</sub> CO <sub>3</sub>	2.88	2.60	4.34
K <sub>2</sub> CO <sub>3</sub>	4.01	7.22	1.50
KBr	3.02	2.46	0.95
Fe(II)CO <sub>3</sub>	-	-	-
CaCO <sub>3</sub>	-	-	-
H <sub>3</sub> BO <sub>3</sub>	-	-	-
MgCl <sub>2</sub>	12.45	8.76	3.66
Na <sub>2</sub> SO <sub>4</sub>	0.35	2.05	1.24
Na <sub>2</sub> SO <sub>3</sub>	8.54	0.38	5.55
NaH <sub>2</sub> PO <sub>4</sub>	3.90	1.19	0.16
Na <sub>2</sub> HPO <sub>3</sub>	3.15	3.89	1.65
Na <sub>2</sub> H <sub>2</sub> P <sub>2</sub> O <sub>7</sub>	0.30	0.06	0.08
Na <sub>3</sub> P <sub>3</sub> O <sub>9</sub>	5.54	7.40	0
P <sub>2</sub> O <sub>5</sub>	5.75	0	0.26
(C <sub>2</sub> H <sub>5</sub> O) <sub>2</sub> PONH <sub>2</sub>	0.47	5.05	2.05
Seawater	13.12	4.43	2.58

Table A.3. Standard Errors of Mean for Figure 2.9

<b>100 <math>\mu\text{M}</math> additive</b>	<b>[1Fe-0S]<sup>2+</sup> SEM (<math>\mu\text{M}</math>)</b>	<b>[2Fe-2S]<sup>2+</sup> SEM (<math>\mu\text{M}</math>)</b>	<b>[4Fe-4S]<sup>2+</sup> SEM (<math>\mu\text{M}</math>)</b>
Control	16.81	2.07	12.84
NaCl	8.95	2.13	6.66
NaF	4.16	2.54	7.79
Na <sub>2</sub> SiO <sub>3</sub>	4.82	1.24	3.34
Na <sub>2</sub> CO <sub>3</sub>	12.47	1.70	7.72
K <sub>2</sub> CO <sub>3</sub>	1.62	2.70	18.35
Fe(II)CO <sub>3</sub>	9.86	2.13	12.85
CaCO <sub>3</sub>	11.62	2.13	3.39
H <sub>3</sub> BO <sub>3</sub>	18.17	1.98	7.50
MgCl <sub>2</sub>	14.59	1.96	2.20
NaH <sub>2</sub> PO <sub>4</sub>	2.12	0	3.27
Na <sub>2</sub> HPO <sub>3</sub>	13.60	0	4.78
Na <sub>2</sub> H <sub>2</sub> P <sub>2</sub> O <sub>7</sub>	0.79	0	2.93
Na <sub>3</sub> P <sub>3</sub> O <sub>9</sub>	13.51	0	2.64
P <sub>2</sub> O <sub>5</sub>	28.25	0	3.70
(C <sub>2</sub> H <sub>5</sub> O) <sub>2</sub> PONH <sub>2</sub>	17.90	0	6.05

<b>100 mM additive</b>	<b>[1Fe-0S]<sup>2+</sup> SEM (<math>\mu\text{M}</math>)</b>	<b>[2Fe-2S]<sup>2+</sup> SEM (<math>\mu\text{M}</math>)</b>	<b>[4Fe-4S]<sup>2+</sup> SEM (<math>\mu\text{M}</math>)</b>
Control	16.15	0	6.45
NaCl	7.02	3.13	2.58
NaF	0	0	6.71
Na <sub>2</sub> SiO <sub>3</sub>	6.94	0	0.40
Na <sub>2</sub> CO <sub>3</sub>	18.16	3.14	4.04
K <sub>2</sub> CO <sub>3</sub>	4.73	0.45	3.04
Fe(II)CO <sub>3</sub>	-	-	-
CaCO <sub>3</sub>	-	-	-
H <sub>3</sub> BO <sub>3</sub>	22.50	1.43	1.97
MgCl <sub>2</sub>	0	0.23	3.06
NaH <sub>2</sub> PO <sub>4</sub>	29.52	4.61	4.47
Na <sub>2</sub> HPO <sub>3</sub>	0.003	2.53	9.83
Na <sub>2</sub> H <sub>2</sub> P <sub>2</sub> O <sub>7</sub>	18.12	0	0
Na <sub>3</sub> P <sub>3</sub> O <sub>9</sub>	39.74	4.90	6.95
P <sub>2</sub> O <sub>5</sub>	23.22	0.33	0
(C <sub>2</sub> H <sub>5</sub> O) <sub>2</sub> PONH <sub>2</sub>	17.93	0	9.74

<b>0.5 M additive</b>	<b>[1Fe-0S]<sup>2+</sup> SEM (<math>\mu</math>M)</b>	<b>[2Fe-2S]<sup>2+</sup> SEM (<math>\mu</math>M)</b>	<b>[4Fe-4S]<sup>2+</sup> SEM (<math>\mu</math>M)</b>
Control	7.65	1.59	17.15
NaCl	0	1.49	9.31
NaF	14.68	1.20	11.27
Na <sub>2</sub> SiO <sub>3</sub>	5.77	0	1.46
Na <sub>2</sub> CO <sub>3</sub>	20.14	0.25	3.81
K <sub>2</sub> CO <sub>3</sub>	13.53	0	0
Fe(II)CO <sub>3</sub>	-	-	-
CaCO <sub>3</sub>	-	-	-
H <sub>3</sub> BO <sub>3</sub>	-	-	-
MgCl <sub>2</sub>	1.26	0.62	3.16
NaH <sub>2</sub> PO <sub>4</sub>	28.57	4.54	2.08
Na <sub>2</sub> HPO <sub>3</sub>	0	3.35	2.08
Na <sub>2</sub> H <sub>2</sub> P <sub>2</sub> O <sub>7</sub>	1.53	0.01	0
Na <sub>3</sub> P <sub>3</sub> O <sub>9</sub>	14.48	0	0.04
P <sub>2</sub> O <sub>5</sub>	29.76	0.09	0.23
(C <sub>2</sub> H <sub>5</sub> O) <sub>2</sub> PONH <sub>2</sub>	18.87	0	3.63
Seawater	2.96	0	0

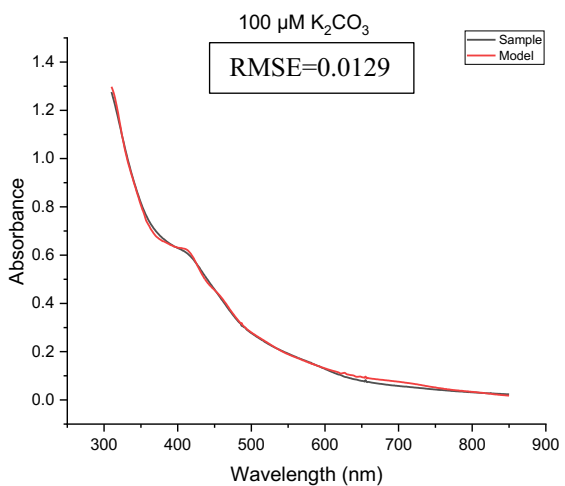
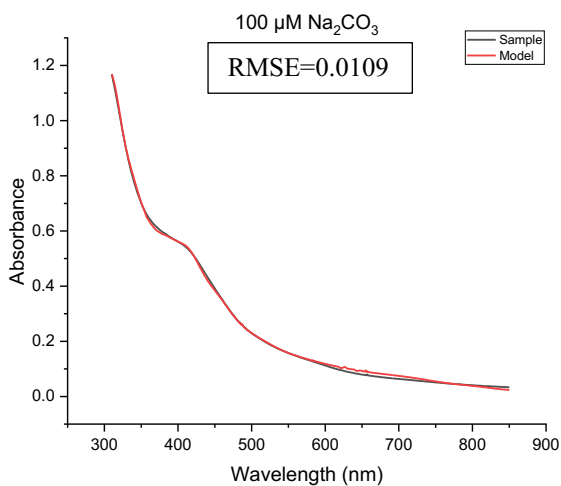
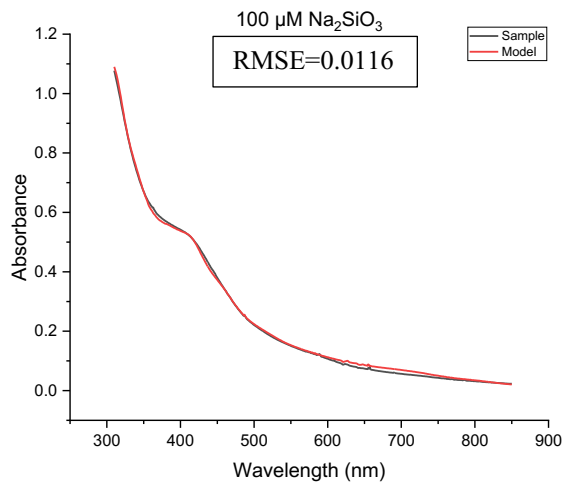
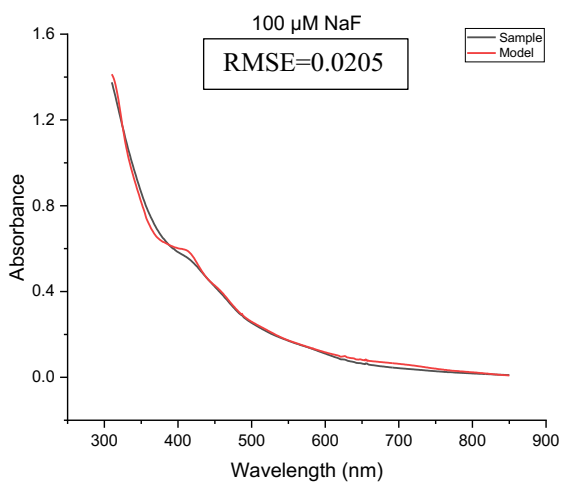
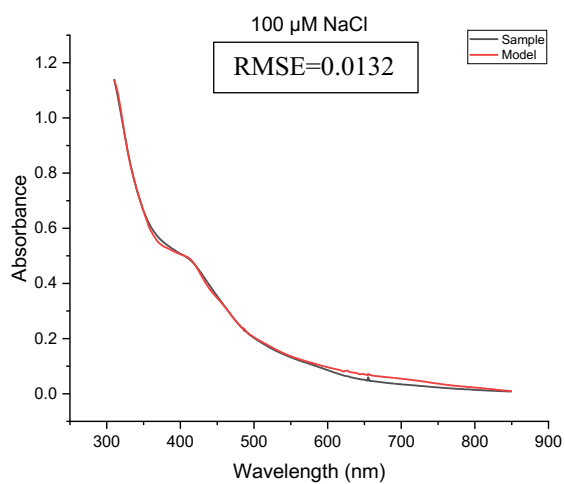
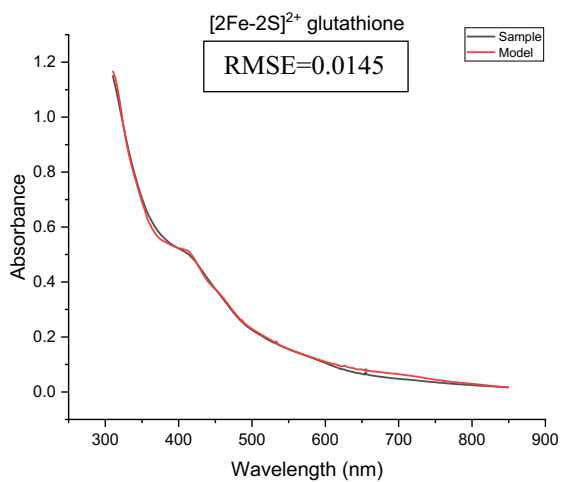
Table A.4. Standard Errors of Mean for Figure 2.15

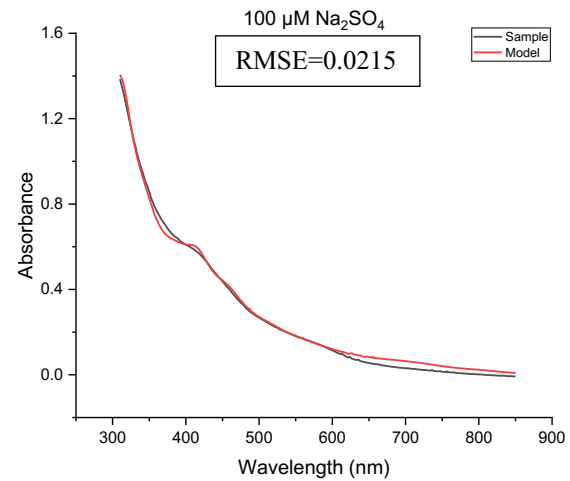
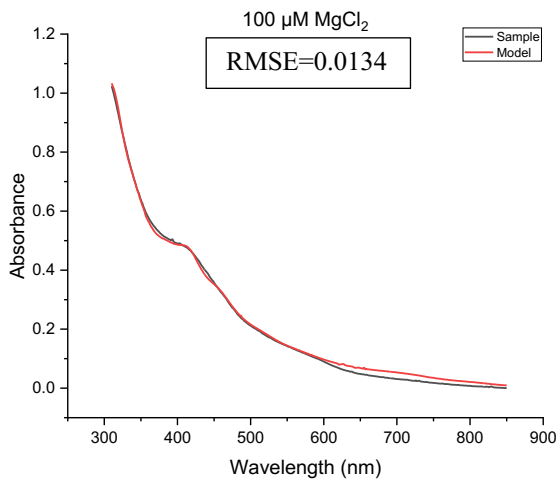
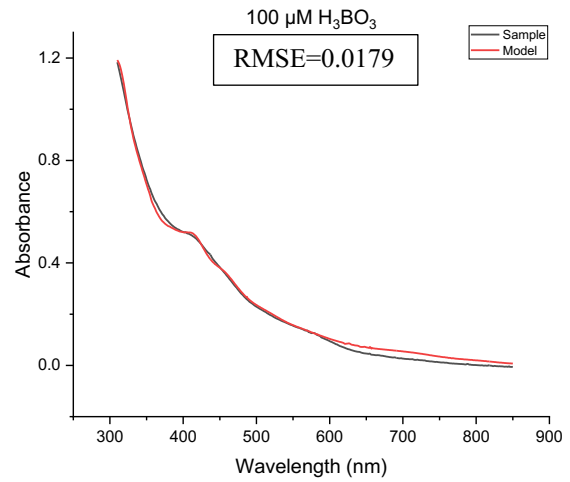
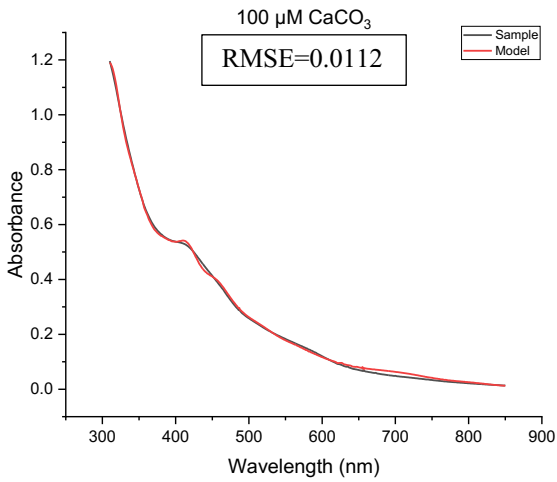
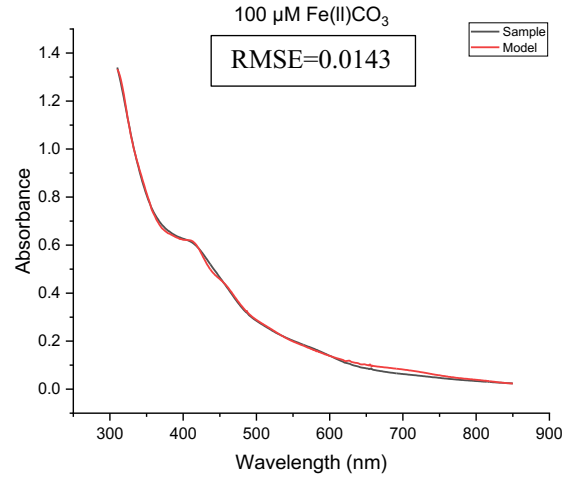
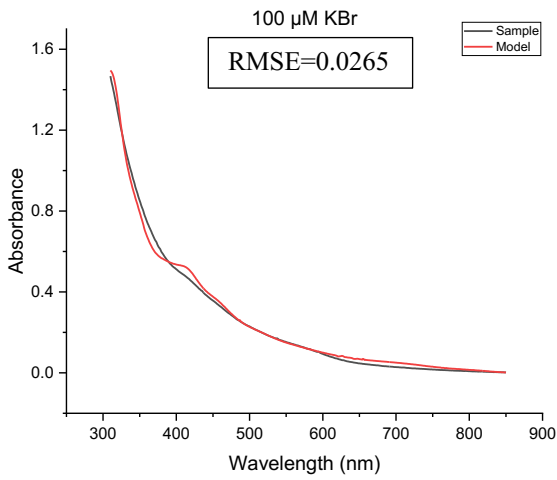
<b>Alkaline Lake pH 10</b>	<b>[1Fe-0S]<sup>2+</sup> SEM (<math>\mu</math>M)</b>	<b>[2Fe-2S]<sup>2+</sup> SEM (<math>\mu</math>M)</b>	<b>[4Fe-4S]<sup>2+</sup> SEM (<math>\mu</math>M)</b>
Glutathione	12.95	3.87	0.74
Ac-Cys-OMe	0	0	0
GCG	0	0	0.08
GCGGCG	0	11.07	22.11
GCPLCG	147.80	37.24	2.71
Sp FdM	5.91	0	0
Pa FdM	0	1.13	0.14

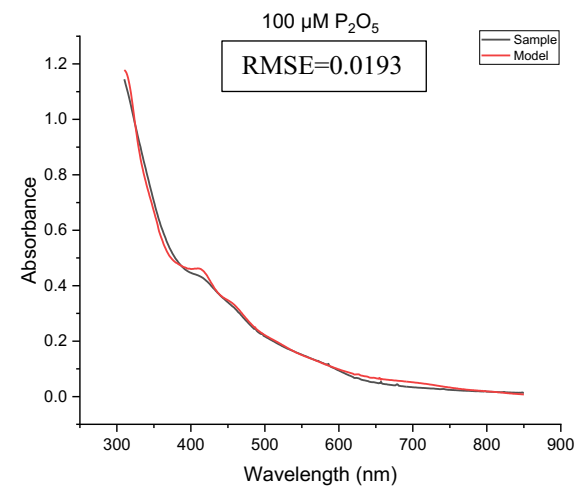
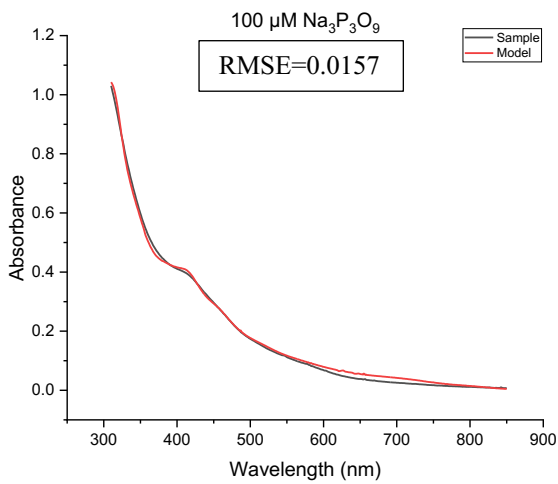
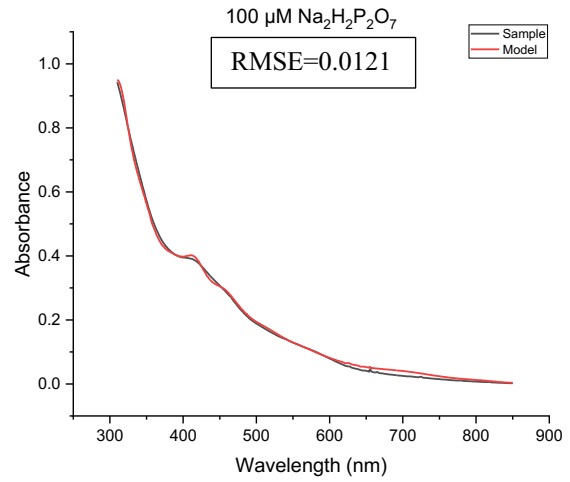
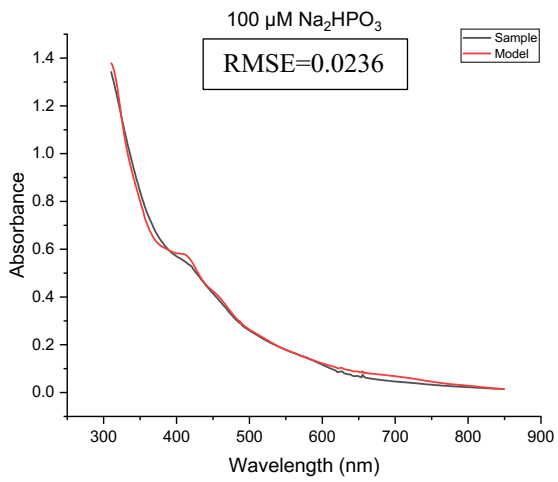
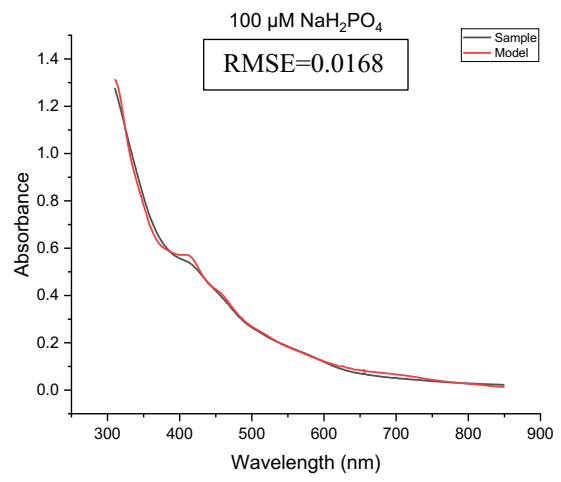
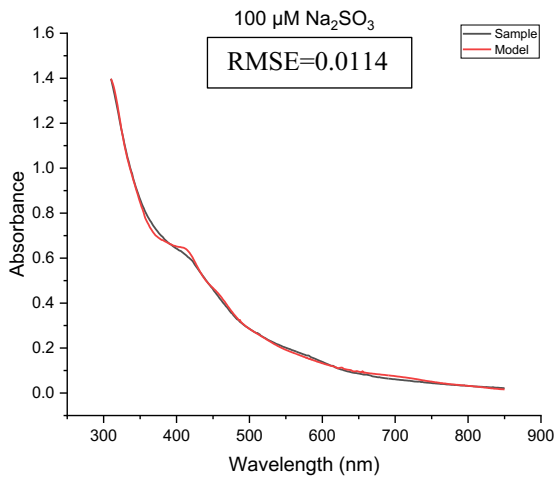
<b>Lost City pH 9</b>	<b>[1Fe-0S]<sup>2+</sup> SEM (<math>\mu</math>M)</b>	<b>[2Fe-2S]<sup>2+</sup> SEM (<math>\mu</math>M)</b>	<b>[4Fe-4S]<sup>2+</sup> SEM (<math>\mu</math>M)</b>
Glutathione	68.46	3.25	2.57
Ac-Cys-OMe	28.50	0	7.91
GCG	8.98	1.80	0.85
GCGGCG	36.18	8.54	2.39
GCPLCG	0	0.59	2.88
Sp FdM	0	2.01	1.43
Pa FdM	17.45	0.87	5.72

<b>Seawater pH 6.5</b>	<b>[1Fe-0S]<sup>2+</sup> SEM (<math>\mu</math>M)</b>	<b>[2Fe-2S]<sup>2+</sup> SEM (<math>\mu</math>M)</b>	<b>[4Fe-4S]<sup>2+</sup> SEM (<math>\mu</math>M)</b>
Glutathione	20.98	0.53	2.55
Ac-Cys-OMe	11.24	2.61	9.81
GCG	4.66	1.19	2.00
GCGGCG	12.03	1.95	2.41
GCPLCG	12.99	2.12	3.96
Sp FdM	0	1.95	1.66
Pa FdM	0	0	5.83

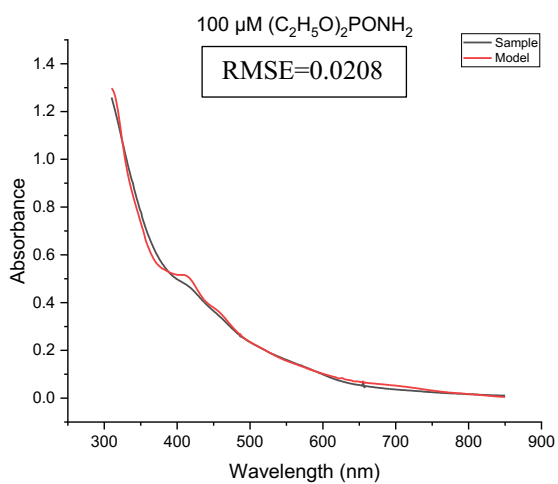
<b>Glacial Brine pH 6.5</b>	<b>[1Fe-0S]<sup>2+</sup> SEM (<math>\mu</math>M)</b>	<b>[2Fe-2S]<sup>2+</sup> SEM (<math>\mu</math>M)</b>	<b>[4Fe-4S]<sup>2+</sup> SEM (<math>\mu</math>M)</b>
Glutathione	0	0.98	0
Ac-Cys-OMe	0	0.25	0.53
GCG	0	0.22	0.86
GCGGCG	1.97	0.47	0.70
GCPLCG	0	0.97	1.68
Sp FdM	0	1.45	6.88
Pa FdM	1.27	0.51	0.11



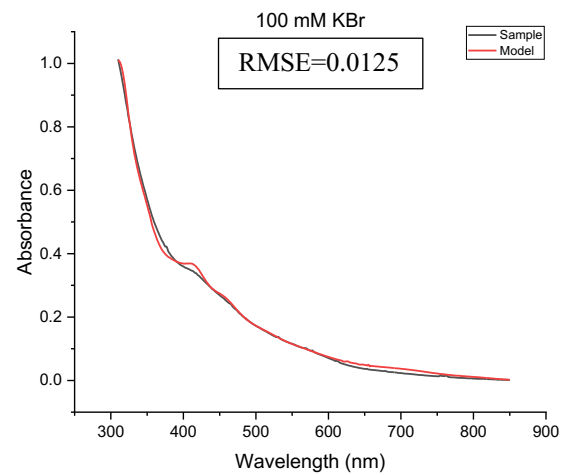
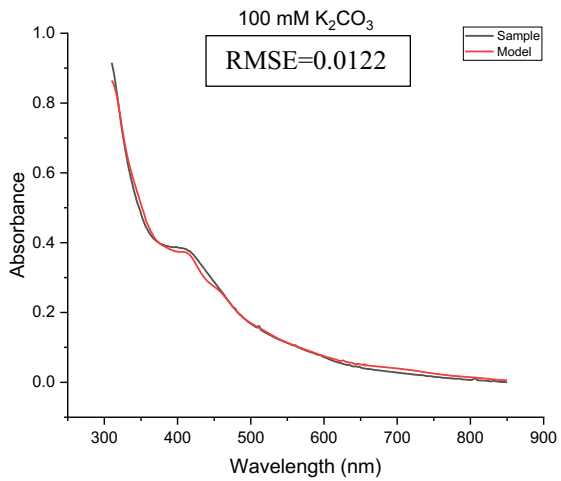
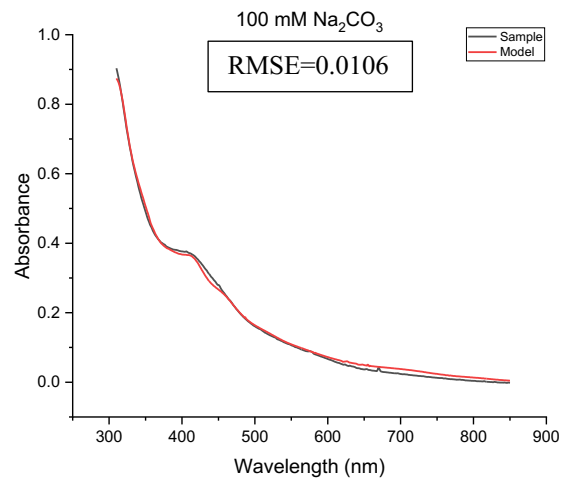
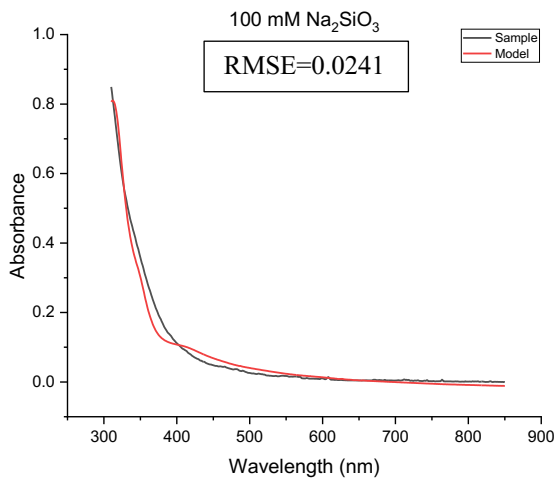
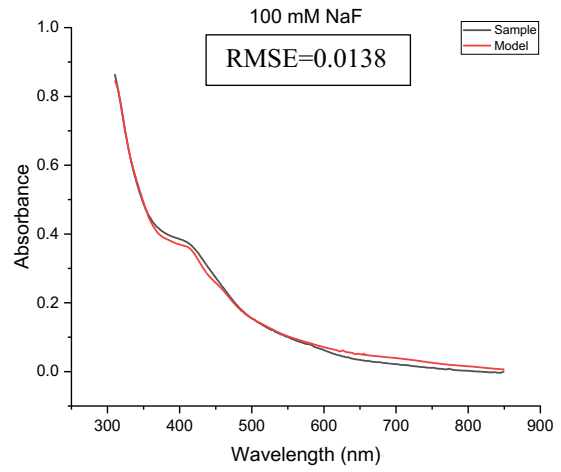
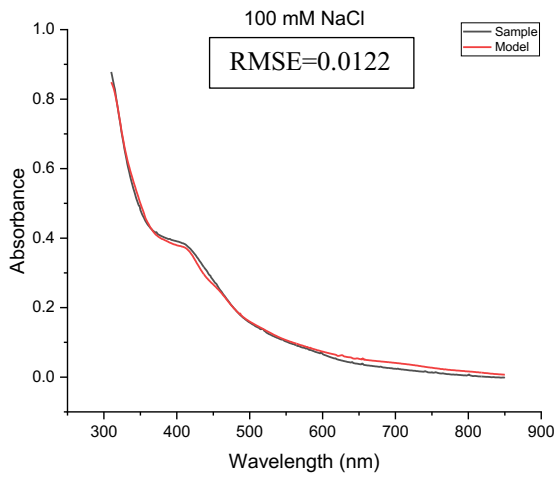


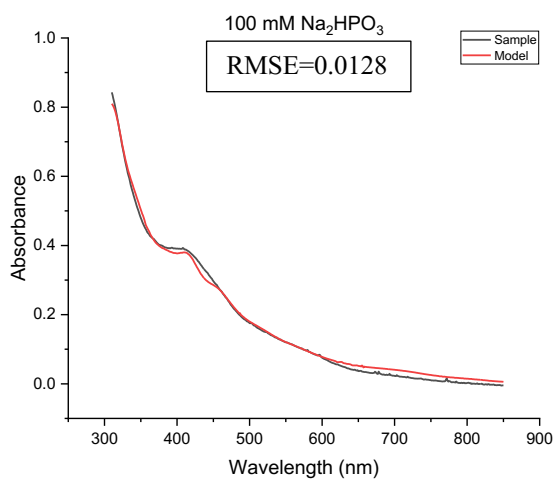
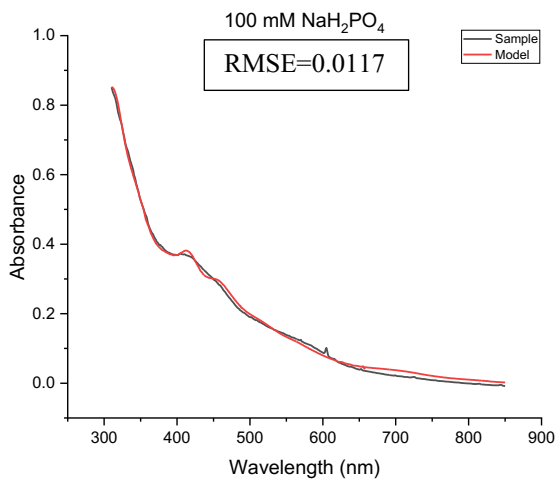
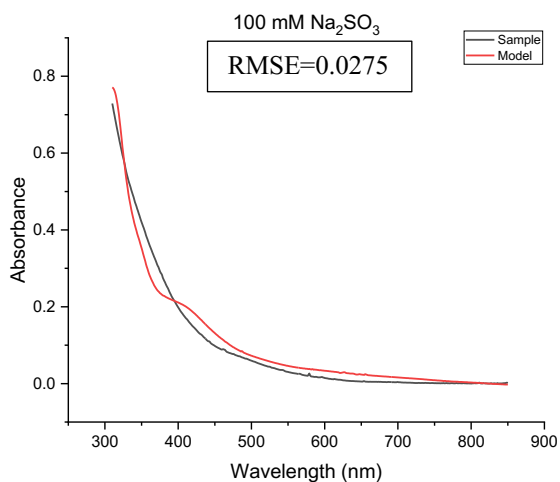
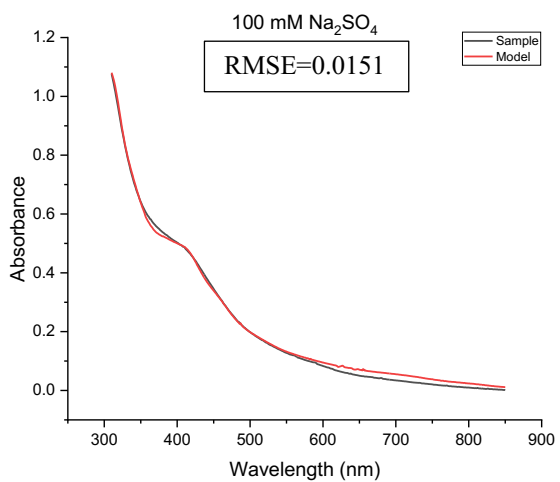
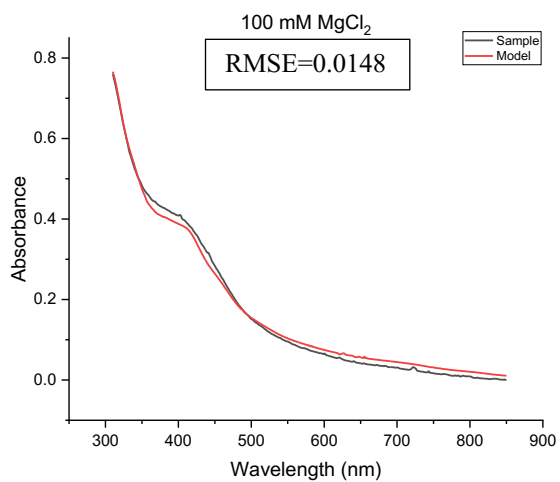
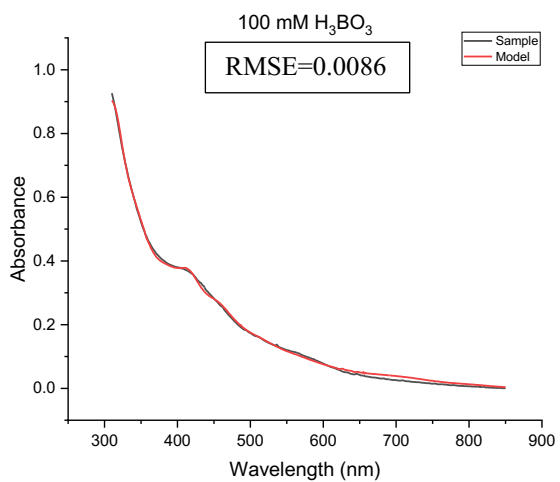


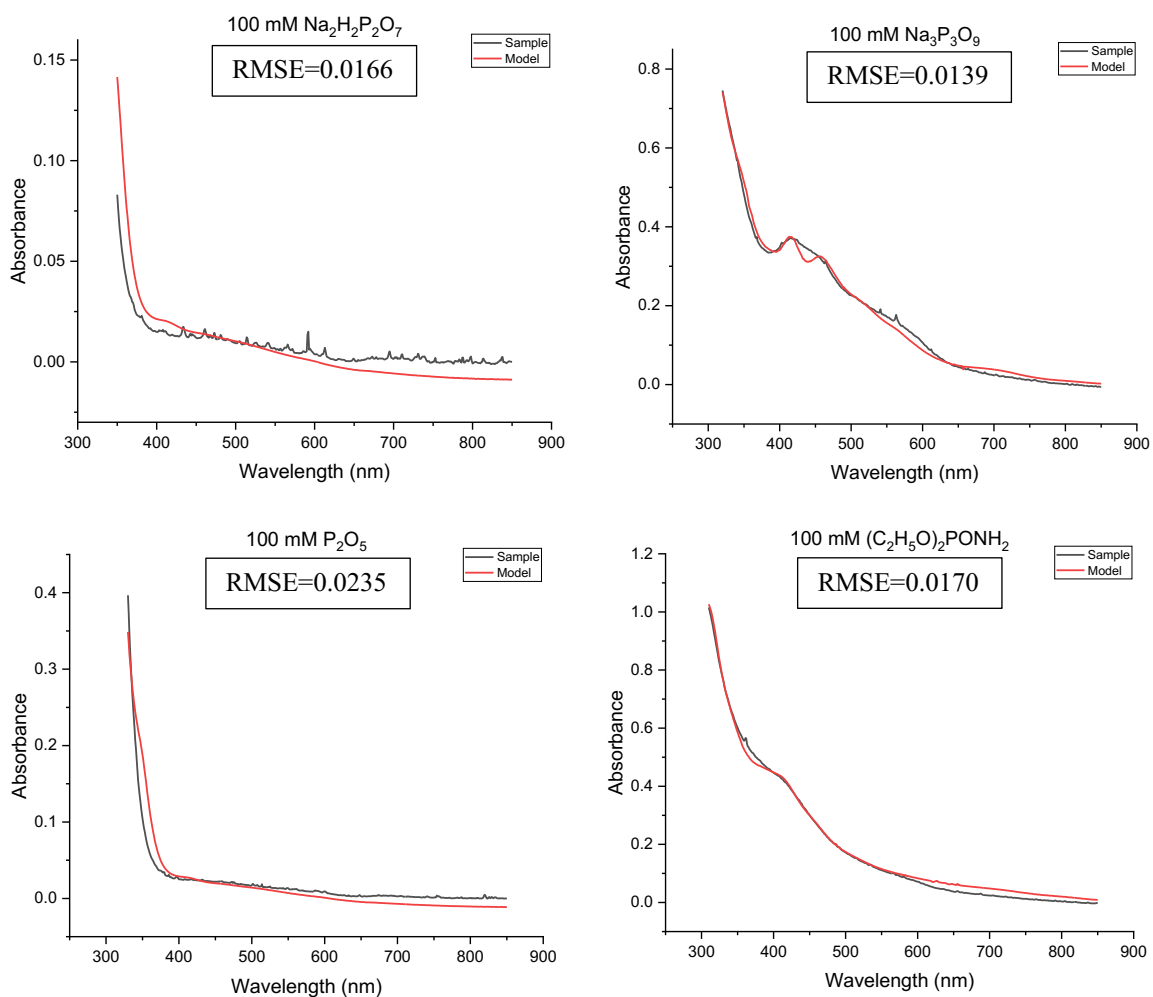




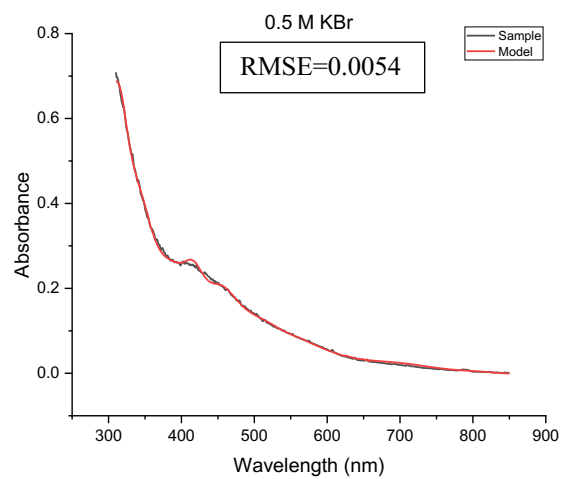
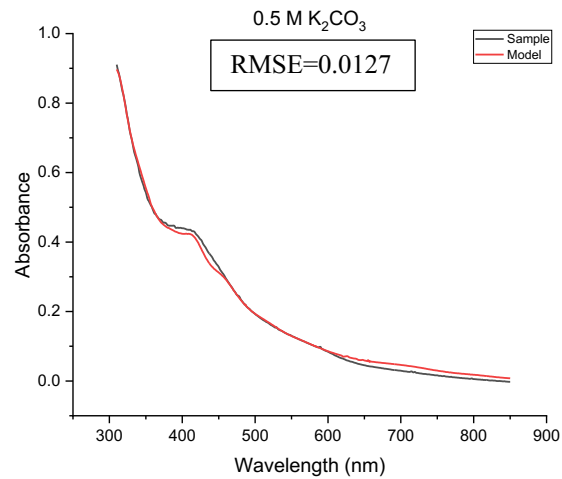
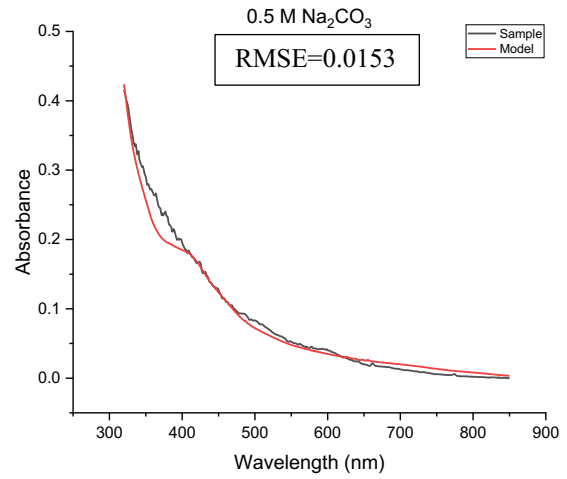
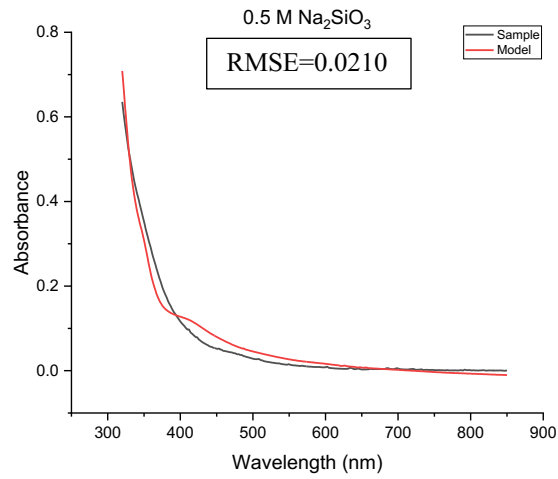
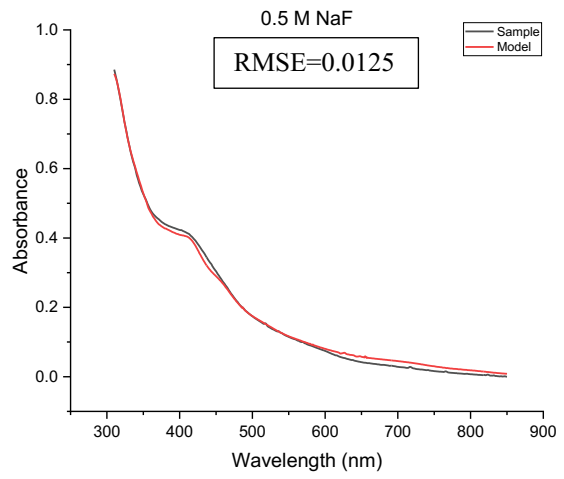
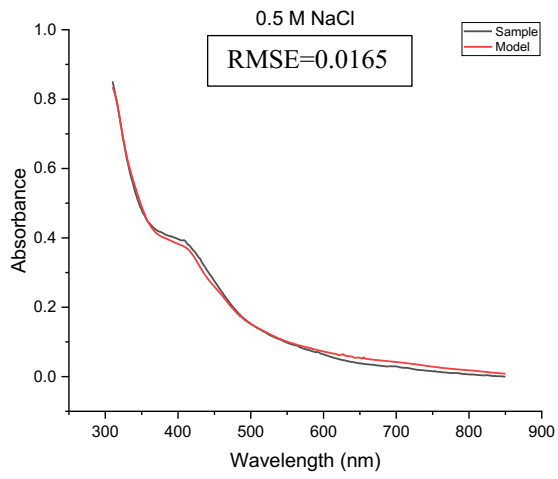
**Figure A.1.** Individual absorption spectra for iron-sulfur glutathione under 100  $\mu\text{M}$  additive conditions. 100  $\mu\text{M}$  additive was added into a solution of 40 mM glutathione, 0.185 mM  $\text{Na}_2\text{S}$ , and 0.5 mM  $\text{FeCl}_3$ , pH 8.7. Black lines are sample spectra, red lines represent fitted models using Fit-FeS. The data here were used to generate the plots in Figure 2.4. All spectra are the average of triplates. Root mean square errors (RMSE) were calculated.

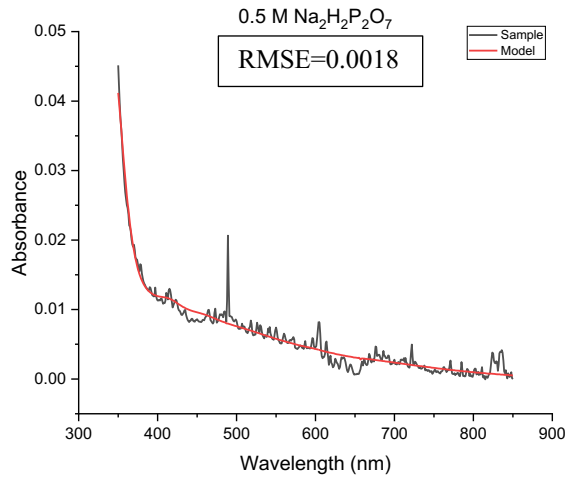
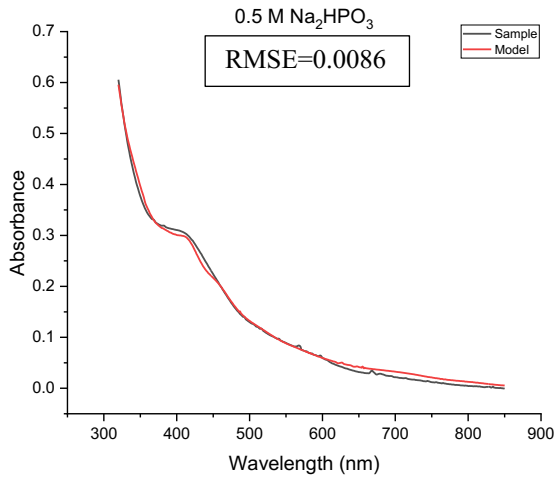
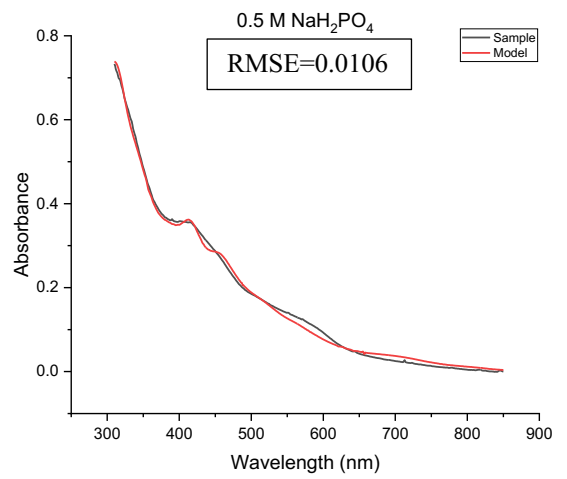
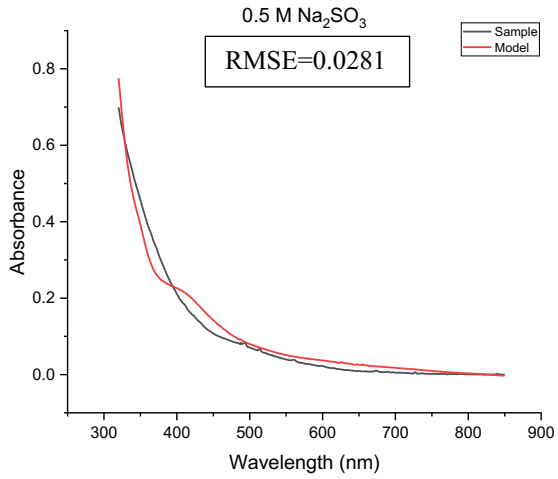
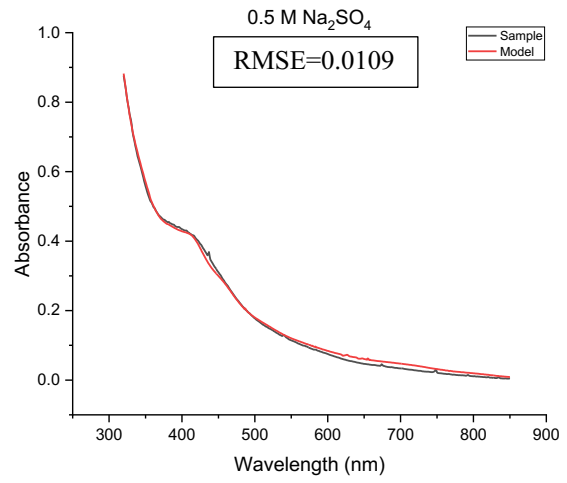
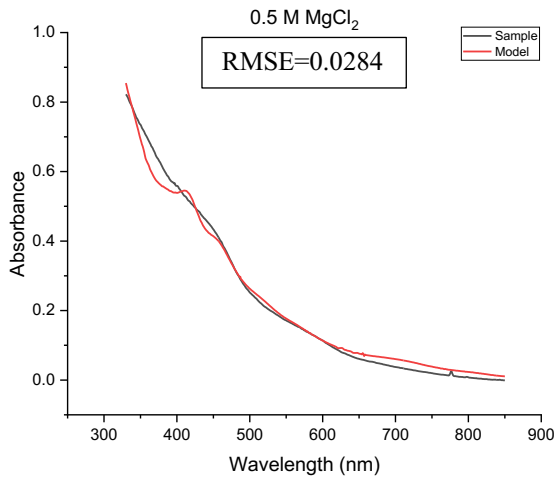


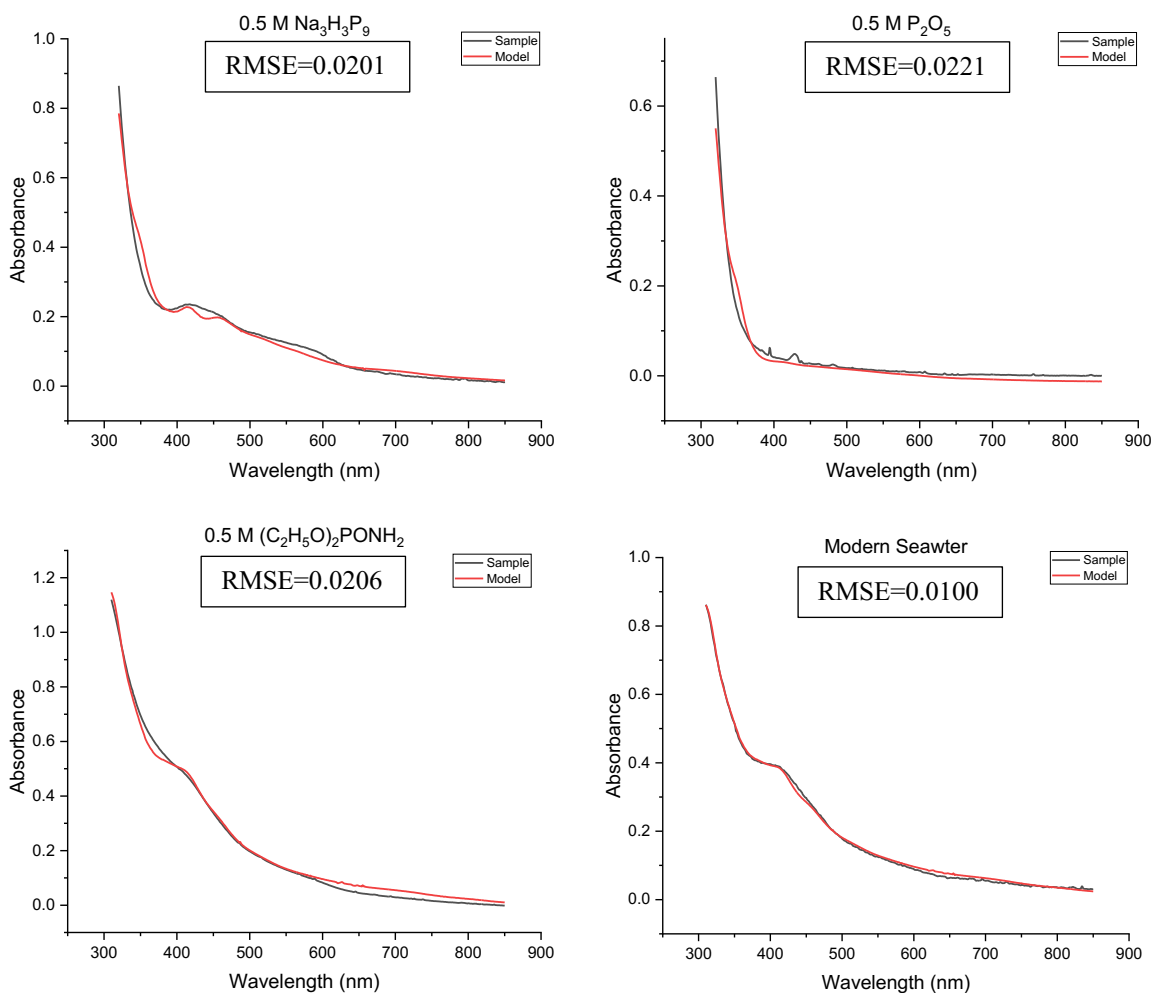




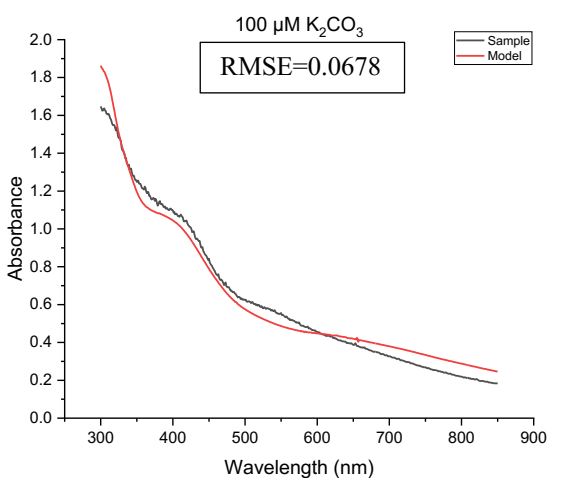
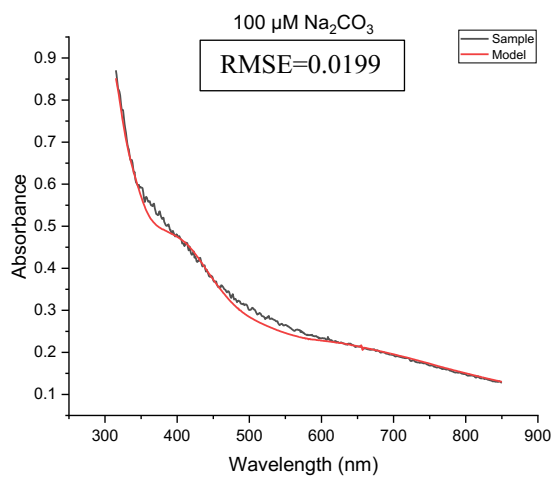
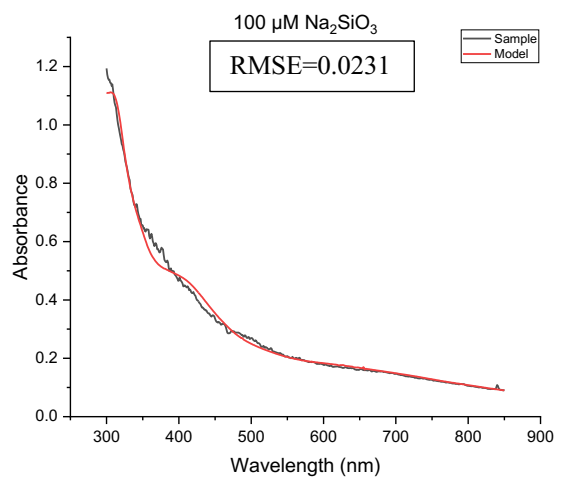
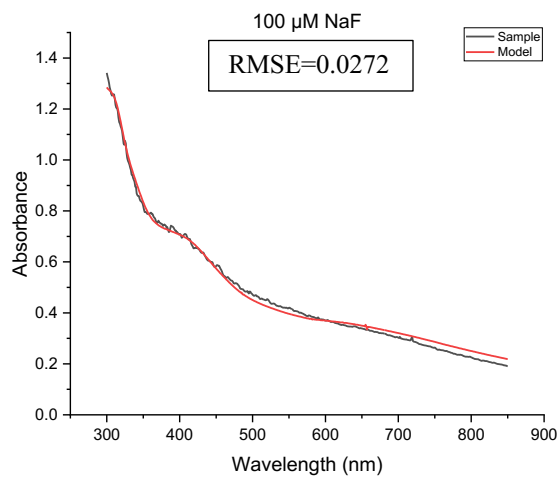
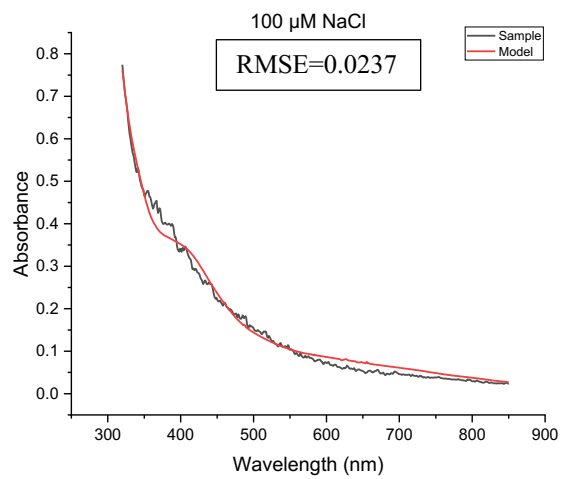
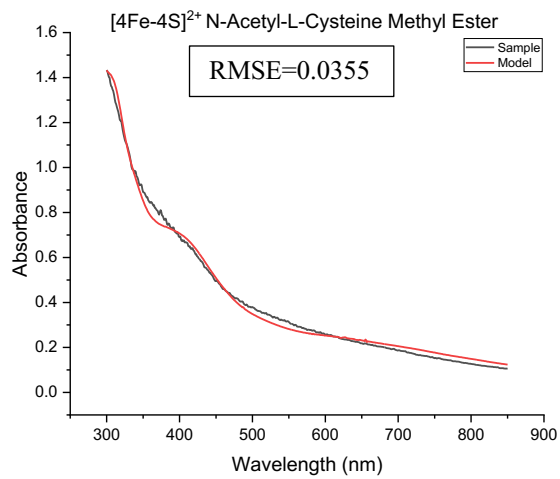
**Figure A.2.** Individual absorption spectra for iron-sulfur glutathione under 100 mM additive conditions. 100 mM additive was added into a solution of 40 mM glutathione, 0.185 mM  $\text{Na}_2\text{S}$ , and 0.5 mM  $\text{FeCl}_3$ , pH 8.7. Black lines are sample spectra, red lines represent fitted models using Fit-FeS. The data here were used to generate the plots in Figure 2.4. All spectra are the average of triplicates. Root mean square errors (RMSE) were calculated.



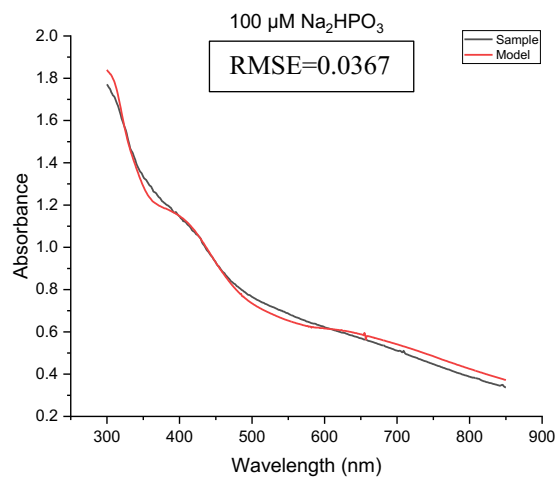
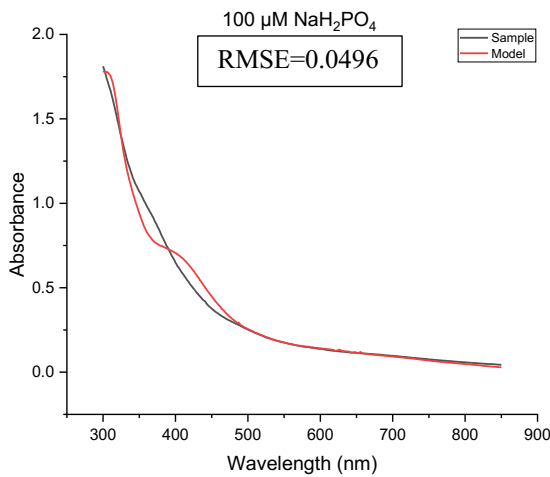
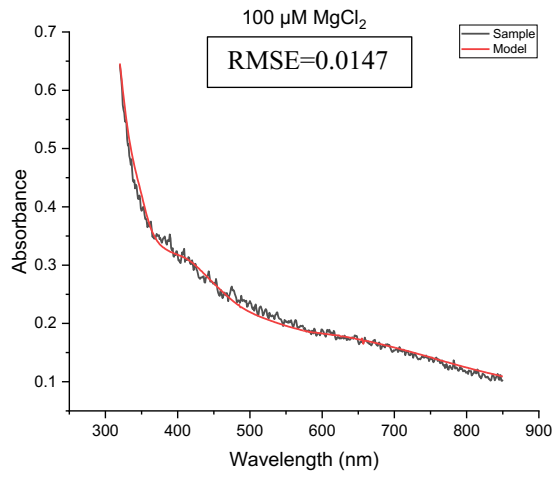
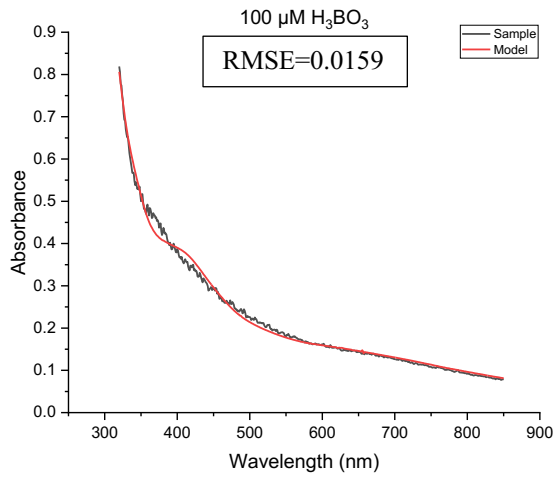
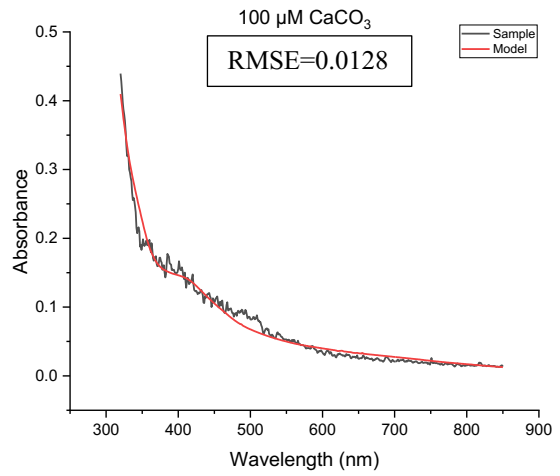
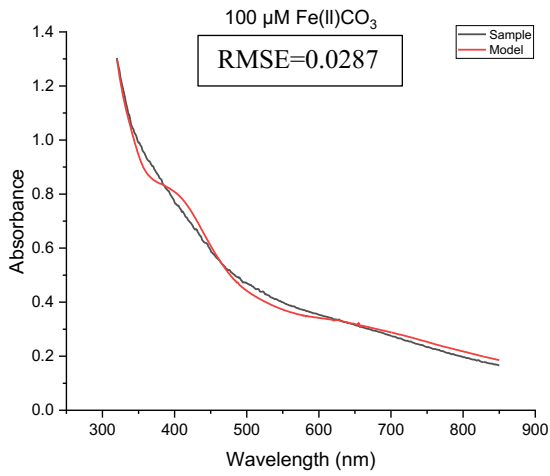


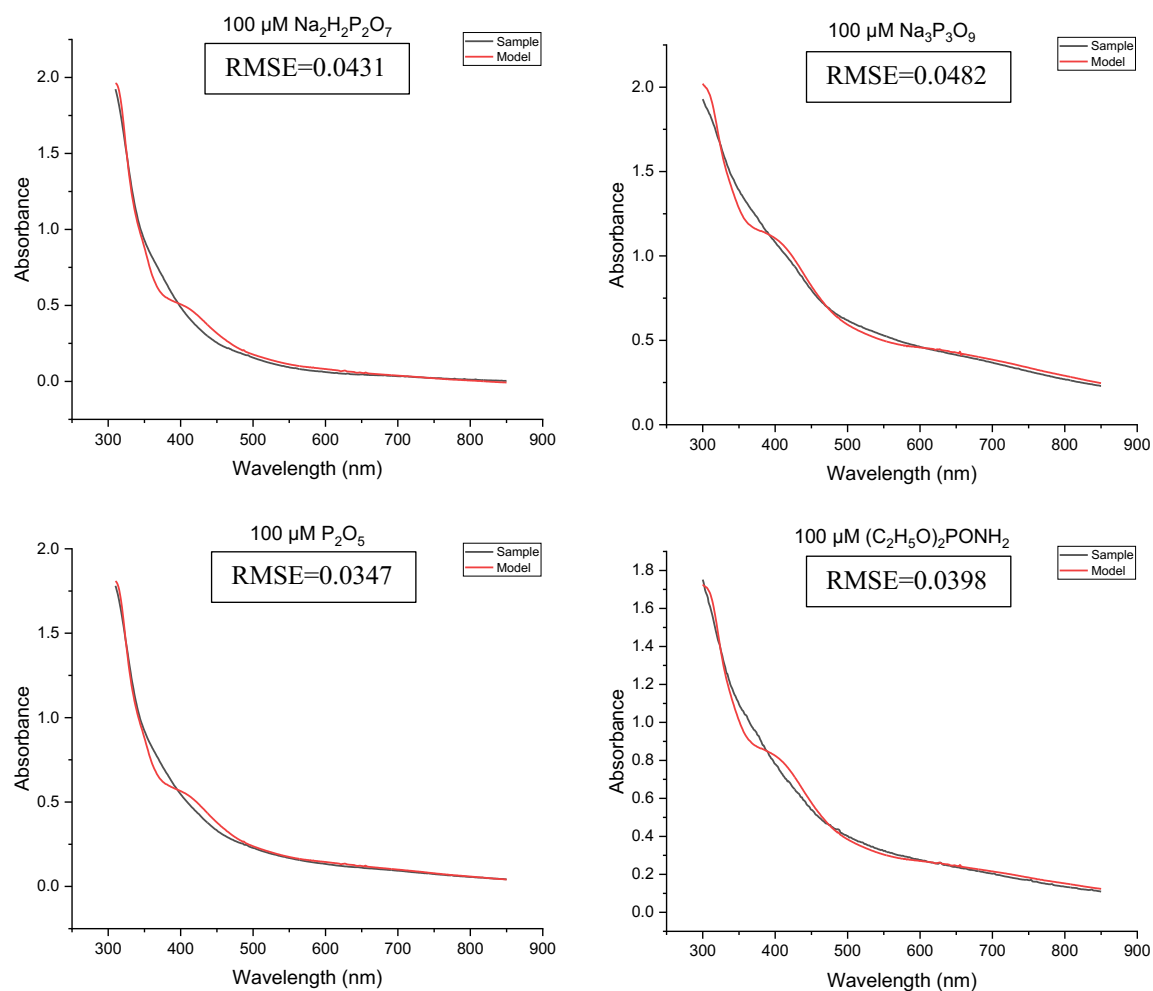


**Figure A.3.** Individual absorption spectra for iron-sulfur glutathione under 0.5 M additive conditions. 0.5 M additive was added into a solution of 40 mM glutathione, 0.185 mM  $\text{Na}_2\text{S}$ , and 0.5 mM  $\text{FeCl}_3$ , pH 8.7. Black lines are sample spectra, red lines represent fitted models using Fit-FeS. The data here were used to generate the plots in Figure 2.4. All spectra are the average of triplicates. Root mean square errors (RMSE) were calculated.

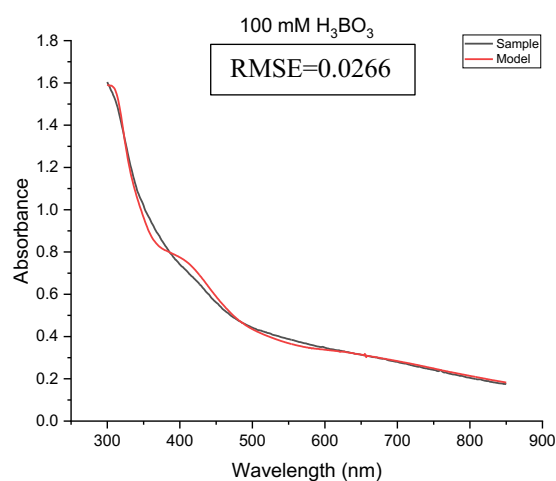
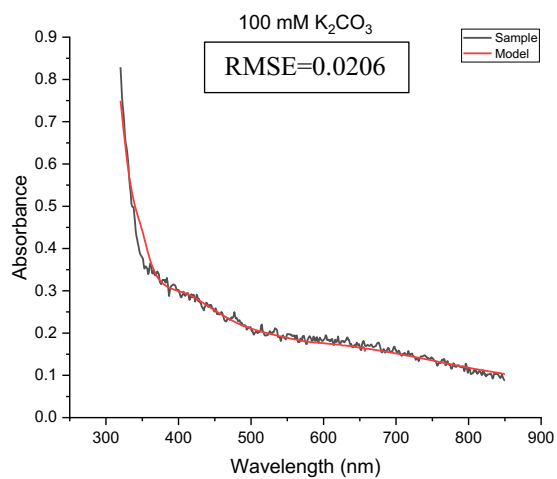
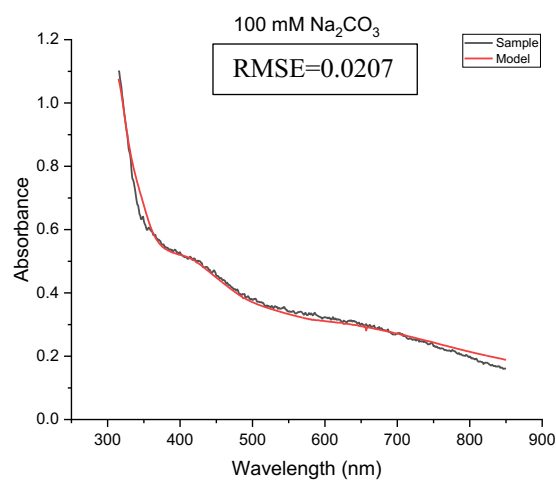
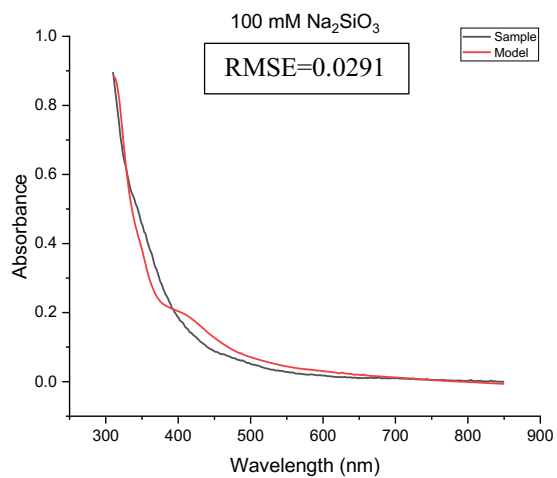
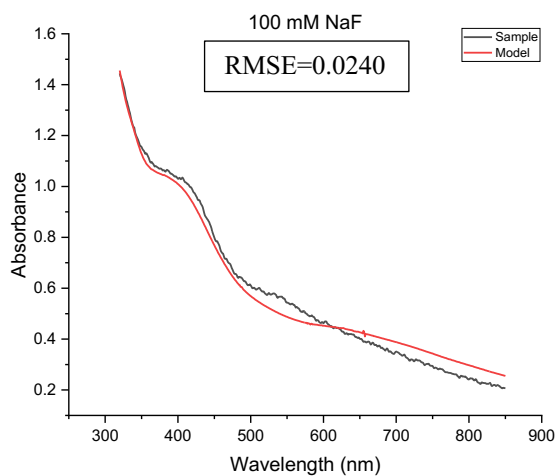
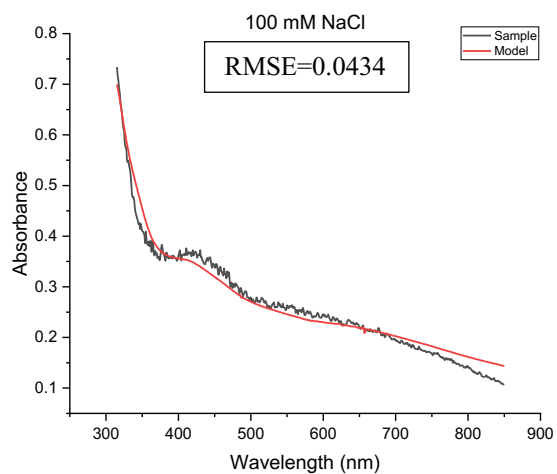


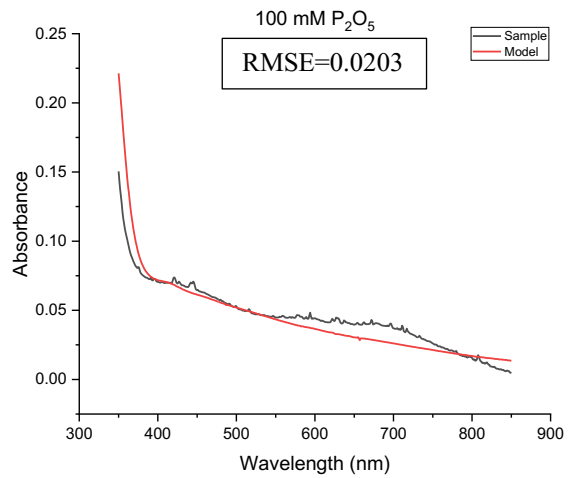
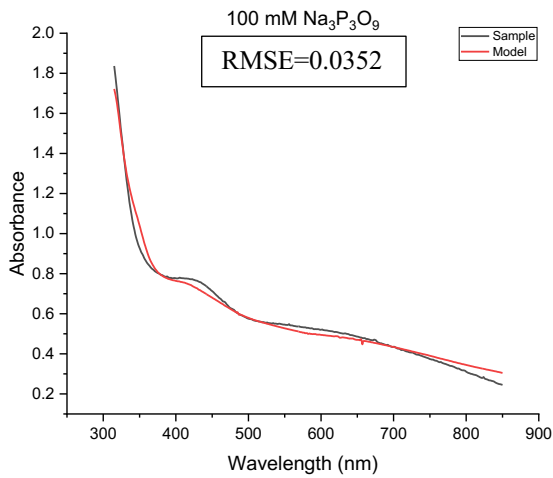
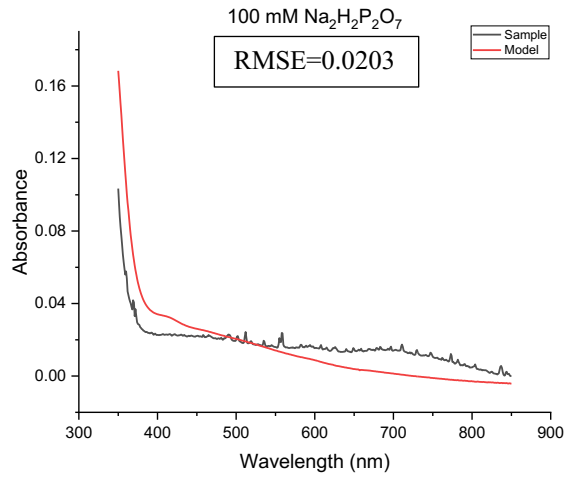
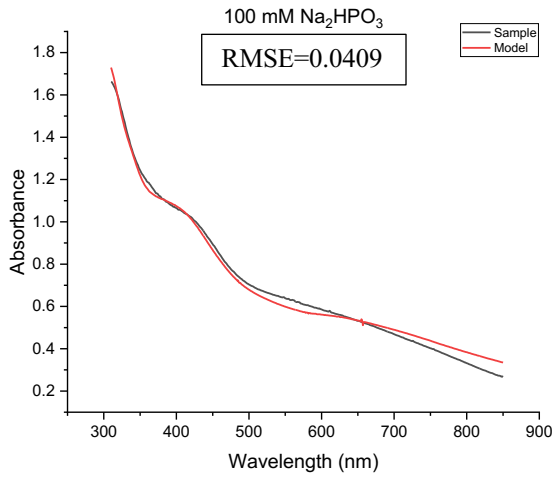
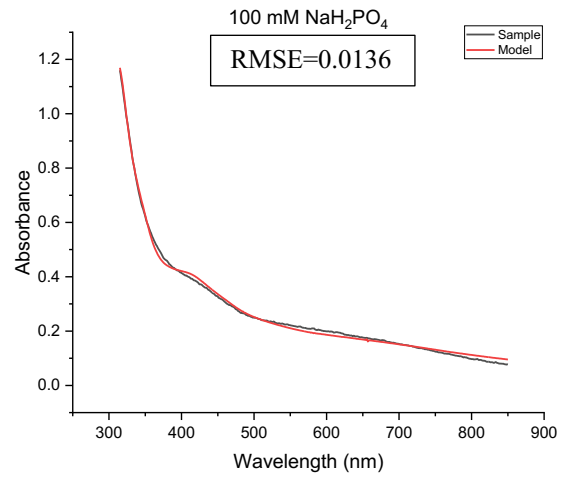
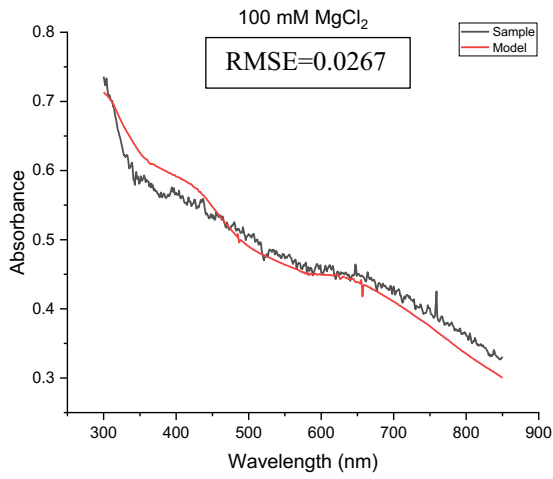


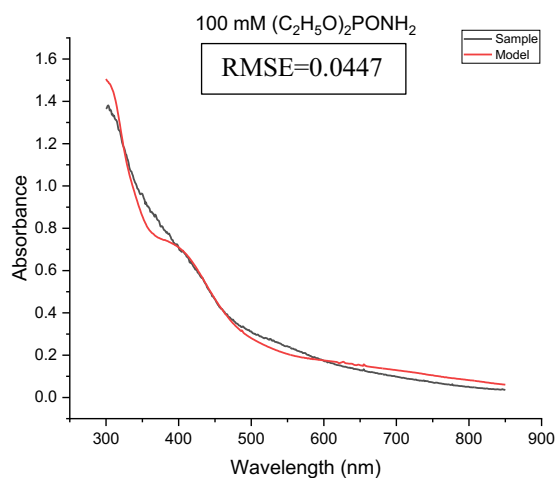




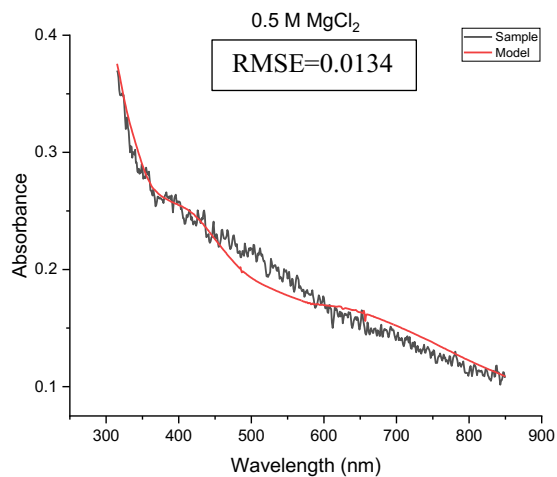
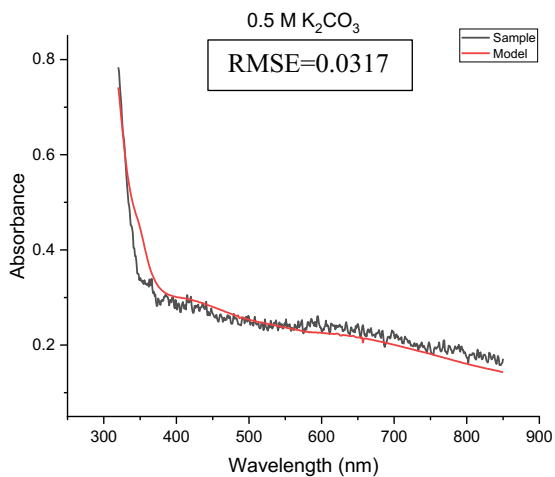
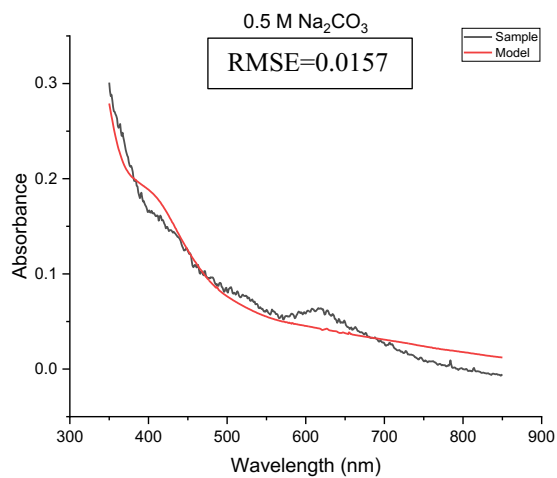
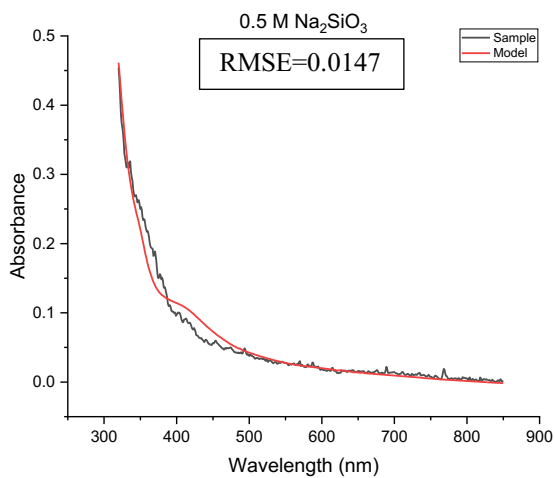
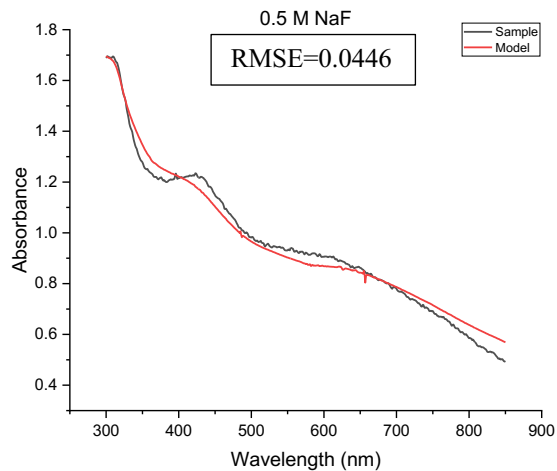
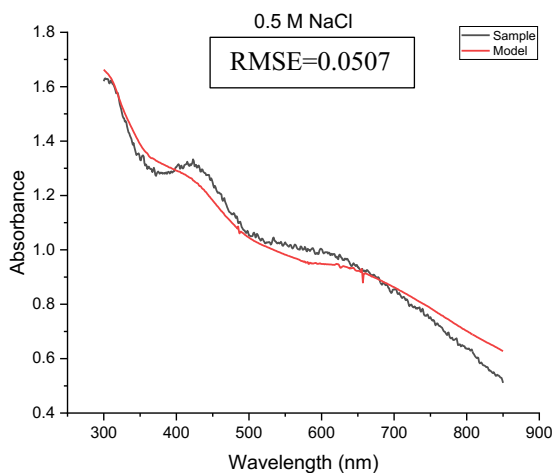
**Figure A.4.** Individual absorption spectra for iron-sulfur N-acetyl-L-cysteine methyl ester under 100 μM additive conditions. 100 μM additive was added into a solution of 5 mM N-acetyl-L-cysteine methyl ester, 0.8 mM  $\text{Na}_2\text{S}$ , and 0.4 mM  $\text{FeCl}_3$ , pH 8.7. Black lines are sample spectra, red lines represent fitted models using Fit-FeS. The data here were used to generate the plots in Figure 2.9. All spectra are the average of triplicates. Root mean square errors (RMSE) were calculated.

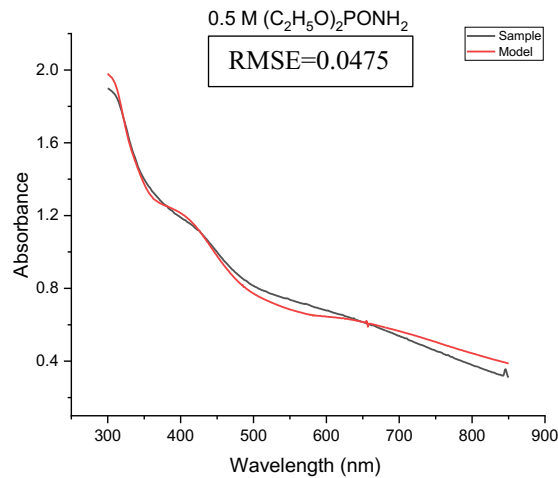
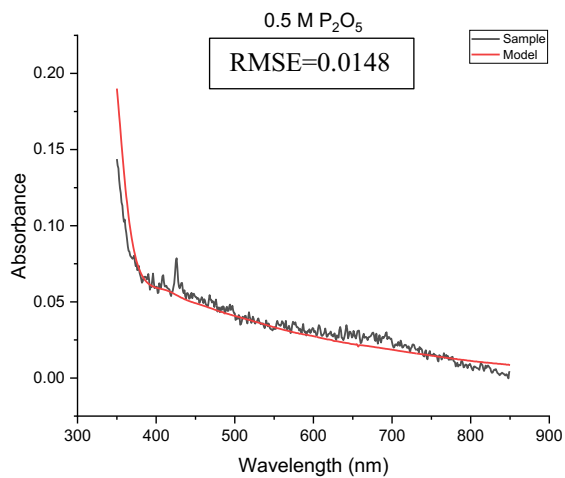
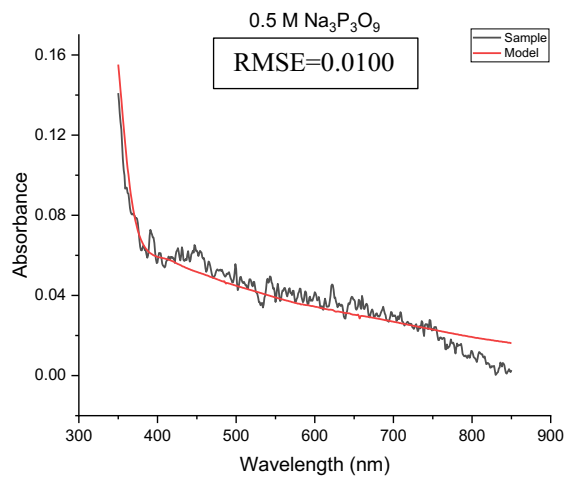
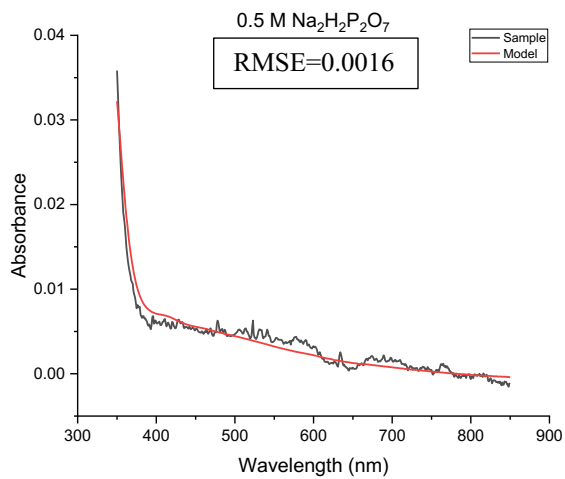
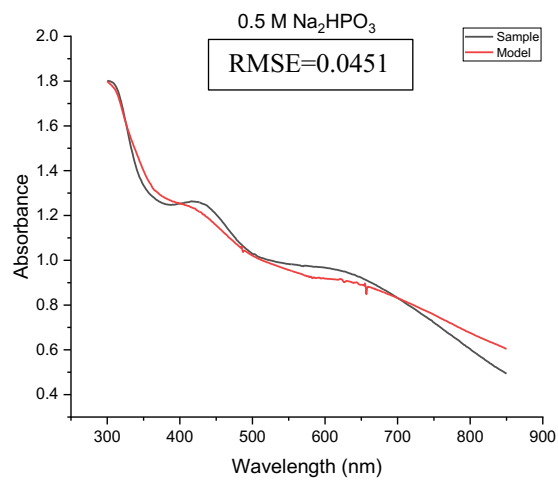
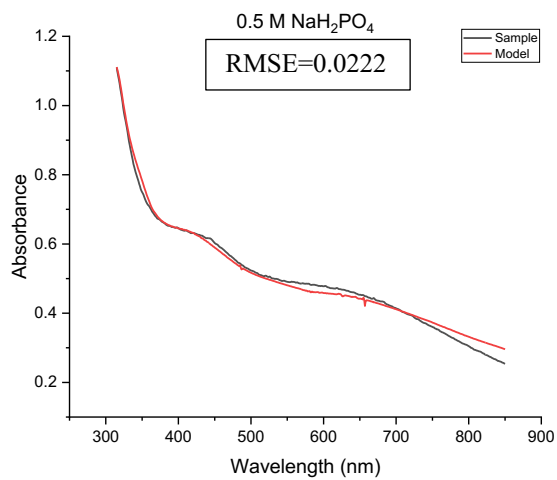


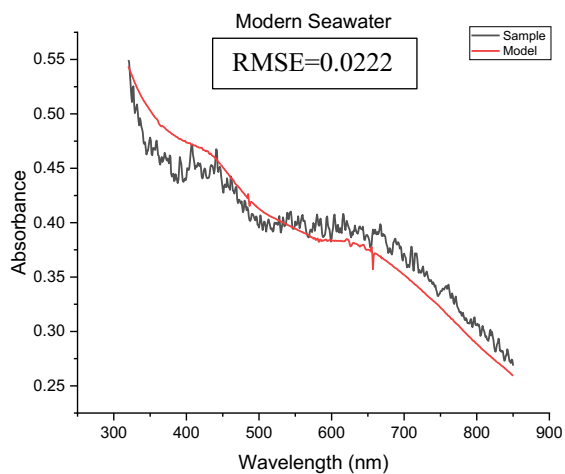




**Figure A.5.** Individual absorption spectra for iron-sulfur N-acetyl-L-cysteine methyl ester under 100 mM additive conditions. 100 mM additive was added into a solution of 5 mM N-acetyl-L-cysteine methyl ester, 0.8 mM Na<sub>2</sub>S, and 0.4 mM FeCl<sub>3</sub>, pH 8.7. Black lines are sample spectra, red lines represent fitted models using Fit-FeS. The data here were used to generate the plots in Figure 2.9. All spectra are the average of triplates. Root mean square errors (RMSE) were calculated.

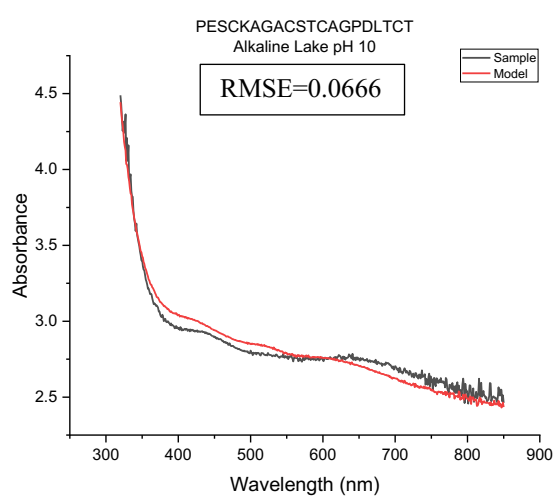
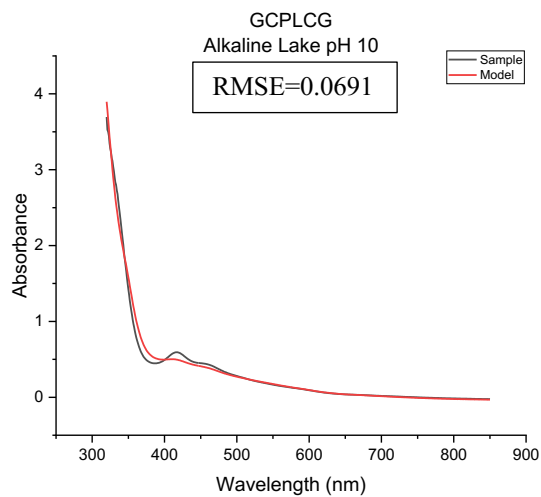
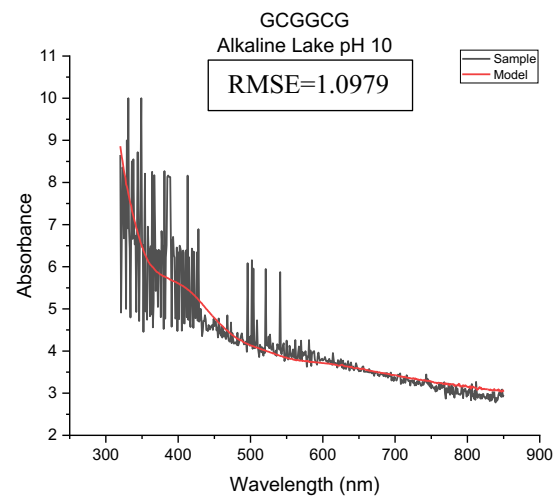
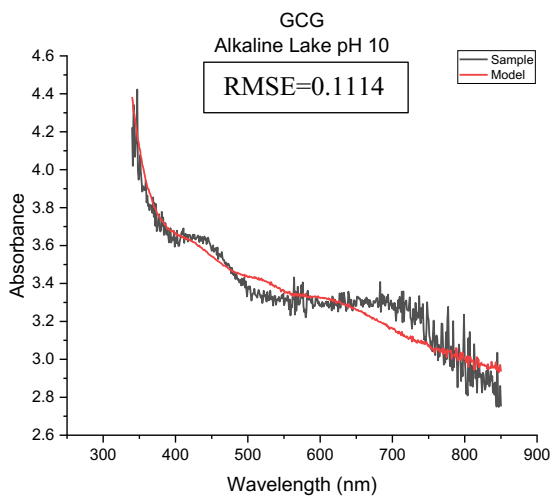
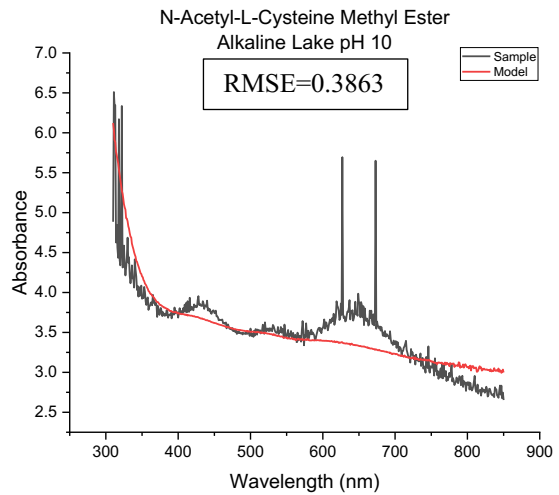
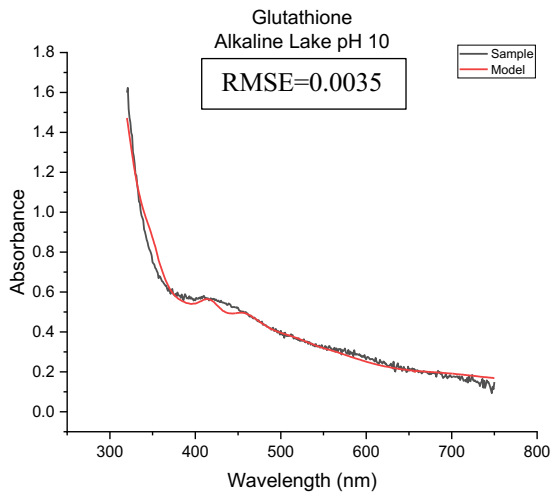


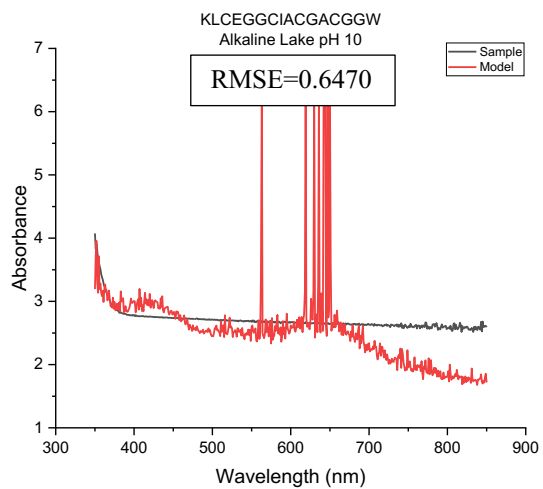




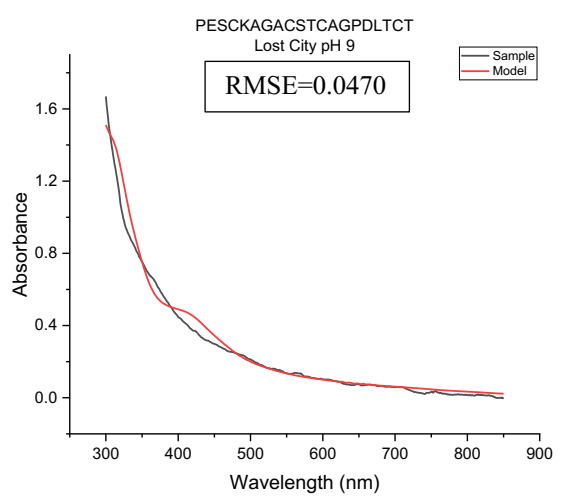
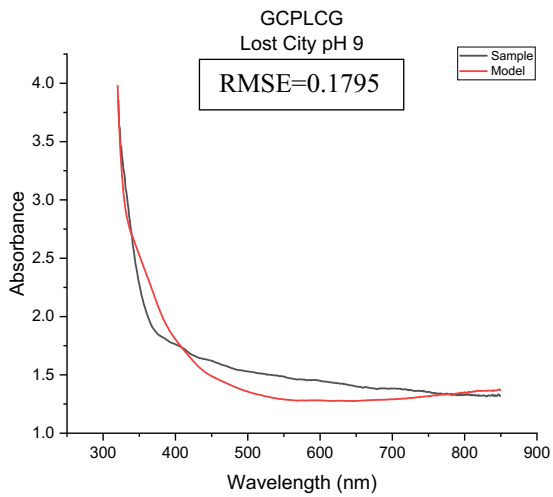
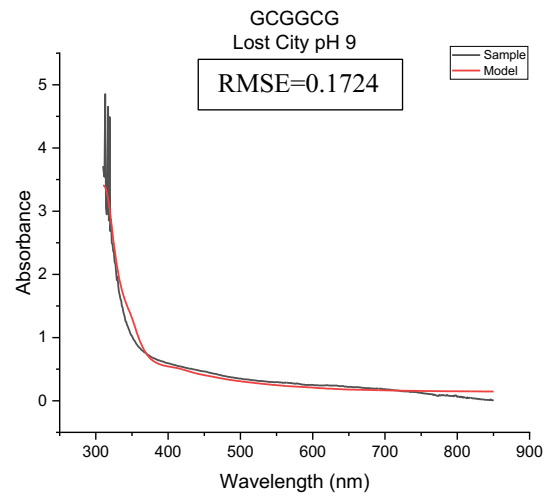
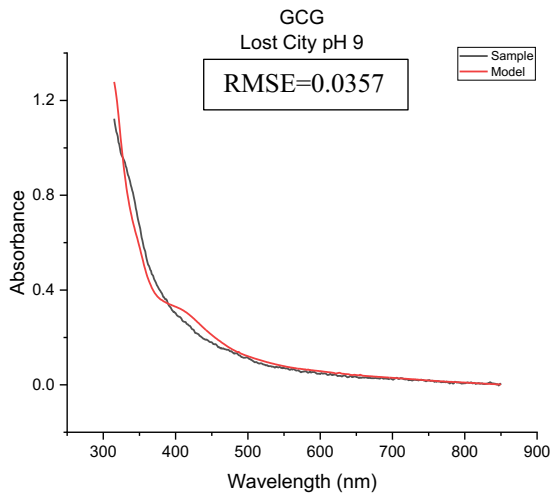
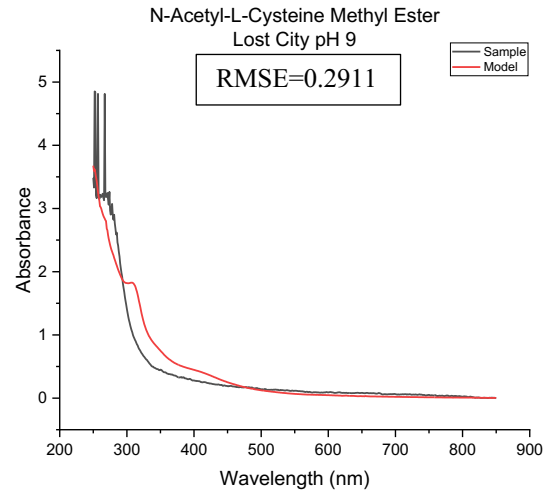
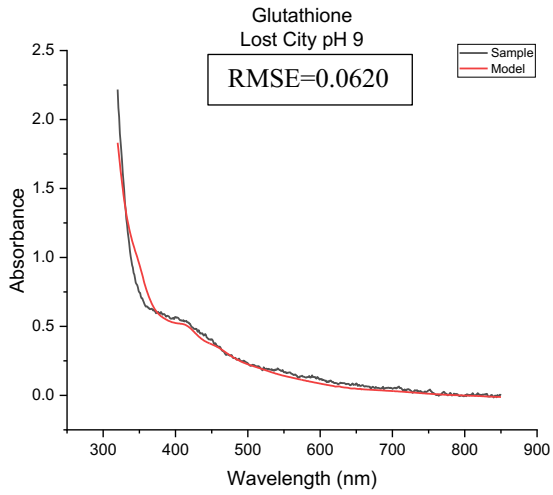
**Figure A.6.** Individual absorption spectra for iron-sulfur N-acetyl-L-cysteine methyl ester under 0.5 M additive conditions. 0.5 M additive was added into a solution of 5 mM N-acetyl-L-cysteine methyl ester, 0.8 mM Na<sub>2</sub>S, and 0.4 mM FeCl<sub>3</sub>, pH 8.7. Black lines are sample spectra, red lines represent fitted models using Fit-FeS. The data here were used to generate the plots in Figure 2.9. All spectra are the average of triplates. Root mean square errors (RMSE) were calculated.

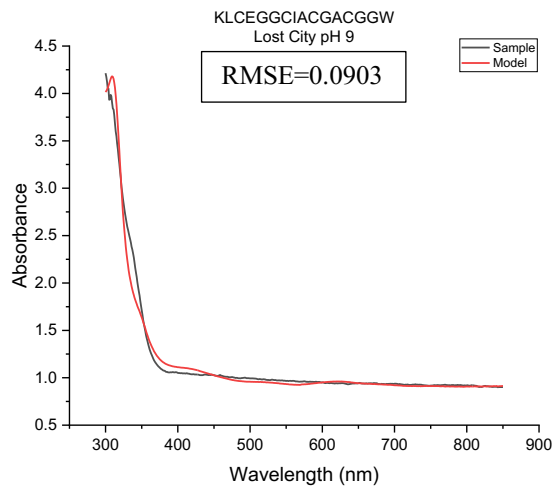




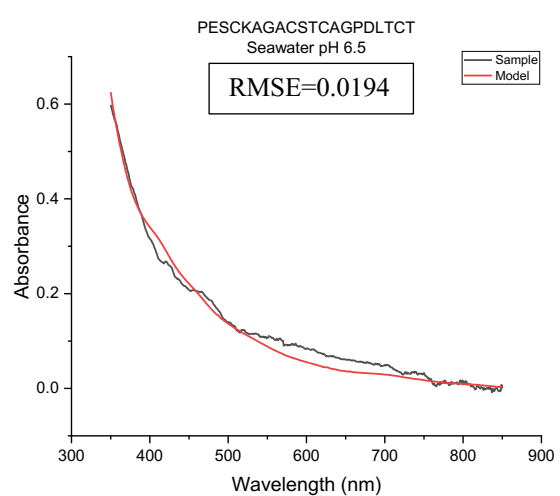
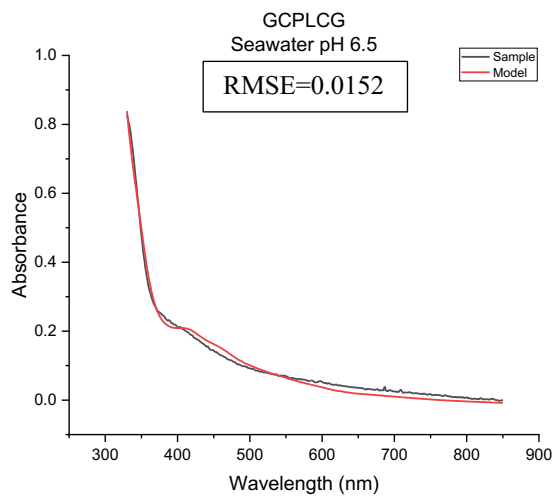
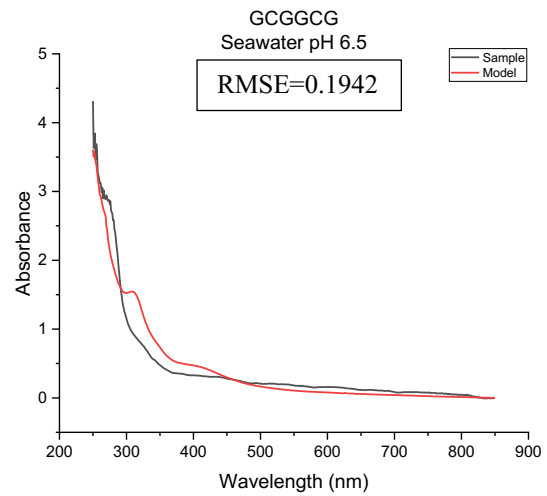
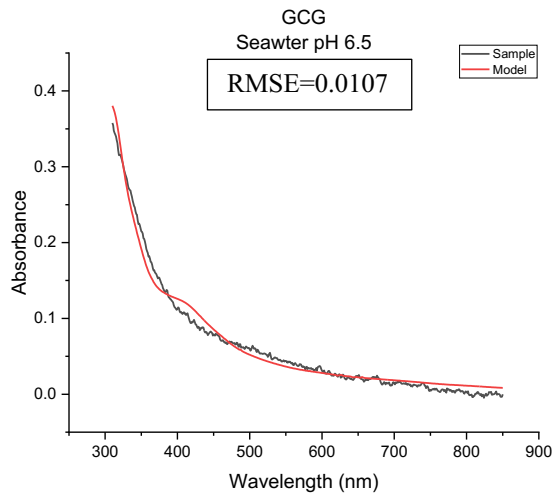
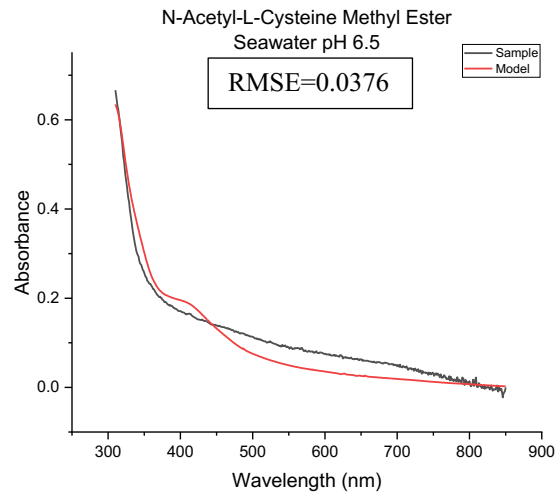
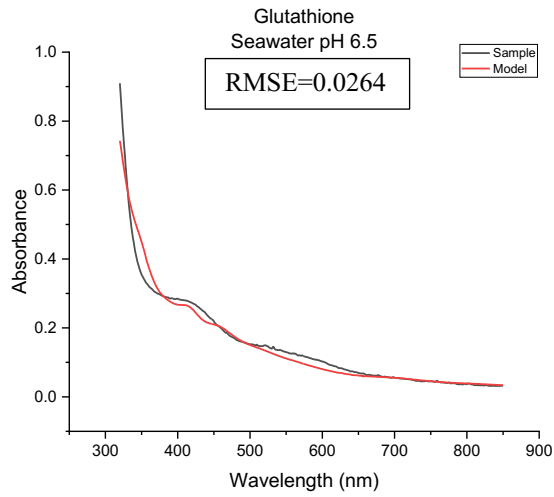


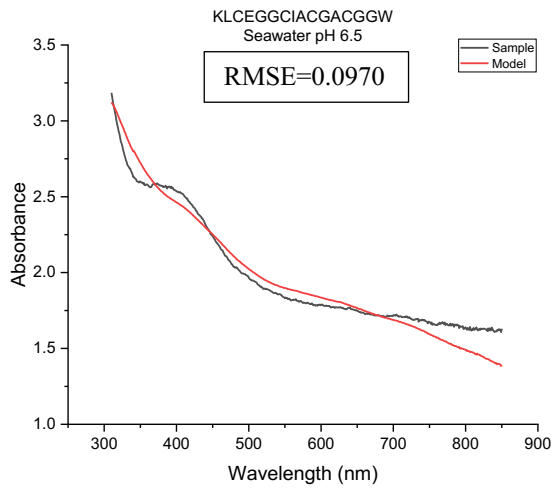
**Figure A.7.** Individual absorption spectra for iron-sulfur peptides under alkaline lake conditions. Black lines are sample spectra, red lines represent fitted models using Fit-FeS. The data here were used to generate the plots in Figure 2.15. All spectra are the average of triplates. Root mean square errors (RMSE) were calculated.



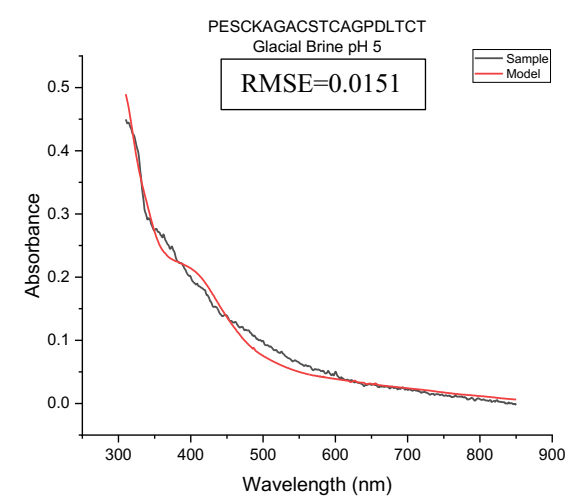
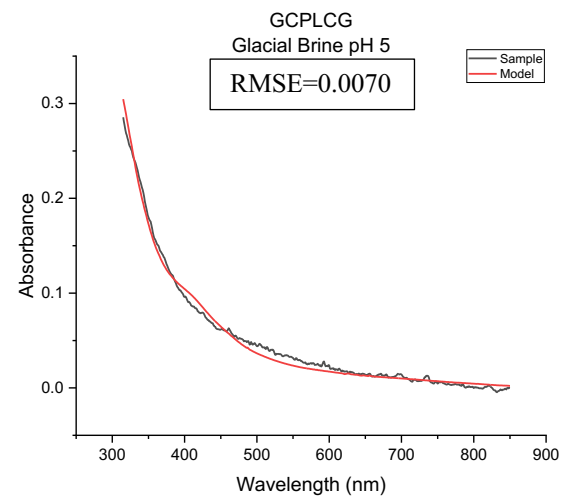
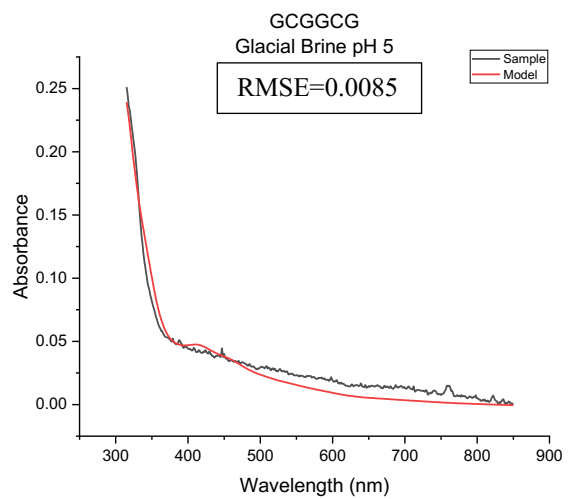
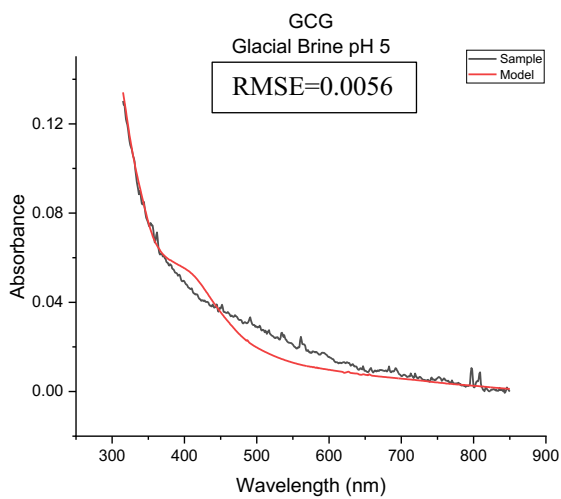
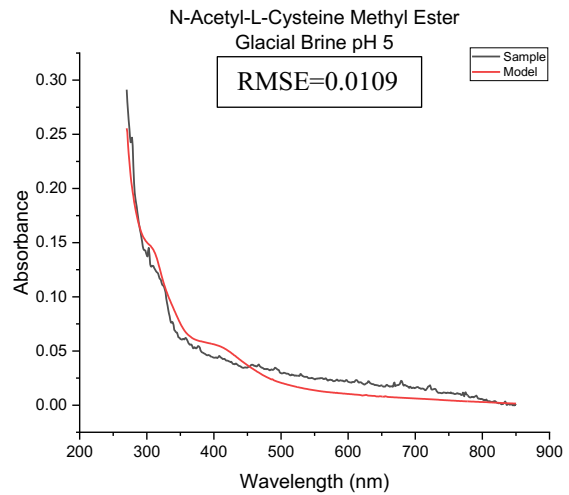
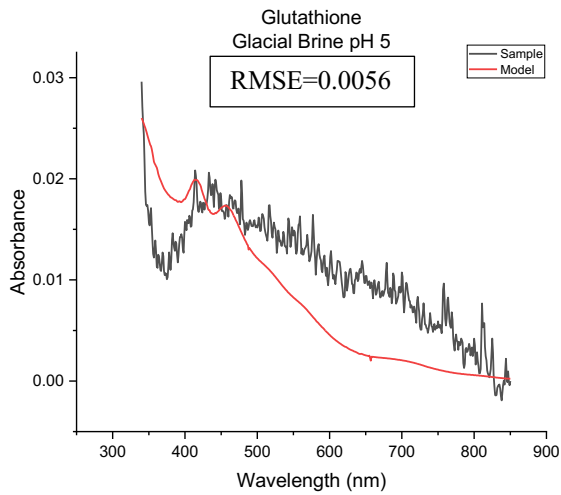


**Figure A.8.** Individual absorption spectra for iron-sulfur peptides under lost city conditions. Black lines are sample spectra, red lines represent fitted models using Fit-FeS. The data here were used to generate the plots in Figure 2.15. All spectra are the average of triplates. Root mean square errors (RMSE) were calculated.





**Figure A.9.** Individual absorption spectra for iron-sulfur peptides under lost city conditions. Black lines are sample spectra, red lines represent fitted models using Fit-FeS. The data here were used to generate the plots in Figure 2.15. All spectra are the average of triplates. Root mean square errors (RMSE) were calculated.



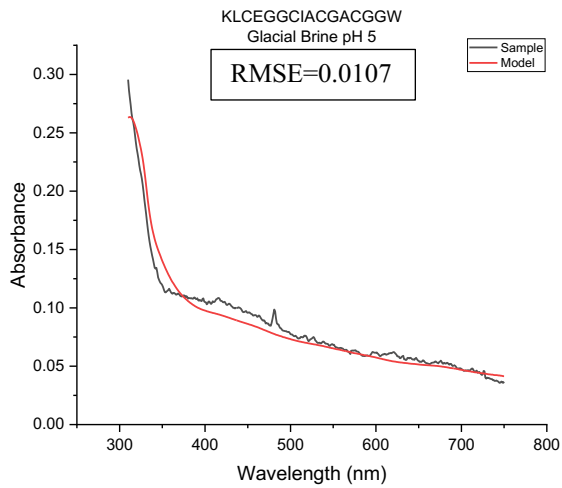


**Figure A.10.** Individual absorption spectra for iron-sulfur peptides under lost city conditions. Black lines are sample spectra, red lines represent fitted models using Fit-FeS. The data here were used to generate the plots in Figure 2.15. All spectra are the average of triplates. Root mean square errors (RMSE) were calculated.

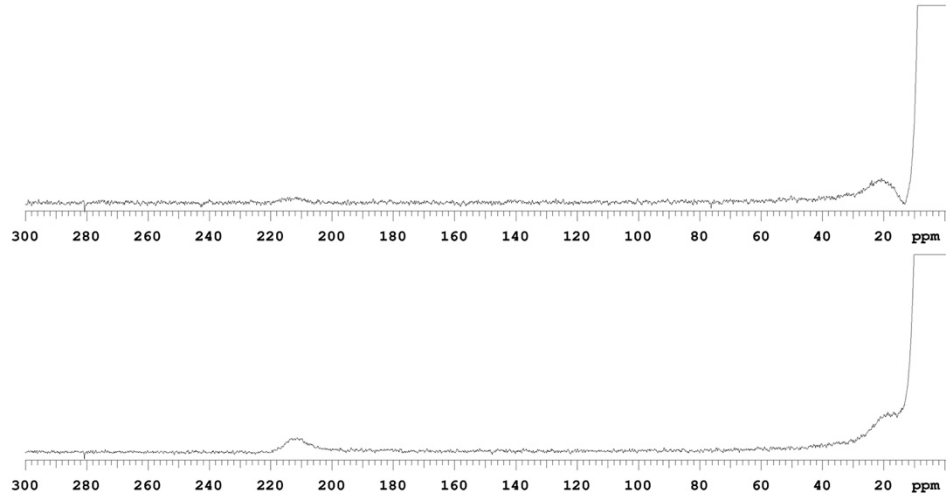


# OpenVnmrj

top- glutathione (alkaline lake) 0 hour  
bottom- glutathione (alkaline lake) 20 hour  
599.927 MHz H1 1D in d2o (ref. to external acetone @ 2.225 ppm)  
temp 26.2 C -> actual temp = 27.0 C, autoxid probe

Department of Chemistry, University of Alberta

Recorded on: 1600, Jul 1 2021	Sweep Width(Hz): 500000	Acquisition Time(s): 0.1	Relaxation Delay(s): 0.25
Pulse Sequence: PRESAT	Digital Res.(Hz/pt): 7.63	Hz per mm(Hz/mm): 769.75	Completed Scans: 1024

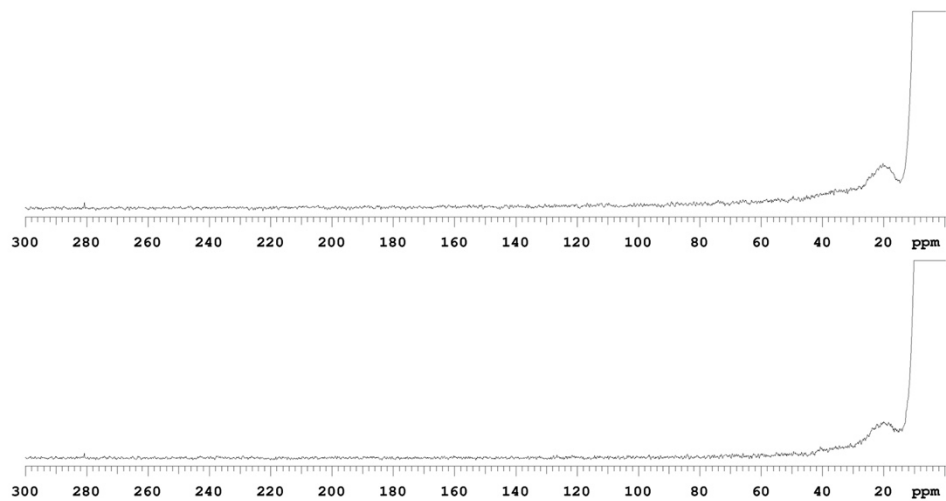


# OpenVnmrj

top-N-acetyl-L-cysteine methyl ester (alkaline lake) 0 hour  
bottom-N-acetyl-L-cysteine methyl ester (alkaline lake) 20 hour  
599.927 MHz H1 1D in d2o (ref. to external acetone @ 2.225 ppm)  
temp 26.2 C -> actual temp = 27.0 C, autoxid probe

Department of Chemistry, University of Alberta

Recorded on: 1600, Aug 5 2021	Sweep Width(Hz): 500000	Acquisition Time(s): 0.1	Relaxation Delay(s): 0.25
Pulse Sequence: PRESAT	Digital Res.(Hz/pt): 7.63	Hz per mm(Hz/mm): 769.75	Completed Scans: 1024

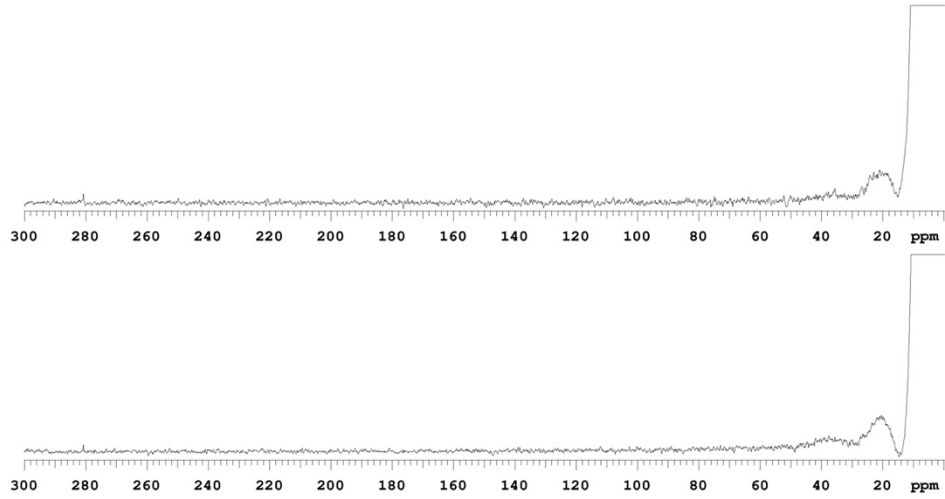


# OpenVnmrj

top-GCG (alkaline lake) 0 hour  
bottom-GCG (alkaline lake) 20 hour  
599.927 MHz H1 1D in d2o (ref. to external acetone @ 2.225 ppm)  
temp 26.2 C -> actual temp = 27.0 C, autoxid probe

Department of Chemistry, University of Alberta

Recorded on: 1600, Aug 5 2021	Sweep Width(Hz): 500000	Acquisition Time(s): 0.1	Relaxation Delay(s): 0.25
Pulse Sequence: PRESAT	Digital Res.(Hz/pt): 7.63	Hz per mm(Hz/mm): 769.75	Completed Scans: 1024

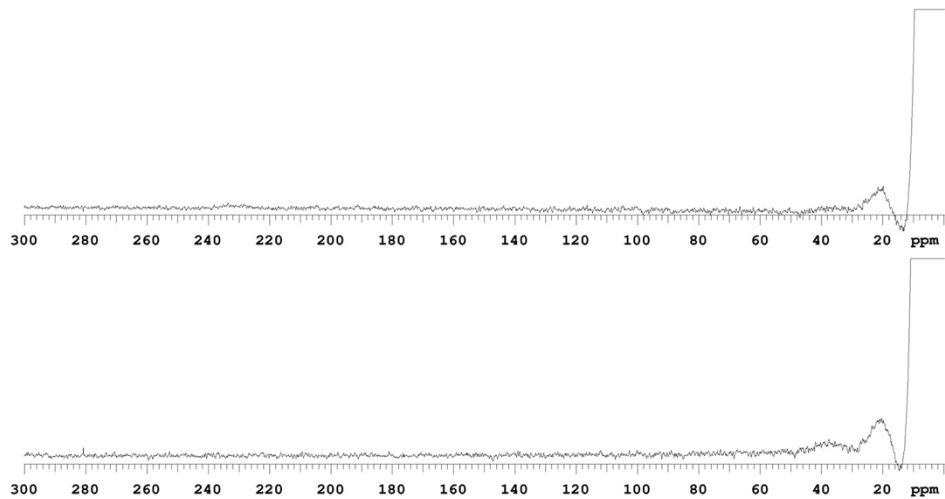


# OpenVnmrj

top-GCGGG (alkaline lake) 0 hour  
bottom-GCGGG (alkaline lake) 20 hour  
599.927 MHz H1 1D in d2o (ref. to external acetone @ 2.225 ppm)  
temp 26.2 C -> actual temp = 27.0 C, autoxid probe

Department of Chemistry, University of Alberta

Recorded on: 1600, Aug 5 2021	Sweep Width(Hz): 500000	Acquisition Time(s): 0.1	Relaxation Delay(s): 0.25
Pulse Sequence: PRESAT	Digital Res.(Hz/pt): 7.63	Hz per mm(Hz/mm): 769.75	Completed Scans: 1024

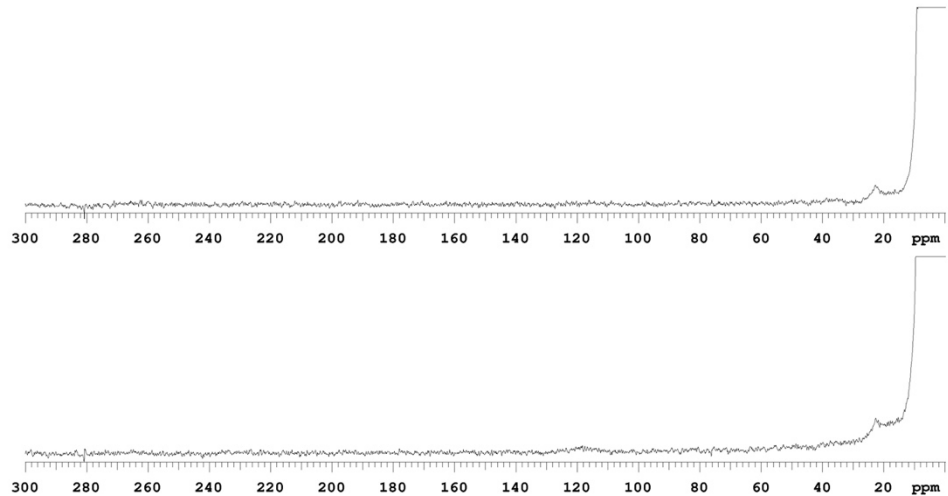


# OpenVnmrj

top-GCLPG (alkaline lake) 0 hour  
bottom-GCLPG (alkaline lake) 20 hour  
599.927 MHz H1 1D in d2o (ref. to external acetone @ 2.225 ppm)  
temp 26.2 C -> actual temp = 27.0 C, autoxid probe

Department of Chemistry, University of Alberta

Recorded on: 1600, Nov 16 2021	Sweep Width(Hz): 500000	Acquisition Time(s): 0.1	Relaxation Delay(s): 0.25
Pulse Sequence: PRESAT	Digital Res.(Hz/pt): 7.63	Hz per mm(Hz/mm): 769.75	Completed Scans: 1024

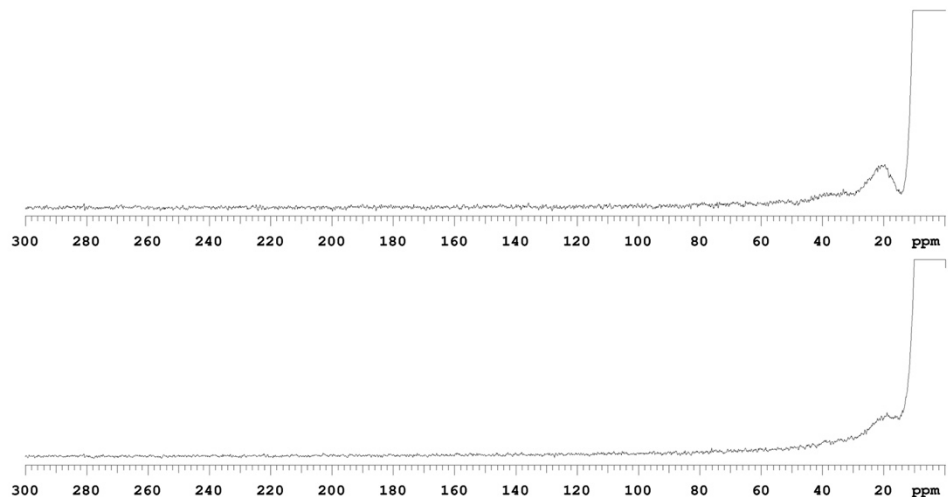


# OpenVnmrj

top-PESCKAGACSTCAGDLTCT (alkaline lake) 0 hour  
bottom-PESCKAGACSTCAGDLTCT (alkaline lake) 20 hour  
599.927 MHz H1 1D in d2o (ref. to external acetone @ 2.225 ppm)  
temp 26.2 C -> actual temp = 27.0 C, autoxid probe

Department of Chemistry, University of Alberta

Recorded on: 1600, Aug 5 2021	Sweep Width(Hz): 500000	Acquisition Time(s): 0.1	Relaxation Delay(s): 0.25
Pulse Sequence: PRESAT	Digital Res.(Hz/pt): 7.63	Hz per mm(Hz/mm): 769.75	Completed Scans: 1024



OpenVnmrj

Department of Chemistry, University of Alberta

Recorded on: 1600, Aug 9 2021  
Pulse Sequence: PRESAT

Sweep Width(Hz): 500000  
Digital Res.(Hz/pt): 7.63

Acquisition Time(s): 0.1  
Hz per mm(Hz/mm): 769.75

Relaxation Delay(s): 0.25  
Completed Scans: 1024

top-KLCEGGCIACGCGGW (alkaline lake) 0 hour  
bottom-KLCEGGCIACGCGGW (alkaline lake) 20 hour  
599.927 MHz  $^1\text{H}$  1D in  $\text{d}_2\text{O}$  (ref. to external acetone @ 2.225 ppm)  
temp 26.2 C -> actual temp = 27.0 C, autoxid probe

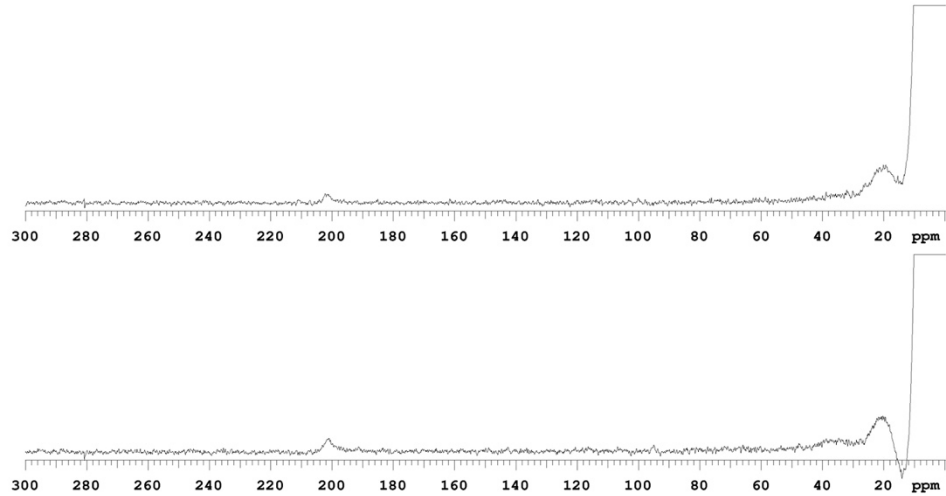


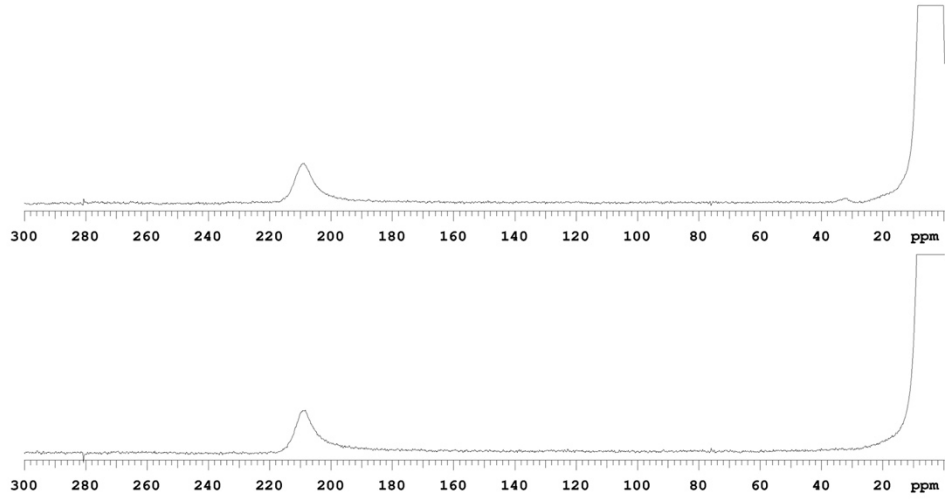
Figure A.11. Paramagnetic  $^1\text{H}$  NMR spectra of iron-sulfur peptides under alkaline lake conditions.

# OpenVnmrj

top- glutathione (lost city) 0 hour  
bottom- glutathione (lost city) 20 hour  
599.927 MHz H1 1D in d2o (ref. to external acetone @ 2.225 ppm)  
temp 26.2 C -> actual temp = 27.0 C, autoxid probe

Department of Chemistry, University of Alberta

Recorded on: 1600, Jul 26 2021	Sweep Width(Hz): 500000	Acquisition Time(s): 0.1	Relaxation Delay(s): 0.25
Pulse Sequence: PRESAT	Digital Res.(Hz/pt): 7.63	Hz per mm(Hz/mm): 769.75	Completed Scans: 1024

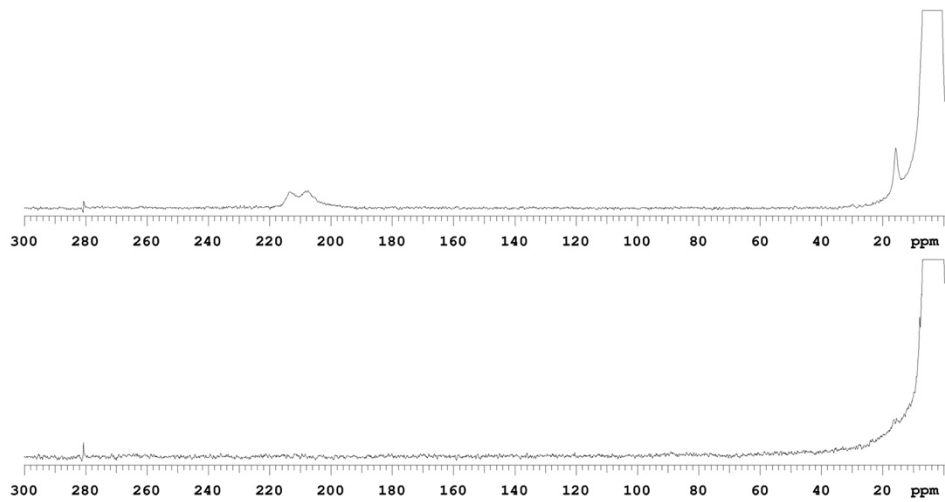


# OpenVnmrj

top-N-acetyl-L-cysteine methyl ester (lost city) 0 hour  
bottom-N-acetyl-L-cysteine methyl ester (lost city) 20 hour  
599.927 MHz H1 1D in d2o (ref. to external acetone @ 2.225 ppm)  
temp 26.2 C -> actual temp = 27.0 C, autoxid probe

Department of Chemistry, University of Alberta

Recorded on: 1600, Jul 30 2021	Sweep Width(Hz): 500000	Acquisition Time(s): 0.1	Relaxation Delay(s): 0.25
Pulse Sequence: PRESAT	Digital Res.(Hz/pt): 7.63	Hz per mm(Hz/mm): 769.75	Completed Scans: 1024



# OpenVnmrj

Department of Chemistry, University of Alberta

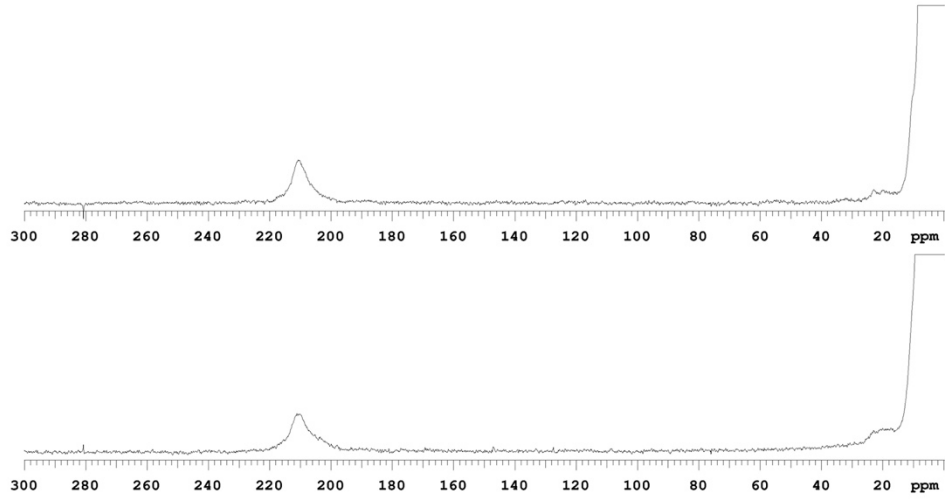
Recorded on: **1600, Jul 30 2021**  
Pulse Sequence: **PRESAT**

Sweep Width(Hz): **500000**  
Digital Res.(Hz/pt): **7.63**

Acquisition Time(s): **0.1**  
Hz per mm(Hz/mm): **769.75**

Relaxation Delay(s): **0.25**  
Completed Scans: **1024**

top-GCG (lost city) 0 hour  
bottom-GCG (lost city) 20 hour  
599.927 MHz H1 1D in d2o (ref. to external acetone @ 2.225 ppm)  
temp 26.2 C -> actual temp = 27.0 C, autoxid probe



# OpenVnmrj

Department of Chemistry, University of Alberta

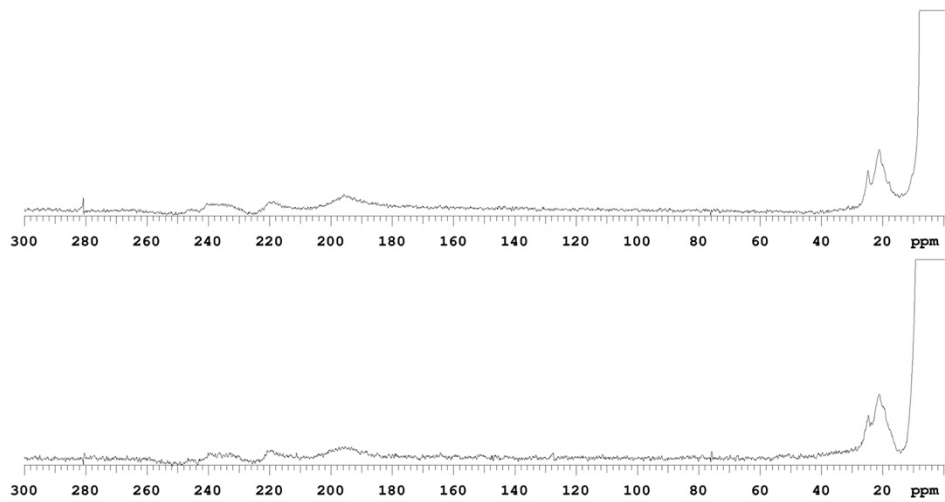
Recorded on: **1600, Jul 30 2021**  
Pulse Sequence: **PRESAT**

Sweep Width(Hz): **500000**  
Digital Res.(Hz/pt): **7.63**

Acquisition Time(s): **0.1**  
Hz per mm(Hz/mm): **769.75**

Relaxation Delay(s): **0.25**  
Completed Scans: **1024**

top-GCGGCG (lost city) 0 hour  
bottom-GCGGCG (lost city) 20 hour  
599.927 MHz H1 1D in d2o (ref. to external acetone @ 2.225 ppm)  
temp 26.2 C -> actual temp = 27.0 C, autoxid probe

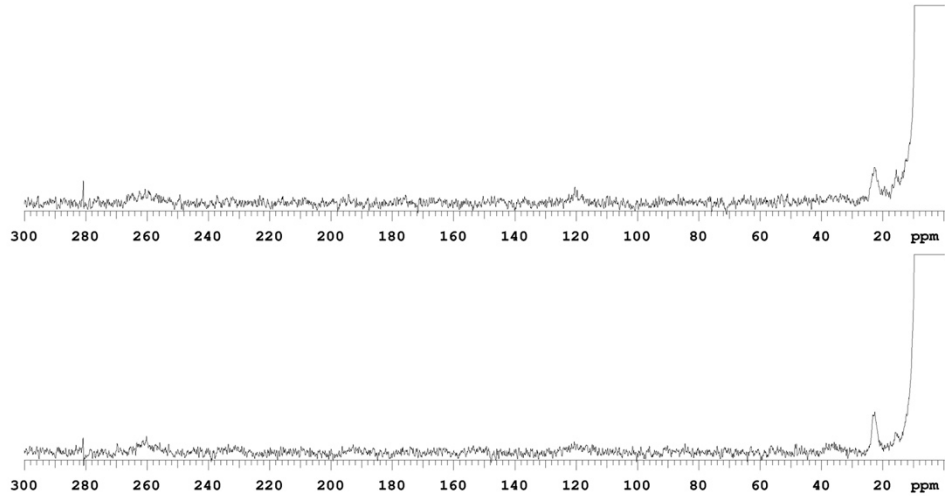


# OpenVnmrj

Department of Chemistry, University of Alberta

Recorded on: <b>1600, Nov 16 2021</b>	Sweep Width(Hz): <b>500000</b>	Acquisition Time(s): <b>0.1</b>	Relaxation Delay(s): <b>0.25</b>
Pulse Sequence: <b>PRESAT</b>	Digital Res.(Hz/pt): <b>7.63</b>	Hz per mm(Hz/mm): <b>769.75</b>	Completed Scans: <b>1024</b>

top-GCPLCG (lost city) 0 hour  
bottom-GCPLCG (lost city) 20 hour  
599.927 MHz H1 1D in d2o (ref. to external acetone @ 2.225 ppm)  
temp 26.2 C -> actual temp = 27.0 C, autoxid probe

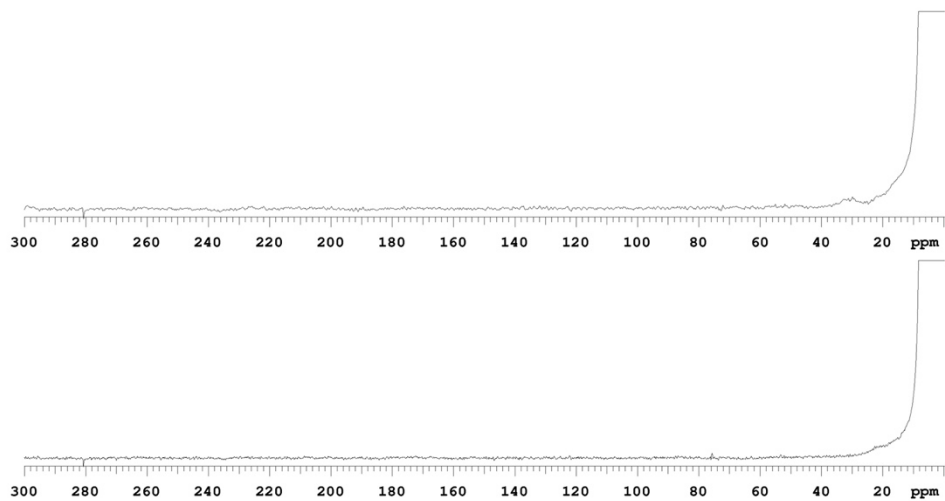


# OpenVnmrj

Department of Chemistry, University of Alberta

Recorded on: <b>1600, Jul 30 2021</b>	Sweep Width(Hz): <b>500000</b>	Acquisition Time(s): <b>0.1</b>	Relaxation Delay(s): <b>0.25</b>
Pulse Sequence: <b>PRESAT</b>	Digital Res.(Hz/pt): <b>7.63</b>	Hz per mm(Hz/mm): <b>769.75</b>	Completed Scans: <b>1024</b>

top-PESCKAGACSTCAGPDLTCT (lost city) 0 hour  
bottom-PESCKAGACSTCAGPDLTCT (lost city) 20 hour  
599.927 MHz H1 1D in d2o (ref. to external acetone @ 2.225 ppm)  
temp 26.2 C -> actual temp = 27.0 C, autoxid probe



OpenVnmrj

Department of Chemistry, University of Alberta

Recorded on: 1600, Aug 9 2021  
Pulse Sequence: PRESAT

Sweep Width(Hz): 500000  
Digital Res.(Hz/pt): 7.63

Acquisition Time(s): 0.1  
Hz per mm(Hz/mm): 769.75

Relaxation Delay(s): 0.25  
Completed Scans: 1024

top-KLCEGGCIACGCGGW (lost city) 0 hour  
bottom-KLCEGGCIACGCGGW (lost city) 20 hour  
599.927 MHz H1 1D in d2o (ref. to external acetone @ 2.225 ppm)  
temp 26.2 C -> actual temp = 27.0 C, autoxid probe

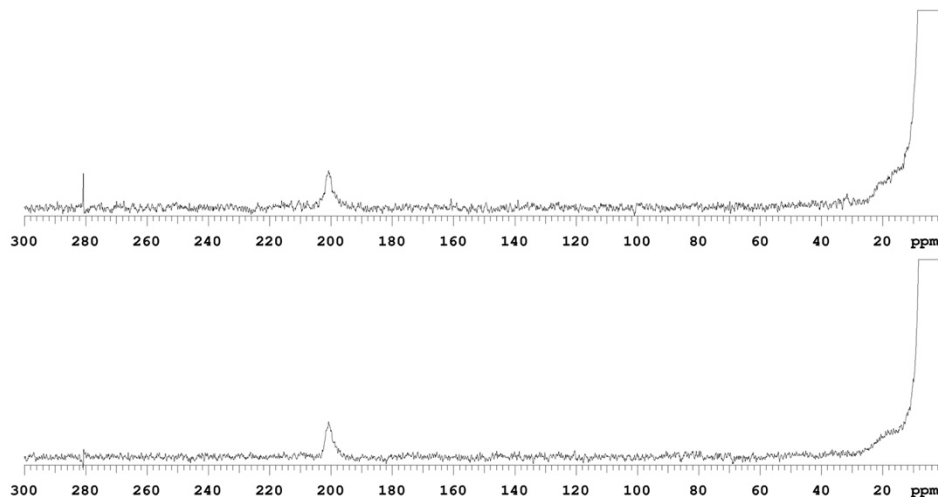


Figure A.12. Paramagnetic  $^1\text{H}$  NMR spectra of iron-sulfur peptides under lost city conditions.

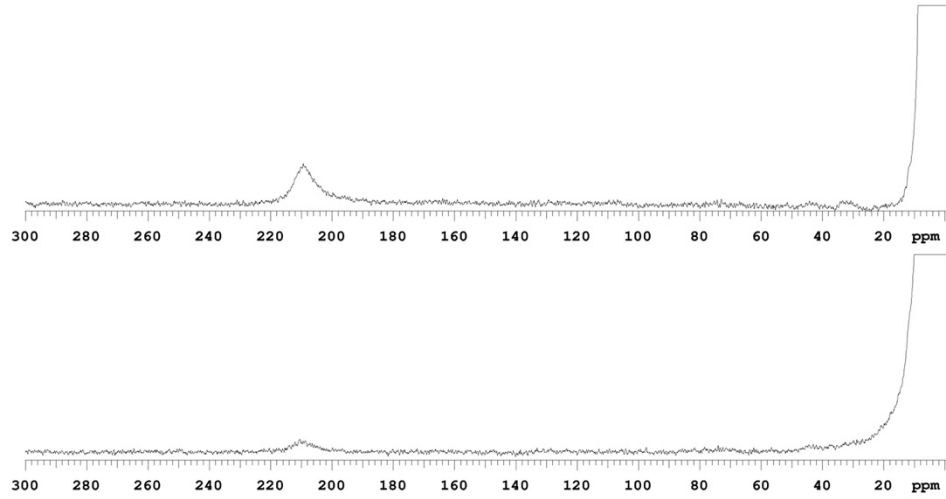


# OpenVnmrj

top- glutathione (seawater) 0 hour  
bottom- glutathione (seawater) 20 hour  
599.927 MHz H1 1D in d2o (ref. to external acetone @ 2.225 ppm)  
temp 26.2 C -> actual temp = 27.0 C, autoxid probe

Department of Chemistry, University of Alberta

Recorded on: 1600, Jun 11 2021	Sweep Width(Hz): 500000	Acquisition Time(s): 0.1	Relaxation Delay(s): 0.25
Pulse Sequence: PRESAT	Digital Res.(Hz/pt): 7.63	Hz per mm(Hz/mm): 769.75	Completed Scans: 1024

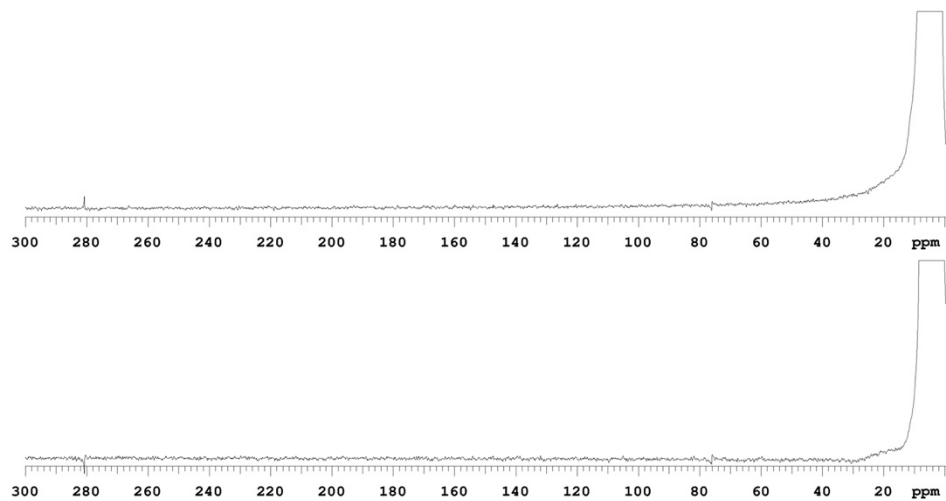


# OpenVnmrj

top-N-acetyl-L-cysteine methyl ester (seawater) 0 hour  
bottom-N-acetyl-L-cysteine methyl ester (seawater) 20 hour  
599.927 MHz H1 1D in d2o (ref. to external acetone @ 2.225 ppm)  
temp 26.2 C -> actual temp = 27.0 C, autoxid probe

Department of Chemistry, University of Alberta

Recorded on: 1600, Aug 2 2021	Sweep Width(Hz): 500000	Acquisition Time(s): 0.1	Relaxation Delay(s): 0.25
Pulse Sequence: PRESAT	Digital Res.(Hz/pt): 7.63	Hz per mm(Hz/mm): 769.75	Completed Scans: 1024

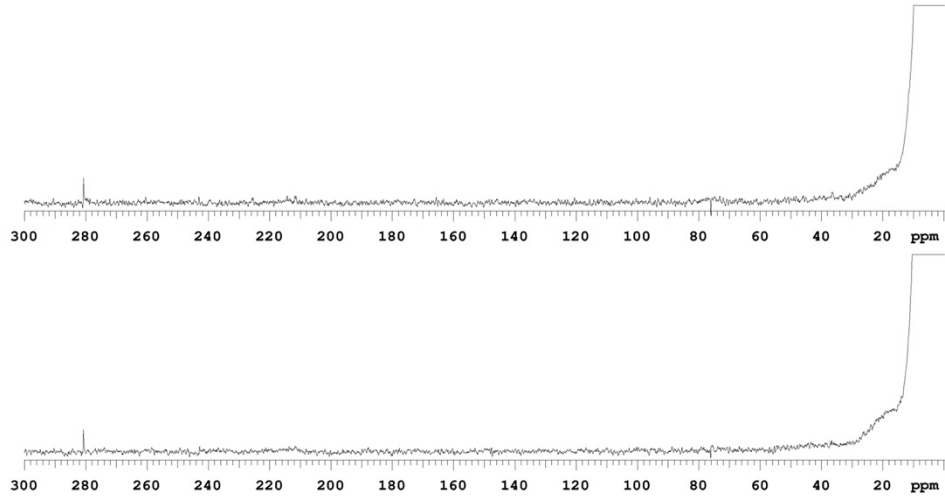


# OpenVnmrj

top-GCG (seawater) 0 hour  
bottom-GCG (seawater) 20 hour  
599.927 MHz <sup>1</sup>H 1D in d<sub>2</sub>O (ref. to external acetone @ 2.225 ppm)  
temp 26.2 C -> actual temp = 27.0 C, autoxid probe

Department of Chemistry, University of Alberta

Recorded on: 1600, Aug 2 2021	Sweep Width(Hz): 500000	Acquisition Time(s): 0.1	Relaxation Delay(s): 0.25
Pulse Sequence: PRESAT	Digital Res.(Hz/pt): 7.63	Hz per mm(Hz/mm): 769.75	Completed Scans: 1024

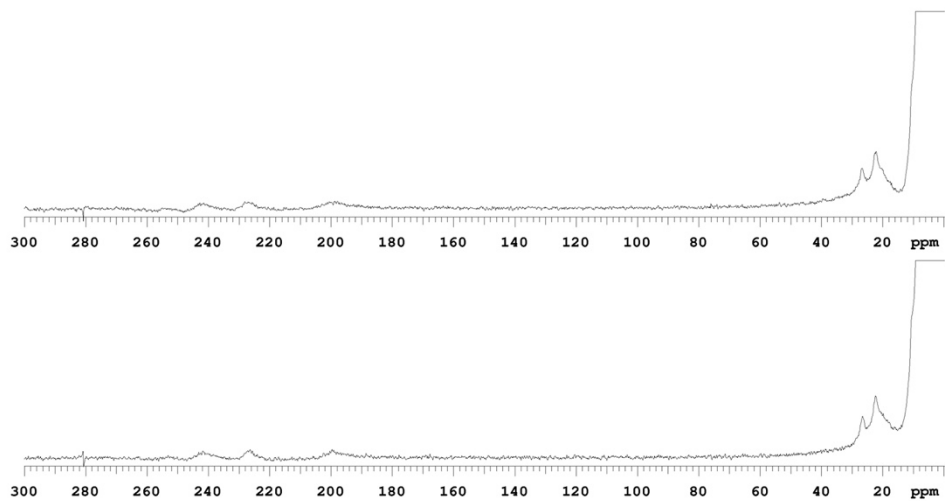


# OpenVnmrj

top-GCGGGG (seawater) 0 hour  
bottom-GCGGGG (seawater) 20 hour  
599.927 MHz <sup>1</sup>H 1D in d<sub>2</sub>O (ref. to external acetone @ 2.225 ppm)  
temp 26.2 C -> actual temp = 27.0 C, autoxid probe

Department of Chemistry, University of Alberta

Recorded on: 1600, Aug 2 2021	Sweep Width(Hz): 500000	Acquisition Time(s): 0.1	Relaxation Delay(s): 0.25
Pulse Sequence: PRESAT	Digital Res.(Hz/pt): 7.63	Hz per mm(Hz/mm): 769.75	Completed Scans: 1024

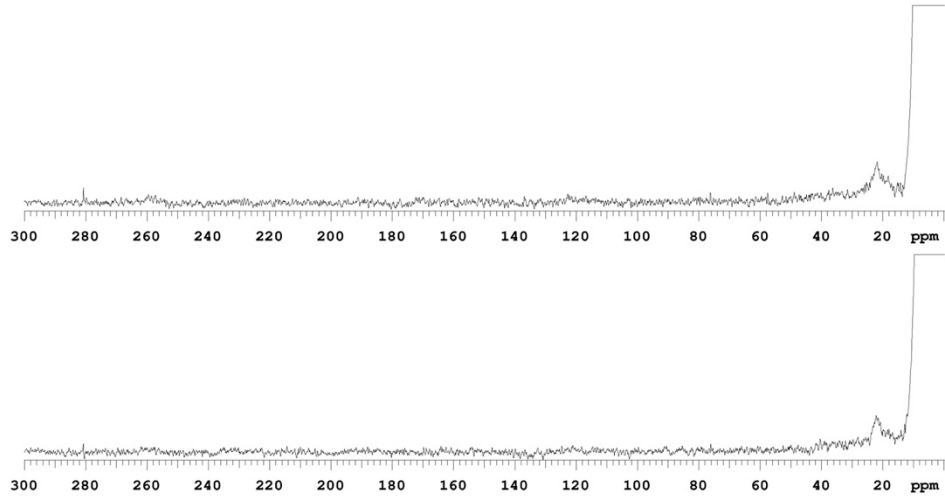


# OpenVnmrj

top-GCPLCG (seawater) 0 hour  
bottom-GCPLCG (seawater) 20 hour  
599.927 MHz H1 1D in d2o (ref. to external acetone @ 2.225 ppm)  
temp 26.2 C -> actual temp = 27.0 C, autoxid probe

Department of Chemistry, University of Alberta

Recorded on: 1600, Nov 16 2021	Sweep Width(Hz): 500000	Acquisition Time(s): 0.1	Relaxation Delay(s): 0.25
Pulse Sequence: PRESAT	Digital Res.(Hz/pt): 7.63	Hz per mm(Hz/mm): 769.75	Completed Scans: 1024

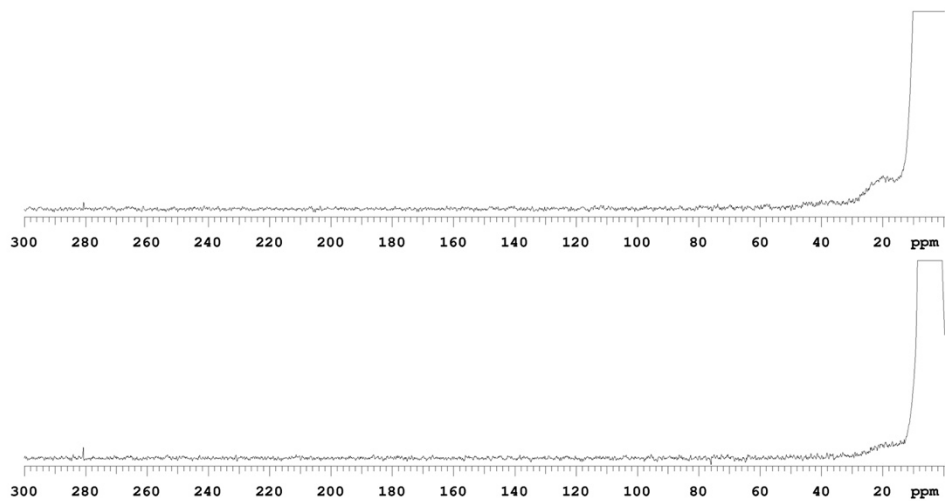


# OpenVnmrj

top-PESCKAGACSTCAGPDLTCT (seawater) 0 hour  
bottom-PESCKAGACSTCAGPDLTCT (seawater) 20 hour  
599.927 MHz H1 1D in d2o (ref. to external acetone @ 2.225 ppm)  
temp 26.2 C -> actual temp = 27.0 C, autoxid probe

Department of Chemistry, University of Alberta

Recorded on: 1600, Aug 4 2021	Sweep Width(Hz): 500000	Acquisition Time(s): 0.1	Relaxation Delay(s): 0.25
Pulse Sequence: PRESAT	Digital Res.(Hz/pt): 7.63	Hz per mm(Hz/mm): 769.75	Completed Scans: 1024



OpenVnmrj

Department of Chemistry, University of Alberta

Recorded on: 1600, Aug 6 2021  
Pulse Sequence: PRESAT

Sweep Width(Hz): 500000  
Digital Res.(Hz/pt): 7.63

Acquisition Time(s): 0.1  
Hz per mm(Hz/mm): 769.75

Relaxation Delay(s): 0.25  
Completed Scans: 1024

top-KLCEGGCIACGCGGW (seawater) 0 hour  
bottom-KLCEGGCIACGCGGW (seawater) 20 hour  
599.927 MHz H1 1D in d2o (ref. to external acetone @ 2.225 ppm)  
temp 26.2 C -> actual temp = 27.0 C, autoxid probe

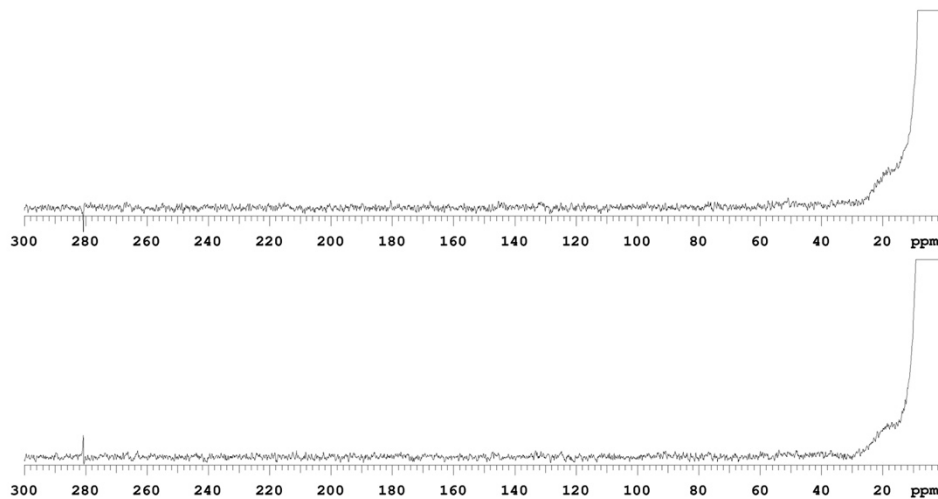


Figure A.13. Paramagnetic  $^1\text{H}$  NMR spectra of iron-sulfur peptides under seawater conditions.

Department of Chemistry, University of Alberta

Recorded on: **1600, Jul 26 2021**  
Pulse Sequence: **PRESAT**

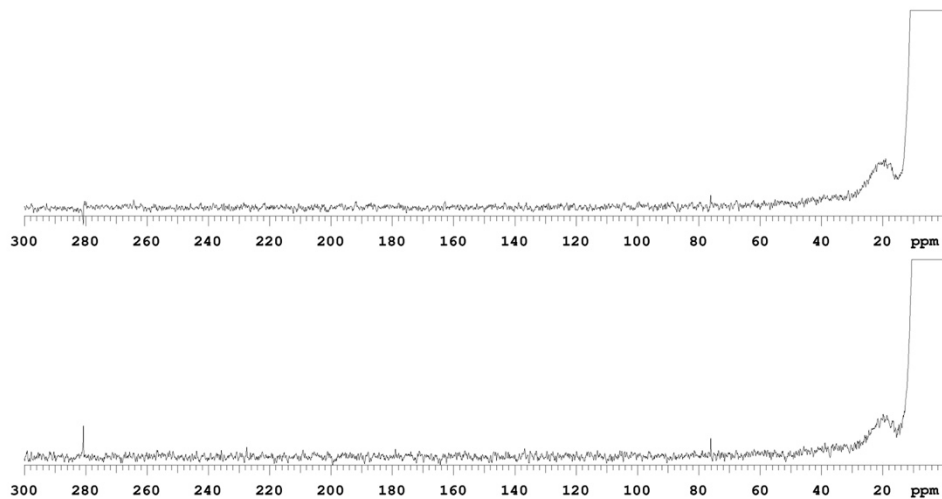
Sweep Width(Hz): **500000**  
Digital Res.(Hz/pt): **7.63**

Acquisition Time(s): **0.1**  
Hz per mm(Hz/mm): **769.75**

Relaxation Delay(s): **0.25**  
Completed Scans: **1024**

## OpenVnmrj

top- glutathione (glacial brine) 0 hour  
bottom- glutathione (glacial brine) 20 hour  
599.927 MHz H1 1D in d2o (ref. to external acetone @ 2.225 ppm)  
temp 26.2 C -> actual temp = 27.0 C, autoxid probe



Department of Chemistry, University of Alberta

Recorded on: **1600, Aug 4 2021**  
Pulse Sequence: **PRESAT**

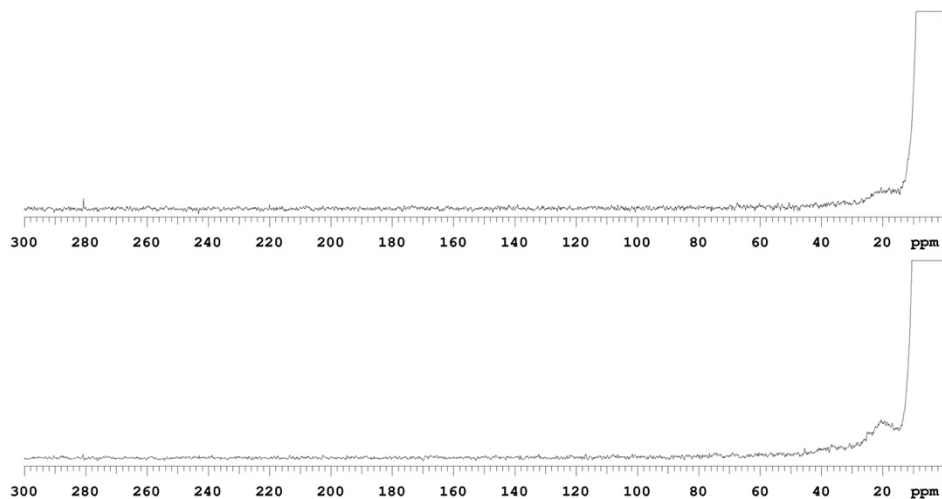
Sweep Width(Hz): **500000**  
Digital Res.(Hz/pt): **7.63**

Acquisition Time(s): **0.1**  
Hz per mm(Hz/mm): **769.75**

Relaxation Delay(s): **0.25**  
Completed Scans: **1024**

## OpenVnmrj

top-N-acetyl-L-cysteine methyl ester (glacial brine) 0 hour  
bottom-N-acetyl-L-cysteine methyl ester (glacial brine) 20 hour  
599.927 MHz H1 1D in d2o (ref. to external acetone @ 2.225 ppm)  
temp 26.2 C -> actual temp = 27.0 C, autoxid probe

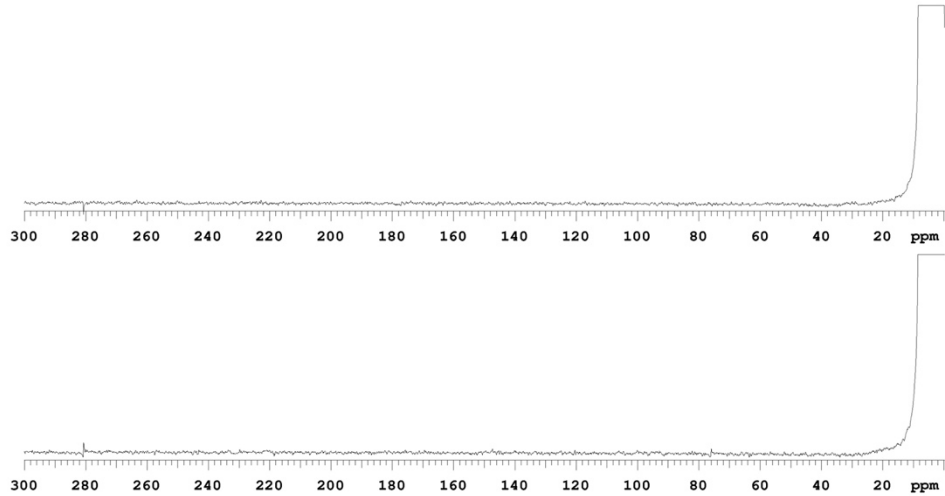


# OpenVnmrj

top-GCG (glacial brine) 0 hour  
bottom-GCG (glacial brine) 20 hour  
599.927 MHz H1 1D in d2o (ref. to external acetone @ 2.225 ppm)  
temp 26.2 C -> actual temp = 27.0 C, autoxid probe

Department of Chemistry, University of Alberta

Recorded on: 1600, Aug 2 2021	Sweep Width(Hz): 500000	Acquisition Time(s): 0.1	Relaxation Delay(s): 0.25
Pulse Sequence: PRESAT	Digital Res.(Hz/pt): 7.63	Hz per mm(Hz/mm): 769.75	Completed Scans: 1024

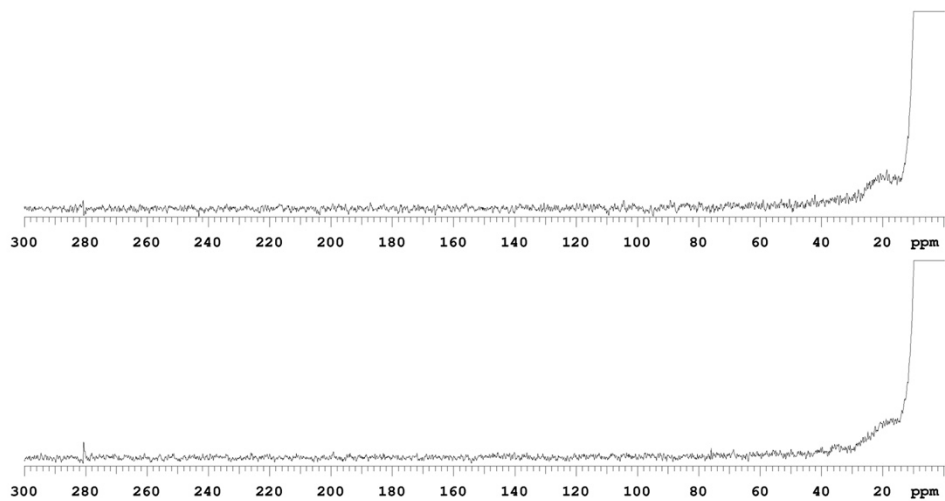


# OpenVnmrj

top-GCGGGC (glacial brine) 0 hour  
bottom-GCGGGC (glacial brine) 20 hour  
599.927 MHz H1 1D in d2o (ref. to external acetone @ 2.225 ppm)  
temp 26.2 C -> actual temp = 27.0 C, autoxid probe

Department of Chemistry, University of Alberta

Recorded on: 1600, Aug 4 2021	Sweep Width(Hz): 500000	Acquisition Time(s): 0.1	Relaxation Delay(s): 0.25
Pulse Sequence: PRESAT	Digital Res.(Hz/pt): 7.63	Hz per mm(Hz/mm): 769.75	Completed Scans: 1024

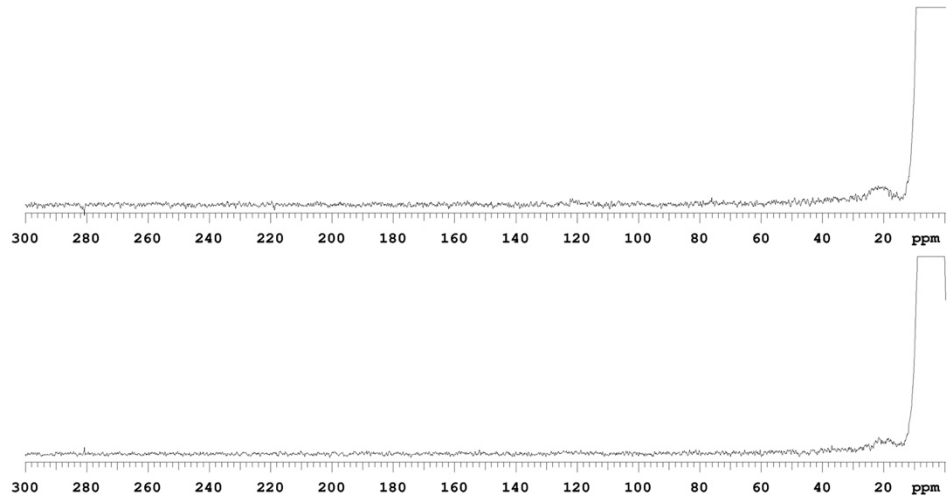


# OpenVnmrj

top-GCPLCG (glacial brine) 0 hour  
bottom-GCPLCG (glacial brine) 20 hour  
599.927 MHz H1 1D in d2o (ref. to external acetone @ 2.225 ppm)  
temp 26.2 C -> actual temp = 27.0 C, autoxid probe

Department of Chemistry, University of Alberta

Recorded on: 1600, Nov 16 2021	Sweep Width(Hz): 500000	Acquisition Time(s): 0.1	Relaxation Delay(s): 0.25
Pulse Sequence: PRESAT	Digital Res.(Hz/pt): 7.63	Hz per mm(Hz/mm): 769.75	Completed Scans: 1024

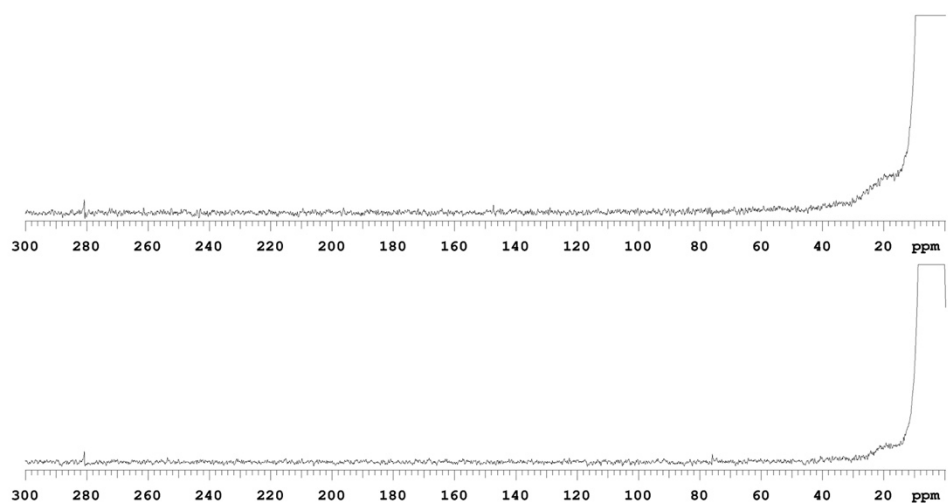


# OpenVnmrj

top-PESCKAGACSTCAGPDLTCT (glacial brine) 0 hour  
bottom-PESCKAGACSTCAGPDLTCT (glacial brine) 20 hour  
599.927 MHz H1 1D in d2o (ref. to external acetone @ 2.225 ppm)  
temp 26.2 C -> actual temp = 27.0 C, autoxid probe

Department of Chemistry, University of Alberta

Recorded on: 1600, Aug 4 2021	Sweep Width(Hz): 500000	Acquisition Time(s): 0.1	Relaxation Delay(s): 0.25
Pulse Sequence: PRESAT	Digital Res.(Hz/pt): 7.63	Hz per mm(Hz/mm): 769.75	Completed Scans: 1024



# OpenVnmrj

Department of Chemistry, University of Alberta

Recorded on: 1600, Aug 6 2021  
Pulse Sequence: PRESAT

Sweep Width(Hz): 500000  
Digital Res.(Hz/pt): 7.63

Acquisition Time(s): 0.1  
Hz per mm(Hz/mm): 769.75

Relaxation Delay(s): 0.25  
Completed Scans: 1024

top-KLCEGGCIACGACGGW (glacial brine) 0 hour  
bottom-KLCEGGCIACGACGGW (glacial brine) 20 hour  
599.927 MHz H1 1D in d2o (ref. to external acetone @ 2.225 ppm)  
temp 26.2 C -> actual temp = 27.0 C, autoxid probe

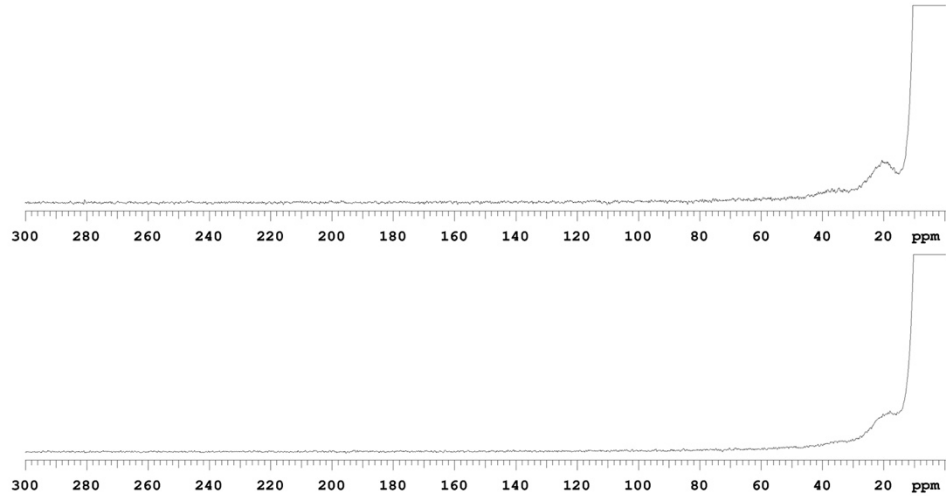


**Figure A.14.** Paramagnetic <sup>1</sup>H NMR spectra of iron-sulfur peptides under glacial brine conditions.